REVIEW

Dark matter and dark energy interactions: theoretical challenges, cosmological implications and observational signatures

IOP Publishing Reports on Progress in Physics
Rep. Prog. Phys. 79 (2016) 096901 (49pp) doi:10.1088/0034-4885/79/9/096901

Review

Dark matter and dark energy interactions: theoretical challenges, cosmological implications and observational signatures

B Wang[1], E Abdalla[2], F Atrio-Barandela[3] and D Pavón[4]

[1] Department of Physics and Astronomy, Shanghai Jiao Tong University, People's Republic of China
[2] Instituto de Fisica, Universidade de São Paulo, Brazil
[3] Física Teórica, Universidad de Salamanca, Spain
[4] Departamento de Física, Universidad Autónoma de Barcelona, Spain

E-mail: wang_b@sjtu.edu.cn, eabdalla@usp.br, atrio@usal.es and diego.pavon@uab.es

Received 30 August 2015, revised 17 April 2016
Accepted for publication 23 May 2016
Published 12 August 2016

Abstract

Models where dark matter and dark energy interact with each other have been proposed to solve the coincidence problem. We review the motivations underlying the need to introduce such interaction, its influence on the background dynamics and how it modifies the evolution of linear perturbations. We test models using the most recent observational data and we find that the interaction is compatible with the current astronomical and cosmological data. Finally, we describe the forthcoming data sets from current and future facilities that are being constructed or designed that will allow a clearer understanding of the physics of the dark sector.

Keywords: dark matter, dark energy, interaction

(Some figures may appear in colour only in the online journal)

1. Introduction

The first observational evidence that the universe entered a period of accelerated expansion was obtained when supernovae type Ia (SNIa) were found to be fainter than expected [281, 282, 313, 314]. This fact has been confirmed by many independent observations such as temperature anisotropies of the cosmic microwave background (CMB) [286, 292, 351], inhomogeneities in the matter distribution [104, 361], the integrated Sachs–Wolfe (ISW) effect [73], baryon acoustic oscillations (BAO) [128], weak lensing (WL) [106], and gamma-ray bursts [206]. Within the framework of general relativity (GR), the accelerated expansion is driven by a new energy density component with negative pressure, termed dark energy (DE). The nature of this unknown matter field has given rise to a great scientific effort in order to understand its properties.

The observational evidence is consistent with a cosmological constant Λ driving the present epoch of the accelerated expansion and a dark matter (DM) component giving rise to galaxies and their distributions [230, 288, 292]. The DM is assumed to have negligible pressure and temperature and is termed Cold. Thanks to the agreement with observations the model is commonly known as Λ CDM, to indicate the nature of its main components. While favored by the observations, the model is not satisfactory from the theoretical point of view: the value of the cosmological constant is many orders of magnitude smaller than what it was estimated in Particle Physics [388]. It was suggested soon that DE could be dynamic, evolving with time [84, 232, 276]. This new cosmological model also suffers from a severe fine-tune problem known as *coincidence problem* [418] that can be expressed with the following simple terms: if the time variation of matter and DE are very different why are their current values so similar? Cosmological models where DM and DE do not evolve separately but interact with each other were first introduced to justify the

currently small value of the cosmological constant [392, 393] but they were found to be very useful to alleviate the coincidence problem. In this review we will summarize the theoretical developments and the observational evidence on the reality and nature of a DM/DE interaction and the forthcoming observational facilities that could eventually lead to its detection.

The emergence of galaxies and large scale structure (LSS) is driven by the growth of matter density perturbations which themselves are connected to the anisotropies of the CMB [273]. An interaction between the components of the dark sector will affect the overall evolution of the universe and its expansion history. The growth of matter and baryon density perturbations, the pattern of temperature anisotropies of the CMB and the evolution of the gravitational potential at late times would be different than in the concordance model. These observables are directly linked to the underlying theory of gravity [192, 389] and, consequently, the interaction could be constrained with observations of the background evolution and the emergence of LSS.

This review is organized as follows: in this introduction we describe the concordance model and its theoretical liminations that motivates the introduction of interacting models. Since the nature of DE and DM are currently unknown, in section 2 we introduce two possible and different approaches to describe the DE and the DM: fluids and scalar fields. Based on general considerations like the holographic principle, we discuss why the interaction within the dark sector is to be expected. In section 3 we review the influence of the interaction on the background dynamics. We find that a DM/DE interaction could solve the coincidence problem and satisfy the second law of thermodynamics. In section 4 the evolution of matter density perturbations is described for the phenomenological fluid interacting models. In section 5 we discuss how the interaction modifies the non-linear evolution and the subsequent collapse of density perturbations. In section 6 we describe the main observables that are used in section 7 to constrain the interaction. Finally, in section 8 we describe the present and future observational facilities and their prospects to measure or constrain the interaction. In table 1 we list the acronyms used in this review.

1.1. The concordance model

The current cosmological model is described by the Friedmann–Robertson–Walker (FRW) metric, valid for a homogeneous and isotropic universe [387]

$$\mathrm{d}s^2 = -\mathrm{d}t^2 + a^2(t)\left[\frac{\mathrm{d}r^2}{1-Kr^2} + r^2\mathrm{d}\theta^2 + r^2\sin^2\theta\mathrm{d}^2\phi\right], \qquad (1)$$

where $a(t)$ is the scale factor at time t, the present time is denoted by t_0 and the scale factor is normalized to $a(t_0) = 1$; K is the Gaussian curvature of the space-time. We have chosen units $c = 1$ but we will reintroduce the speed of light when needed. A commonly used reparametrization is the *conformal time*, defined implicitly as $\mathrm{d}t = a(\tau)\mathrm{d}\tau$. In terms of this coordinate, the line element is

Table 1. List of commonly used acronyms.

Acronym	Meaning
A–P	Alcock–Paczynski
BAO	Baryon accoustic oscillations
CDM	Cold dark matter
CL	Confidence level
CMB	Cosmic microwave background
DE	Dark energy
DETF	Dark energy task force
DM	Dark matter
EoS	Equation of state
EISW	Early integrated Sachs–Wolfe
FRW	Friedman–Robertson–Walker
ISW	Integrated Sachs–Wolfe
KSZ	Kinematic Sunyaev–Zeldovich
LBG	Lyman break galaxies
LHS	Left hand side (of an equation)
LISW	Late integrated Sachs–Wolfe
LSS	Large scale structure
MCMC	Monte Carlo Markov chain
RHS	Right hand side (of an equation)
RSD	Redshift space distortions
SL	Strong lensing
SNIa	Supernova type Ia
SW	Sachs–Wolfe
TSZ	Thermal Sunyaev–Zeldovich
WL	Weak lensing

$$\mathrm{d}s^2 = a^2(\tau)\left[-\mathrm{d}\tau^2 + \frac{\mathrm{d}r^2}{1-Kr^2} + r^2\mathrm{d}\theta^2 + r^2\sin^2\theta\mathrm{d}^2\phi\right]. \qquad (2)$$

If we describe the matter content of the universe as a perfect fluid with mean energy density ρ and pressure p, Friedmann's equations are [212]

$$H^2 + \frac{K}{a^2} = \frac{8\pi G}{3}\sum\rho_i + \frac{\Lambda}{3}, \qquad (3)$$

$$\frac{\ddot{a}}{a} = -\frac{4\pi G}{3}\sum(\rho_i + 3p_i) + \frac{\Lambda}{3}, \qquad (4)$$

where $H = \dot{a}/a$ is the Hubble function and ρ_i, p_i are the energy density and pressure of the different matter components, related by an equation of state (EoS) parameter $\omega_i = p_i/\rho_i$. In terms of the conformal time, the expression $\mathcal{H} = a^{-1}(\mathrm{d}a/\mathrm{d}\tau) = aH$ is used. Usually densities are measured in units of the critical density: $\Omega = \rho/\rho_{\mathrm{cr}}$ with $\rho_{\mathrm{cr}} = 3H^2/(8\pi G)$. The curvature term can be brought to the right hand side (RHS) by defining $\rho_K = -3K/(8\pi G a^2)$. As a matter of convention, a sub-index '0' denotes the current value of any given quantity. Due to the historically uncertain value of the Hubble constant, its value is usually quoted as $H_0 = 100h\ \mathrm{kms}^{-1}\ \mathrm{Mpc}^{-1}$ so the parameter h encloses the observational uncertainty.

The cosmological constant provides the simplest explanation of the present period of accelerated expansion. When Λ is positive and dominates the RHS of equation (4) then $\ddot{a} > 0$ and the expansion is accelerated. The accelerated expansion can also be described by the deceleration parameter

Table 2. Cosmological parameters of the ΛCDM model, derived from the CMB temperature fluctuations measured by Planck with the addition of external data sets.

$H_0/(\mathrm{kms}^{-1}\,\mathrm{Mpc}^{-1})$	67.74 ± 0.46
$\Omega_{b,0}\,h^2$	$0.022\,30 \pm 0.000\,14$
$\Omega_{c,0}\,h^2$	0.1188 ± 0.0010
$\Omega_{\Lambda,0}$	0.6911 ± 0.0062
$\Omega_{K,0}$	$0.0008^{+0.0040}_{-0.0039}$
ω_d	$-1.019^{+0.075}_{-0.080}$

Note: Error bars are given at the 68% confidence level. The data for curvature and EoS parameter are constraints on 1-parameter extensions to the base ΛCDM model for combinations of Planck power spectra, Planck lensing and external data. The errors are at the 95% confidence level. Data taken from [293].

$q = -\ddot{a}/(aH^2) < 0$. If we set the cosmological constant to zero in equations (3) and (4), it can be reintroduced as a fluid with energy density $\rho_\Lambda = \Lambda/(8\pi G)$ and an EoS parameter $\omega_\Lambda = -1$. In addition to the cosmological constant and the curvature terms the concordance model includes other energy density components: Baryons (b), Cold DM (c), and Radiation (r), characterized by the EoS parameters $\omega_b = \omega_c = 0$ and $\omega_r = 1/3$, respectively. Then, equation (4) can be expressed as $\sum \Omega_i = 1$ where the sum extends over all energy densities, $i = (b, c, \Lambda, K, r)$.

If the source of the accelerated expansion is DE (d), its EoS parameter could be constant or vary with time but has to satisfy $\omega_d < -1/3$. The ΛCDM refers to the specific case when $\omega_d = -1$.

In table 2 we present the most recent values given by the Planck Collaboration derived by fitting the ΛCDM model to the measured CMB anisotropies and other external data sets [292]. The quoted errors are given at the 68% confidence level (CL). When more general models with 1-parameter extensions to the base ΛCDM model are fit to the same data, it is possible to derive constraints on the curvature and a constant DE EoS parameter. In these two cases, the quoted error bars are at the 95% CL. The table shows that in the ΛCDM model the energy density budget is dominated by ρ_Λ and ρ_c. Other components like massive neutrinos or the curvature ρ_K are not dynamically important and will not be considered in this review.

1.2. Observational magnitudes

The first evidence of the present accelerated expansion came when comparing the measured brightness of SNIa at redshifts $z \geqslant 0.4$ to their flux expected in different cosmological models [281, 313]. The method relies on measuring distances using *standard candles*, sources with well known intrinsic properties. In Cosmology, distances are measured very differently than in the Minkowski space-time, they are parametrized in terms of the time travelled by the radiation from the source to the observer by magnitudes such as the redshift and look-back time. Depending on the observational technique, distances are numerically different and their comparison provides important information on the parameters defining the metric. The most commonly used distance estimators are luminosity and angular diameter distances.

1.2.1. Redshift z. If ν_e and ν_0 are the frequencies of a line at the source and at the observer, the redshift of the source is defined as $z = (\nu_e/\nu_0) - 1$. In Cosmology, the redshift is directly related to the expansion factor at the time of emission t_e and observation t_0 as [387]

$$1 + z = \frac{a(t_0)}{a(t_e)}. \tag{5}$$

Due to the expansion of the universe, spectral lines are shifted to longer wavelengths from the value measured in the laboratory. The redshift measures the speed at which galaxies recede from the observer but it is not a measure of distance; the inhomogeneities in the matter distribution generate peculiar velocities that add to the velocity due to the Hubble expansion. Objects with the same redshift could be at different distances from the observer if they are not comoving with the Hubble flow. The redshift can be used to define the time variation of cosmological magnitudes. For instance, equation (3) can be written in terms of the EoS parameter as

$$E(z) = \frac{H(z)}{H_0} = \left(\sum_i \Omega_{i,0} f_i(z)\right)^{1/2},$$
$$f_i(z) = \exp\left[3\int_0^z \frac{1 + \omega_i(z')}{1 + z'}\mathrm{d}z'\right], \tag{6}$$

where the sum extends over all energy density components, $i = (b, c, d, r)$.

1.2.2. Luminosity distance D_L. The distance obtained by comparing the luminosity L of a standard candle to its measured flux F is known as luminosity distance $D_\mathrm{L} = \sqrt{L/4\pi F}$. For the flat universe, the luminosity distance is given in terms of the cosmological parameters in the form [387]

$$D_\mathrm{L} = (1 + z) c H_0^{-1} \int_0^z \frac{\mathrm{d}z'}{E(z')}, \tag{7}$$

The Hubble function (see equation (6)) encodes the information on the time evolution of the different energy components.

1.2.3. Angular diameter distance D_A. The distance resulting from the ratio of the intrinsic size of a standard ruler x to the angle θ subtended in the sky is $D_\mathrm{A} = x/\theta$. It can be expressed in terms of the Hubble function as

$$D_\mathrm{A} = \frac{c H_0^{-1}}{(1 + z)} \int_0^z \frac{\mathrm{d}z'}{E(z')}, \tag{8}$$

From equations (7) and (8) these distances verify $D_\mathrm{L} = (1 + z)^2 D_\mathrm{A}$.

1.2.4. Look-back time t_L and age of cosmological sources. The look-back time is defined as the difference between the age of the universe today and its age at some redshift z

$$t_\mathrm{L}(z) = H_0^{-1} \int_0^z \frac{\mathrm{d}z'}{(1 + z')E(z')} \equiv t_0 - t_\mathrm{age}(z) - df, \tag{9}$$

where $t_{\rm age}(z) = t_{\rm L}(z_{\rm F}) - t_{\rm L}(z)$ and $z_{\rm F}$ is the redshift of the formation of a source observed. If t_0 is the age of the universe today, then the look-back time is $t_{\rm L}(z) = t_{\rm L}(z_{\rm F}) - t_{\rm age}(z) = t_0 - t_{\rm age}(z) - df$, with $df = t_0 - t_{\rm L}(z_{\rm F})$. From stellar population synthesis one can estimate the age of a particular galaxy and compute its look-back time. Since the redshift of formation of the object is not directly observable, look-back time as tests of cosmological models can only be applied when many similar objects are observed at different redshifts in order to marginalize over the nuisance parameter df [87].

1.3. Problems with the concordance model

Although the concordance model fits reasonably well all the available data, it suffers from two fine-tune initial value problems: the cosmological constant and the coincidence problem.

1.3.1. The cosmological constant problem. Table 2 shows that today $\Omega_\Lambda \sim 1$ which implies that $\Lambda \sim 3H_0^2$. The corresponding energy density is a constant of amplitude $\rho_\Lambda = 10^{-47}\,({\rm GeV})^4$. The cosmological constant can be interpreted as the energy density of the vacuum. At the Planck scale, the contribution to the quantum vacuum of the ground state of all known matter fields is $\rho_{\rm vac} = 10^{74}\,({\rm GeV})^4$, 121 orders of magnitude larger [388]. Therefore, the initial conditions for the concordance model requires setting a value of ρ_Λ that is several orders of magnitude smaller than the theoretical expectation.

1.3.2. The coincidence problem. The energy density associated to the cosmological constant, ρ_Λ, is constant in time but the DM density varies as $\rho_c \propto a(t)^{-3}$. The CMB blackbody temperature, that today is $T_0 = 2.5 \times 10^{-4}$ eV and scales as $T = T_0/a(t)$, can be used to relate the current ratio of the matter to cosmological constant energy density to its value at the Planck energy scale, $T_{\rm Planck} = 10^{19}$ GeV, as

$$\frac{\rho_\Lambda}{\rho_m(t_{\rm Planck})} = \frac{\rho_\Lambda}{\rho_{m,0}}\left(\frac{T_{\rm Planck}}{T_0}\right)^{-3} \simeq 10^{-95}. \qquad (10)$$

This expression shows that the initial values of the energy densities associated to matter and cosmological constant would not be very likely fixed by random processes. At the Planck time, the initial conditions are heavily tuned by 95 orders of magnitude [418].

The problem of the initial conditions in the 'concordance' model has led to study different alternatives such as scalar fields, fluids with negative pressure and different EoS [4, 84, 232, 306]; these models are termed *quintessence* if $\omega_d > -1$ and *phantom* if $\omega_d < -1$. Other popular alternatives are *k-essence*, a scalar field with a non-canonical kinetic energy term [33, 94, 96, 332] and the Chaplygin gas, a fluid with EoS $p \propto \rho^{-\alpha}$ ($\alpha > 0$) [194, 341]. Yet, these models suffer similar fine-tune problems [97] and do not fit the observations better than the 'concordance' model. Furthermore, the cosmological constant enjoys a solid motivation since it can be interpreted as the vacuum energy density while the alternative models do not.

1.4. Why interacting DM/DE models?

Most cosmological models implicitly assume that matter and DE only interact gravitationally. In the absence of further interactions, energy is conserved for each component,

$$\frac{{\rm d}\rho_i}{{\rm d}t} + 3H(1+\omega_i)\rho_i = 0. \qquad (11)$$

where $i = (b, c, d, r)$. In view of the unknown nature of both DE and DM, it is difficult to describe these components in term of a well established theory. Since DE and DM dominate the energy content of the universe today, it is equally reasonable to assume that these dark components could interact among themselves [75] and with other components. A few properties can be derived from observations: (A) The DE must contribute with a negative pressure to the energy budget while the DM pressure is small, possibly zero. (B) The DE coupling with baryons is probably negligible, being tightly constrained by local gravity measurements [159, 276]. (C) Coupling with radiation is also very difficult since photons will no longer follow a geodesic path and light deflection of stellar sources during solar eclipses would contradict the observations. (D) The coupling between DE and DM must also be small since the concordance model, where the DE is a cosmological constant and by definition non-interacting, is an excellent fit to the data. Of all these possibilities, a DM/DE interaction is the most attractive since it can either solve the coincidence problem by allowing solutions with a constant DM/DE ratio at late times or alleviate it, if the ratio varies more slowly than in the concordance model.

Modified gravity models can be expressed in terms of the DE/DM interaction in the Einstein frame (see section 2.8). This equivalence to a DM/DE interaction could be interpreted as an extension of the gravitational theory beyond the scope of GR, which gives further motivation to our study. Unfortunately, since we neither have a clear understanding of the nature of DM nor of DE, the nature of their interaction is also an unsolved problem. There is no clear consensus on what interaction kernel is the most adequate and different versions, based on multiple considerations, coexist in the literature. Ultimately, this is a question that must be resolved observationally.

2. Interacting DM/DE models

The present observational data is insufficient to determine the nature of the DE, leaving a great freedom to construct models. The cosmological constant can be interpreted as a fluid with an EoS parameter $\omega_\Lambda = -1$ (see section 1.1) or, equivalently, it can be seen as a scalar field with a vanishing kinetic energy [212]. Following this example, it is often assumed that the DE is part of the field theory description of Nature, an approach that has been extremely successful when applied to the early universe. Such an effort is not just a pure theoretical attempt of understanding, but also a step towards a general characterization of the dark sector.

The lack of information on the nature and dynamics of DM and DE makes it difficult to describe these components from first principles, in terms of well established physical theories. The DE can be treated as a fluid, a scalar field, a vector field, etc, and assumptions like the *holographic principle* can be made to construct models. We will review these approaches and further we will include the interactions between these DE descriptions with DM to show how they can be used to solve some of the shortcomings of the concordance model. More details can be found in [72].

2.1. Phenomenological fluid models

In the concordance model the energy density of each fluid component $i = (r, b, c, d)$, radiation, baryons, CDM and DE, respectively, is conserved separately: $\dot{\rho}_i + 3H(1+\omega_i)\rho_i = 0$ (equation (11)). In interacting models, the total energy density of the dark sector is conserved, but the DM and DE densities evolve as

$$\dot{\rho}_c + 3H\rho_c = Q, \tag{12}$$

$$\dot{\rho}_d + 3H(1+\omega_d)\rho_d = -Q, \tag{13}$$

where Q represents the interaction kernel. In the absence of a fundamental theory the quantity Q cannot be derived from first principles. The interaction introduces only a small correction to the evolution history of the universe; if $|Q| \gg 0$, then either the universe would have remained in the matter dominated regime (if $Q > 0$) or the universe would have not experienced a matter dominated period, altering the formation of galaxies and large scale structure (if $Q < 0$). As in particle physics, one would expect the kernel to be a function of the energy densities involved, ρ_d, ρ_c and of time, H^{-1}. The Taylor expansion of the interaction terms at first order would be: $Q = H(\xi_2\rho_d + \xi_1\rho_c)$, where the coefficients ξ_1, ξ_2 are constants to be determined observationally. Given the lack of information, it is convenient to use a single parameter instead of two. Three choices can be made here: $\xi_1 = 0$, $\xi_2 = 0$ and $\xi_1 = \xi_2$. This leads to the following kernels

$$Q = H\xi_1\rho_c; \quad Q = H\xi_2\rho_d; \quad Q = H\xi(\rho_d + \rho_c). \tag{14}$$

In table 3 we present the phenomenological models that will be considered in this review. We distinguish phantom and quintessence EoS parameters and we analyze only those models with stable density perturbations (see section 4).

The underlying reason why the interaction alleviates the coincidence problem is simple to illustrate. Due to the interaction, the ratio of energy densities $r = \rho_c/\rho_d$ evolves with the scale factor as $r \propto a^{-\zeta}$, where ζ is a constant parameter in the range [0, 3]. The deviation of ζ from zero quantifies the severity of the coincidence problem. When $\zeta = 3$ the solution corresponds to the ΛCDM model with $\omega_\Lambda = -1$ and $Q = 0$. If $\zeta = 0$ then $r =$ const. and the coincidence problem is solved [416]. As examples, let us now consider two specific kernels.

2.1.1. A solution of the coincidence problem. The interest of model IV is that it has attractor solutions with a constant DM/DE ratio, $r = \rho_c/\rho_d =$ const.. In fact, the past attractor solution is unstable and evolves towards the future attractor solution. To verify this behavior, we write the equation of the DM/DE ratio

$$\frac{\mathrm{d}r}{\mathrm{d}t} = -3\Gamma H r, \quad \Gamma = -\omega_d - \xi^2\frac{(\rho_c+\rho_d)^2}{3\rho_c\rho_d}, \tag{15}$$

and stationary solutions are obtained imposing $r_s\Gamma(r_s) = 0$. If, to simplify, we hold ω_d constant, then

$$r_s^{\pm} = -1 + 2b \pm 2\sqrt{b(b-1)}, \quad b = -\frac{3\omega_d}{4\xi} > 1. \tag{16}$$

Of these two stationary solutions, the past solution r_s^+ is unstable while the future solution r_s^- is stable [98, 414]. As the universe expands, $r(t)$ will evolve from r_s^+ to the attractor solution r_s^- avoiding the coincidence problem. This DE fluid model can also be seen as a scalar field with a power law potential at early times followed by an exponential potential at late times [261]. In figure 1 we represent the energy densities of the model with kernel $Q = H\xi(\rho_c + \rho_d)$. In (a) the value of the coupling constant $\xi = 0.1$ was chosen to show that the universe undergoes a baryon domination period, altering the sequence of cosmological eras. This value of ξ would not fit the observations since during most of the matter dominated period baryons would dominate the formation of galaxies and this process would proceed more slowly within shallower potential wells. The matter-radiation equality would occur after recombination so that the anisotropies of the CMB would be altered. In (b) the smaller value gives rise to the correct sequence of cosmological eras.

Model III has also been extensively studied in the literature [20, 85, 157, 386]. In this case the ratio evolves as

$$\dot{r} = H[\xi_1(1+r) + 3\omega_d]; \tag{17}$$

$$r = -(3\omega_d + \xi_1)r_0/\{\xi_1 r_0 - (1+z)^{-(3\omega_d+\xi_1)}[\xi_1(1+r_0) + 3\omega_d]\}, \tag{18}$$

where $r_0 = r(t_0)$ is the current DM/DE density ratio. Equation (18) does not have future attractor solutions with $r =$ const.; the interaction alleviates the coincidence problem but does not solve it. The time evolution of the ratio for different kernels is illustrated in figure 2 for a DE EoS $\omega_d = -1.1$. In (a) the ratio in model IV is constant both in the past and in the future. In (b) model III the ratio is constant in the past but in the future it will evolve with time, but the variation is $|(\dot{r}/r)_0| \leqslant H_0$, slower than in ΛCDM, alleviating the coincidence problem.

Table 3. Phenomenological interacting models considered in this review.

Model	Q	DE EoS
I	$\xi_2 H\rho_d$	$-1 < \omega_d < 0$
II	$\xi_2 H\rho_d$	$\omega_d < -1$
III	$\xi_1 H\rho_c$	$\omega_d < -1$
IV	$\xi H(\rho_c + \rho_d)$	$\omega_d < -1$

2.1.2. Statefinder parameters and the coincidence problem. At the background level, it is possible to choose models with

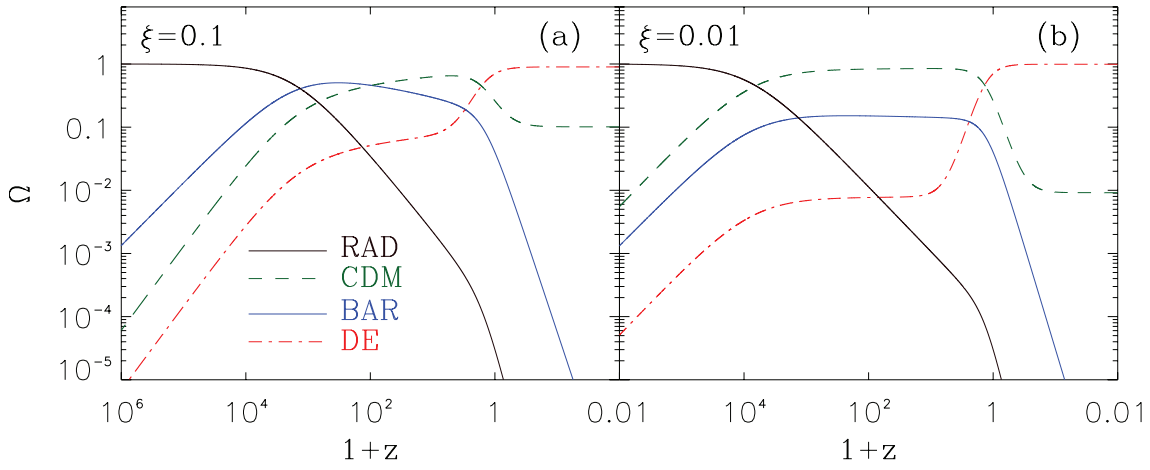

Figure 1. Evolution of energy densities on an interacting DM/DE model with kernel $Q = H\xi(\rho_d + \rho_c)$. Lines correspond to: baryons (solid), DM (dashed), DE (dot–dashed) with an EoS parameter $\omega_d = -1.1$ and radiation (triple dot–dashed). In (a) $\xi = 0.1$ and in (b) $\xi = 0.01$.

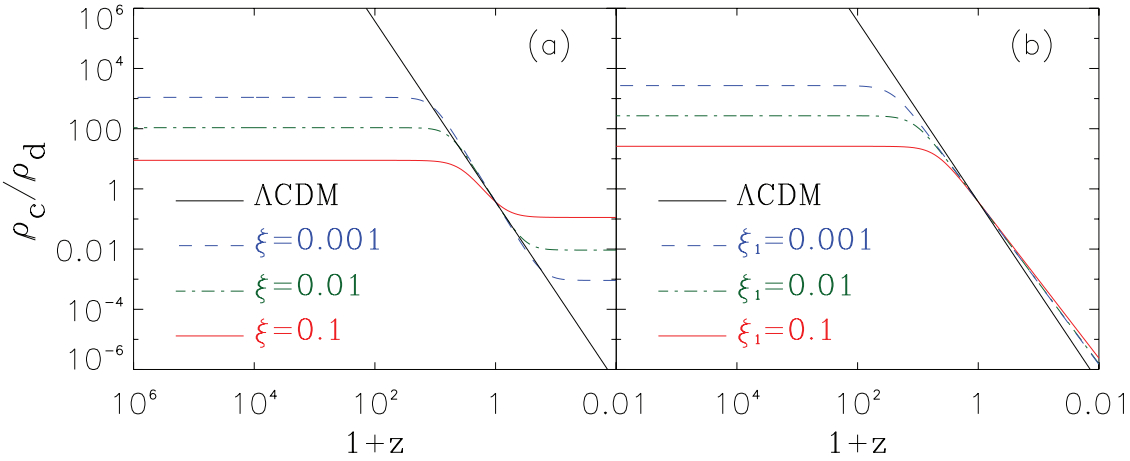

Figure 2. Evolution of the ratio of DM to DE densities for different model parameters. (a) corresponds to model IV and (b) to model III. The solid line, common to both panels, corresponds to the concordance model, while the dashed lines correspond to different interaction kernel parameters.

a varying EoS parameter such that it reproduces the same Hubble function $H(z)$ as the DM/DE interaction models. Then, observables such as angular and luminosity distances or look-back time can not be used to test the interaction. One exception is when DE decays into DM, since $\omega_d(z)$ would take imaginary values [86]. At the background level, the dimensionless parameters

$$\chi = \frac{1}{aH^3}\frac{\mathrm{d}^3 a}{\mathrm{d}t^3}, \quad s = \frac{\chi - 1}{3(q - \frac{1}{2})}, \tag{19}$$

first introduced in [320], are more useful to discriminate cosmological models. For instance, if $\omega_d = \text{const.}$ and the energy density ratio scales as a power law of the scale factor, $r \propto a^{-\zeta}$ then

$$\chi = 1 + \frac{9}{2}\frac{\omega_d}{1 + r_0(1+z)^\zeta}\left[1 + \omega_d - \left(\omega_d + \frac{\zeta}{3}\right)\frac{r_0(1+z)^\zeta}{1 + r_0(1+z)^\zeta}\right], \tag{20}$$

$$s = 1 + \omega_d - \left(\omega_d + \frac{\zeta}{3}\right)\frac{r_0(1+z)^\zeta}{1 + r_0(1+z)^\zeta}, \tag{21}$$

and as indicated in section 2.1, a lower value of ζ corresponds to a model with a less severe coincidence problem. In figure 3 we represent the function $\chi(s)$ for three values of ζ to demonstrate that lower values of ζ correspond to lower curves in the $s - \chi$. Hence, for any specific model, the statefinder parameters are useful to determine the severity of the coincidence problem. In the particular case of the concordance model, these parameters are constants: $\chi = 1$ and $s = 0$ and any deviation for those values would be an observational evidence against the concordance model. Similar conclusions have been reached by [114].

2.2. More forms of the interaction kernels from phenomenology

Here we briefly consider further phenomenological proposals of interaction kernels, not included in table 3, that have also been discussed in the literatures:

(i) $Q = \xi H\, \rho_c\, \rho_d/(\rho_c + \rho_d)$. At early times ($\rho_c \gg \rho_d$) it is seen that r diverges as $a \to 0$, see figure 23 in [86]. Further, using equation (4) in [86] and that the above expression approaches (in that limit) to $Q \approx \xi H \rho_d$, it follows that ξ is constrained to be $\xi \approx ar^{-1}\,(dr/da) - 3\omega_d$.

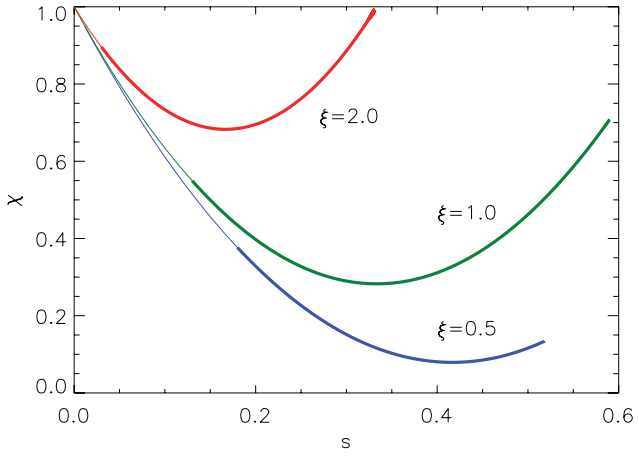

Figure 3. Selected curves $\chi(s)$ for a DE EoS parameter $\omega_d = -1.1$ and r_0 =3/7 and three different values of ξ. The thick lines correspond to the past evolution in the interval $z = [0, 20]$ and the thin lines to the future evolution in $z = [-0.9, 0]$.

(ii) $Q = -\xi(\dot{\rho}_c + \dot{\rho}_d)$ [325]. This model interpolates between radiation dominance and a far future de Sitter phase and is in good agreement with observational data; however, the DM component is not exactly cold, $\omega_c = 0.049^{+0.181}_{-0.460}$.

(iii) $Q = 3(\Gamma_d \rho_d + \Gamma_c \rho_c)$ this interaction term was motivated by models in reheating, curvaton, and decay of DM into radiation. In order to alleviate the coincidence problem and allow the ratio r to be positive and finite at early and late times, the constant coefficients Γ must have opposite signs and satisfy $\Gamma_d > \Gamma_c$. In this kind of models the matter perturbations stay finite at all times. However, with these models we are unable to solve the coincidence problem and, simultaneously, ensure that ρ_c and ρ_d never become negative [82]. In the particular case that Γ_c vanished these constraints can be met, but the DE dominated phase would be transitory and the universe would revert to DM domination in contradiction to the second law of thermodynamics [305]. Further, r would diverge irrespectively of whether both Γ coefficients were different from zero or just one of them.

(iv) $Q = \rho_{n0}\, a^{-3(1+\omega_n)}\, \dot{f}\,(\phi)$, this interaction term is not given *a priori* but ascertained from the cosmic dynamics [375]. Here $f(\phi)$ is a function of the scalar field, ϕ, which interacts with the dominant background fluid (matter or radiation) and plays the role of a cosmological constant since the corresponding EoS is set to -1. This function obeys $f \propto t^3$, and the subindex n stands for matter and radiation in the dust and radiation eras, respectively. In this scenario Q is fixed to zero in the early inflation phase and the last de Sitter expansion but it differs from zero in both the radiation and matter eras.

(v) In the scenario proposed in [376] DE (in the form of a cosmological constant), DM and radiation arise from the action of a Higgs-like mechanism on an underlying tachyon field. A small time dependent perturbation in the EoS of the cosmological constant, so that $\omega_d = -1 + \varepsilon(t)$, leads to a small shift in the EoS of radiation and matter. The pressure of the latter results slightly negative whence it contributes to drive the acceleration. The three components interact non-gravitationally with each other via two interaction terms, namely, $Q_1 = \alpha\dot{\bar{\rho}}_d$ and $Q_2 = \beta\dot{\bar{\rho}}_r$ (the over-bars indicates that we are dealing with the shifted energy densities). Different dynamics follow depending on whether $|Q_1| > |Q_2|$ or $|Q_2| > |Q_1|$ or $Q_1 = Q_2$.

(vi) In [342] the interaction was taken in the form $Q = \alpha\dot{\rho}_c$, $Q = \beta\dot{\rho}_d$, and also $Q = \sigma(\dot{\rho}_c + \dot{\rho}_d)$. In all three instances no baryonic matter is considered and $\omega_d > -1$. In each case the analysis of the corresponding autonomous system reveals the existence of a late time stable attractor such that the ratio between both energy densities is of the order of unity, thus solving the coincidence problem.

Other linear and nonlinear kernels and their background evolution have been extensively studied in [99].

2.3. Scalar fields in cosmology

From the observational point of view, phenomenological fluid models are viable candidates of DM and DE; they fit the observational data with realistic interaction kernels [378, 381], although they are not motivated by a dynamical principle. Alternative formulations are usually based on a particle field approach. This choice not only has been very useful to describe the physics of the early universe, but in this context it also defines what physical principles are involved. The situation is somewhat clearer for the DM, with several candidates defined in terms of extensions of the Standard model. The first DM candidate were massive neutrinos, ruled out since they failed to explain the formation of Large Scale Structure (LSS) [71, 360]. Alternative candidates were sterile neutrinos [122] and axions, introduced to explain CP violation [272]. Similarly, supersymmetry produces candidates such as the axino, the s-neutrino, the gravitino and the neutralino. These particles need to be stable so they must be the lightest supersymmetric particle. This leaves a small number of candidates, basically the neutralino and the gravitino [63]. The situation could be more complex if the DM is not described by a single field but by a whole particle sector with nontrivial structure. In string theory, the second piece of the symmetry $E_8 \otimes E_8$ could describe a sector that would interact with baryonic matter only via gravity [116, 155]. However, in spite of the many candidates that have been proposed and the exhaustive searches that have been carried out in the last decades, no concrete evidence of the particle nature of the DM has emerged.

The nature of DE is an even more troubling question. When the theoretical description of DE is made very general, models can be constructed using a wide variety of choices at the expense of loosing predictability. This great freedom indicates that the description of DE is more a scenario than a physical theory, similarly to what happens with inflationary models. The best guiding principles are simplicity and the consistency of the theoretical foundation. Let us assume that DE can be described in terms of quantum fields. Its pressure should be negative to generate a period of accelerated expansion ($\omega_d \leqslant -1/3$, see equation (3)). Even in this simplified approach, quantum field theory already imposes severe

restrictions if $\omega_d < -1$ [378]. The difficulty of constructing suitable quantum field models is illustrated by the fact that several models correspond to non-renormalizable Lagrangians [19, 40, 245]. There are also models with fermionic [311, 312, 319] and vectorial DE [34, 210, 385, 420]. Although gravity and other fields are purely classical and in spite of gravity being itself non-renormalizable, the need to consider non-renormalizable models is a clear indication that, at the moment, the description of DE must be phenomenological.

2.4. Field description and the DM/DE interaction

The simplest DM description is in terms of fermions with pressure vanishing at decreasing momenta (small energy). Let us consider the following canonical fermionic field Lagrangian, see [409]

$$\mathcal{L} = \sqrt{-g}\,\overline{\Upsilon}(\mathrm{i}\not{\mathcal{D}} - m)\Upsilon + \text{non derivative interactions}. \tag{22}$$

The energy-momentum tensor is defined as $T_{\mu\nu} \equiv e^{-1}e^{a}_{\mu}(\delta\mathcal{L}/\delta \mathrm{e}^{\nu a})$ where $e_{\mu a}$ is the vierbein and e the corresponding determinant. For a fermion field Υ, it is given by

$$T_{\mu\nu} = \frac{\mathrm{i}}{4}(\overline{\Upsilon}\gamma_{\mu}\nabla_{\nu}\Upsilon + \overline{\Upsilon}\gamma_{\nu}\nabla_{\mu}\Upsilon - \nabla_{\mu}\overline{\Upsilon}\gamma_{\nu}\Upsilon - \nabla_{\nu}\overline{\Upsilon}\gamma_{\mu}\Upsilon). \tag{23}$$

For a homogeneous universe the spatial part of the energy-momentum tensor vanishes and so does the pressure. This is not correct for relativistic fermions since the average momentum does not vanish and originates a pressure that, like in the case of massive neutrinos, would alter the formation of LSS. If we consider that DM and DE interact, then this constraint can be evaded since the pressure of each component is not well defined. An interaction gives the freedom to choose what fraction of the pressure corresponds to the DM or to the DE. A natural choice is to take the interaction term to be in the fermionic component, then the corresponding background pressure vanishes and matter behaves as a pressureless fluid. Therefore, hereafter we will describe the DM as a non-relativistic fermion with zero pressure, i.e. the DM is 'cold'. A discussion on what models are compatible with observational constraints is given in [72, 269].

Scalar fields are the quantum fields that provide the simplest description of DE. If K is the kinetic and V the potential energy of the field φ, the energy density and pressure associated to the field would be $\rho_d \sim K + V$ and $p_d \sim K - V$, respectively. If $|V| > K$, it is possible to find configurations where the EoS is negative enough (i.e. $\omega_d < -1/3$) to give rise to a cosmological period of accelerated expansion. In a field theoretic formulation, the interaction is not only allowed but is actually inevitable. In this section we discuss scalar fields with renormalizable Lagrangians and defer to the next section a non-renormalizable case.

A fermionic DM and a renormalizable DE model can be described by the Lagrangian

$$\mathcal{L} = \overline{\Upsilon}(\mathrm{i}\not{\partial})\Upsilon + \mathcal{L}_s(\varphi) + F(\varphi)\overline{\Upsilon}\Upsilon. \tag{24}$$

where $F \equiv F(\varphi)$ is an effective interaction. Any generic Lagrangian would contain an interaction term except if such term is forbidden by a given symmetry [392]. To continue further, let us assume that the DE can be described as an uncharged scalar φ obeying the Lagrangian

$$\mathcal{L}_s(\varphi) = \ell\frac{1}{2}\partial^{\mu}\varphi\partial_{\mu}\varphi - V(\varphi), \tag{25}$$

where $V(\varphi)$ is the scalar field potential (of arbitrary shape). The sign $\ell = -1$ describes a phantom field. For simplicity, we will restrict our study to $\ell = +1$ (see [269] for details) and to the linear relation $F(\varphi) = M - \beta\varphi$. Then M is the usual fermion mass and β a Yukawa coupling constant.

The interaction term in equation (24) couples DM and DE. The Hubble function (equation (3)) for a FRW universe that also includes baryons and radiation becomes [212]

$$H^2 = \frac{8\pi G}{3}\left(\rho_r + \rho_b + \rho_c + \frac{1}{2}\dot{\varphi}^2 + V(\varphi)\right). \tag{26}$$

In this simplified model, the different components evolve separately and their energy densities are independently conserved except for DM and DE. For these two components, the energy-momentum conservation equations are

$$\dot{\rho}_c + 3H\rho_c = -\rho_c\dot{\varphi}\varrho/(1 - \varrho\varphi), \tag{27}$$

$$\ddot{\varphi} + 3H\dot{\varphi} + V'(\varphi) = \rho_c\varrho/(1 - \varrho\varphi), \tag{28}$$

where $\varrho = \beta/M$; dots correspond to time derivatives and primes to derivatives with respect to the scalar field φ. Equations (27) and (28) show that if DM and DE are members of a unified quantum field description, they interact.

Although from the theoretical point of view, quantum field models constitute an improvement over the simpler phenomenological interaction [111], the coupling is still undetermined. Several attempts have been tried, including modifications of the space-time dimensions [408]. Alternative exponential forms of $F(\varphi)$ have been extensively considered in the literature giving different coupling kernels [19, 40, 245, 403]. The field description is a possible understanding on the interaction between dark sectors, however it brings another hidden fine tuning problem which needs to be carefully dealt with.

2.5. Scalar fields as k-essence and tachyons

When renormalizability is not required, models become increasingly more complex. For example, k-essence is a model of a scalar field defined by a non-standard kinetic term

$$\mathcal{L} = p(\varphi, X), \qquad X = \frac{1}{2}(D_{\mu}\varphi D^{\mu}\varphi). \tag{29}$$

If the kinetic term is separable in its variables φ and X, then the k-essence field can be transformed from a tracking background into an effective cosmological constant at the epoch of matter domination [32]. We will restrict our study to this particular Lagrangian because of its simplicity. Our interest is driven by string theory and supergravity where such non-standard kinetic terms appear quite often. The Lagrangian of equation (29) generalizes the simplest scalar field models. In the limit of small spatial derivatives the Lagrangian is equivalent to that of a canonical field.

Another non-renormalizable class of models is related to tachyons in string theory. The tachyon Lagrangian, derived from brane developments is given by [175, 335–340]

$$\mathcal{L}_{\rm tach} = -V(\varphi)\sqrt{(1-\alpha\partial^\mu\varphi\partial_\mu\varphi)}\,. \tag{30}$$

This Lagrangian has the form discussed by [32] and has been used to give general descriptions of the components of the dark sector [56, 57]. It can be implemented in models with interaction. One such interacting Lagrangian is

$$\mathcal{L} = \mathcal{L}_{\rm tach} + \frac{\rm i}{2}\left[\overline{\Upsilon}\gamma^\mu\nabla_\mu\Upsilon - \overline{\Upsilon}\overleftarrow{\nabla}_\mu\gamma^\mu\Upsilon\right] - F(\varphi)\overline{\Upsilon}\Upsilon, \tag{31}$$

where Υ is a fermionic field for DM and φ a bosonic field for DE. The linear (for canonical renormalizable bosons) model $F(\varphi) = M - \beta\varphi$ has been studied in detail (see section 2.4) and shown to be compatible with the observational constraints, although it is not renormalizable because of the bosonic non-linearities [248]. The equations of motion can be derived from equation (31) and for the linear case they read

$$\mathrm{i}\gamma^\mu\nabla_\mu\Upsilon - (M-\beta\varphi)\Upsilon = 0, \tag{32}$$

$$\alpha\nabla_\mu\partial^\mu\varphi + \alpha^2\frac{\partial^\mu\varphi(\nabla_\mu\partial_\sigma\varphi)\partial^\sigma\varphi}{1-\alpha\partial_\mu\varphi\partial^\mu\varphi} + \frac{\mathrm{d}\ln V(\varphi)}{\mathrm{d}\varphi} = \frac{\beta\bar{\Upsilon}\Upsilon}{V(\varphi)}\sqrt{1-\alpha\partial^\mu\varphi\partial_\mu\varphi}\,. \tag{33}$$

Neglecting spatial gradients, the motion of the scalar field becomes

$$\ddot{\varphi} = -(1-\alpha\dot{\varphi}^2)\left[\frac{1}{\alpha}\frac{\mathrm{d}\ln V(\varphi)}{\mathrm{d}\varphi} + 3H\dot{\varphi} - \frac{\beta\bar{\Upsilon}\Upsilon}{\alpha V(\varphi)}\sqrt{1-\alpha\dot{\varphi}^2}\right], \tag{34}$$

where $H = \dot{a}/a$ is the Hubble function. Fermionic current conservation implies

$$\frac{\mathrm{d}(a^3\bar{\Upsilon}\Upsilon)}{\mathrm{d}t} = 0, \quad \Rightarrow \quad \bar{\Upsilon}\Upsilon = \bar{\Upsilon}_0\Upsilon_0 a^{-3}. \tag{35}$$

Let us now show that the Lagrangian of equation (31) gives rise to a cosmological model with an interaction in the dark sector. To that purpose, we compute the energy-momentum tensor (see [248] for details). The energy density and pressure of each component is given by

$$\rho_\varphi = \frac{V(\varphi)}{\sqrt{1-\alpha\dot{\varphi}^2}}, \qquad p_\varphi = -V(\varphi)\sqrt{1-\alpha\dot{\varphi}^2}, \tag{36}$$

$$\rho_\Upsilon = (M-\beta\varphi)\bar{\Upsilon}\Upsilon, \qquad p_\Upsilon = 0. \tag{37}$$

An important consequence of equation (36) is that the EoS parameter of the fluid associated to the DE field is $\omega_\varphi \equiv p_\varphi/\rho_\varphi = -(1-\alpha\dot{\varphi}^2)$. If $\alpha\dot{\varphi}^2 \ll 1$, then the DE acts as an effective cosmological constant. In addition, from equations (36) and (37) the time evolution of the DM and DE energy densities are

$$\dot{\rho}_\varphi + 3H\rho_\varphi(\omega_\varphi + 1) = \beta\dot{\varphi}\bar{\Upsilon}_0\Upsilon_0 a^{-3}, \tag{38}$$

$$\dot{\rho}_\Upsilon + 3H\rho_\Upsilon = -\beta\dot{\varphi}\bar{\Upsilon}_0\Upsilon_0 a^{-3}. \tag{39}$$

and the Friedmann equation (3) becomes

$$H^2 = \frac{8\pi G}{3}\left[\rho_r + \rho_b + (M-\beta\varphi)\bar{\Upsilon}_0\Upsilon_0 a^{-3} + \frac{V(\varphi)}{\sqrt{1-\alpha\dot{\varphi}^2}}\right]. \tag{40}$$

Together with the equations of evolution of baryons and radiation, equations (38)–(40) fully describe the background evolution of the universe. These equations are very similar to the ones used in phenomenological models [133, 164, 165, 381]. The RHS of equations (38) and (39) does not contain the Hubble parameter H explicitly, but it does contain the time derivative of the scalar field, which should behave as the inverse of the cosmological time, thus replacing the Hubble parameter in the phenomenological models.

Analytic solutions have been found in [9, 131, 267] in the pure bosonic case with the potential $V(\varphi) = m^{4+n}\varphi^{-n}$, with m a dimensional constant and n a positive integer. Choosing $n = 2$, leads to a power law expansion of the universe. This model has been shown to be compatible with the observational data [248].

2.6. Holographic DE models

Another set of models are loosely based on heuristic arguments taken from particle physics. The concept of holography [356, 362] has been used to fix the order of magnitude of the DE [227]. To explain the origin of these ideas, let us consider the world as three-dimensional lattice of spin-like degrees of freedom and let us assume that the distance between every two neighboring sites is some small length ℓ. Each spin can be in one of two states. In a region of volume L^3 the number of quantum states will be $N(L^3) = 2^n$, with $n = (L/\ell)^3$ the number of sites in the volume, whence the entropy will be $S \propto (L/\ell)^3 \ln 2$. One would expect that if the energy density does not diverge, the maximum entropy would vary as L^3, i.e. $S \sim L^3\,\lambda_{\rm UV}^3$, where $\lambda_{\rm UV} \equiv \ell^{-1}$ is to be identified with the ultraviolet cut-off. Even in this case, the energy is large enough for the system to collapse into a black hole larger than L^3. Bekenstein suggested that the maximum entropy of the system should be proportional to its area rather than to its volume [54]. In the same vein 't Hooft conjectured that it should be possible to describe all phenomena within a volume using only the degrees of freedom residing on its boundary. The number of degrees of freedom should not exceed that of a two-dimensional lattice with about one binary degree of freedom per Planck area.

Elaborating on these ideas, an effective field theory that saturates the inequality $L^3\,\lambda_{\rm UV}^3 \leqslant S_{\rm BH}$ necessarily includes many states with $R_{\rm s} > L$, where $R_{\rm s}$ is the Schwarzschild radius of the system under consideration [103]. Therefore, it seems reasonable to propose a stronger constraint on the infrared cutoff L that excludes all states lying within $R_{\rm s}$, namely, $L^3\,\lambda_{\rm UV}^4 \leqslant m_{Pl}^2\,L$ (clearly, $\lambda_{\rm UV}^4$ is the zero–point energy density associated to the short-distance cutoff) and we can conclude that $L \sim \lambda_{\rm UV}^{-2}$ and $S_{\rm max} \simeq S_{\rm BH}^{3/4}$. Saturating the inequality and

identifying $\lambda^4_{\rm UV}$ with the holographic DE density is given by [227]

$$\rho_d = \frac{3\wp}{8\pi G L^2}, \tag{41}$$

where $\wp$ is a positive, dimensionless parameter, either constant or very slowly varying with the expansion.

Suggestive as they are, the above ideas provide no indication about how to choose the infrared cutoff in a cosmological context. Different possibilities have been tried with varying degrees of success, namely, the particle horizon [91, 136], the future event horizon [152, 153, 156, 187, 227, 378, 379] and the Hubble horizon. The first choice fails to produced an accelerated expansion. The second presents a circularity problem: for the cosmological event horizon to exist the universe must accelerate (and this acceleration must not stop), i.e. it needs the existence of DE. The third option is the most natural, but $L = H^{-1}$ corresponds to an energy density with $\rho \propto a^{-3}$, i.e. to dust and not to DE. Nevertheless, as we shall see below, if the holographic DE interacts with pressureless matter then it can drive a period of accelerated expansion and alleviate, or even solve, the coincidence problem [271, 417].

2.6.1. Interacting holographic DE. An effective theory based on the holographic principle that produces a period of accelerated expansion requires the following assumptions: (a) the DE density is given by equation (41), (b) $L = H^{-1}$, and (c) DM and holographic DE interact with each other obeying equations (12) and (13). As an example, we will consider the kernel $Q = \xi\rho_d$ where $\xi > 0$ is a rate (model not listed in table 3). In a spatially flat universe, the EoS parameter of the DE for this kernel can be expressed in terms of the interaction ξ parameter and the ratio $r = \rho_c/\rho_d$, namely, $\omega_d = -(1+r)\xi/(3rH)$. As the DE decays into pressureless DM, it gives rise to a negative ω_d and the ratio of the energy densities is a constant, $r_0 = (1-\wp)/\wp$, irrespectively of the value of ξ [271]. When $\xi \propto H$ then $\rho_c, \rho_d \propto a^{-3m}$ with $m = (1+r_0+\omega_d)/(1+r_0)$ and $a \propto t^{2/(3m)}$. Then, the universe will be accelerating if $\omega_d < -(1+r_0)/3$ but if $\xi = 0$, the choice $L = H^{-1}$ does not lead to acceleration.

In conclusion, the interaction will simultaneously solve the coincidence problem and produce a late period of accelerated expansion. Prior to the current epoch the universe had to undergo a period of radiation and matter domination to preserve the standard picture of the formation of cosmic structure. The usual way to introduce these epochs is to assume that the ratio r has not been constant but was (and possibly still is) decreasing. In the present context, a time dependence of r can only be achieved if $\wp$ varies slowly with time, i.e. $0 < \dot\wp/\wp \ll H$. This hypothesis is not only admissible but it is also reasonable since it is natural to expect that the holographic bound only gets fully saturated in the very long run or even asymptotically [304]. There is, however, a different way to recover an early matter dominated epoch. It is straightforward to show that

$$\dot r = 3Hr\left[\omega_d + \frac{1+r}{r}\frac{\xi}{3H}\right]. \tag{42}$$

Then, if $\xi/H \ll 1$ then $|\omega_d| \ll 1$ and the DE itself behaves as pressureless matter, even if $r \simeq$ const.. If we neglect the dynamical effect of curvature, baryons and radiation, from equation (42) and $\rho_d = 3H^2\wp/(8\pi G)$ we obtain $\wp(t) = 1/(1+r(t))$. At late times, $r \to r_0$ and $\wp \to \wp_0$. In this scenario w_d would depend on the fractional change of $\wp$ according to

$$\omega_d = -\left(1+\frac{1}{r}\right)\left[\frac{\xi}{3H} + \frac{\dot\wp}{3H\wp}\right]. \tag{43}$$

Holographic DE must satisfy the dominant energy condition and it is not compatible with a phantom EoS [39] and this additional restriction $\omega_d \geqslant -1$ sets further constraints on ξ and $\wp$ that need to be fulfilled when confronting the model with observations [127, 380, 413]. The model is a simple and elegant option to account for the present era of cosmic accelerated expansion within the framework of standard gravity. Finally, its validity will be decided observationally.

2.6.2. Transition to a new decelerated era? It has been speculated that the present phase of accelerated expansion is just transitory and the universe will eventually revert to a fresh decelerated era. This can be achieved by taking as DE a scalar field whose energy density obeys a suitable ansatz. The EoS parameter ω_d would evolve from values above but close to -1 to much less negative values; the deceleration parameter increases to positive values [89] and the troublesome event horizon that afflicts superstring theories disappears. Interacting holographic models that provide a transition from the deceleration to the acceleration can be shown to be compatible with such a transition, reverting to a decelerating phase. Inspection of equation (43) reveals that $w_d \leqslant -1/3$ when either any of the two terms in the square parenthesis (or both) reach sufficiently small values or the first term is nearly constant and the second becomes enough negative. These possibilities are a bit contrived, especially the second one since -contrary to intuition- the saturation parameter would be decreasing instead of increasing. This counterintuitive behavior is the result of requiring that a decelerated phase follows the period of accelerated expansion for the sole purpose of eliminating the event horizon. But even if data does not suggest existence of a future period of decelerated expansion, we cannot dismiss this possibility offhand. In any case, it should be noted that holographic dark energy proposals that identify the infrared cutoff L with the event horizon radius are unable to produce such transition.

2.7. On the direction of the interaction

An important open question in interacting DM/DE models is in which direction is transferred the energy; does DE decays into DM ($\xi > 0$) or is the other way around ($\xi < 0$)? Although this question will be eventually settled observationally, at present we can explore different options based on physical principles.

Thermodynamic considerations suggest that DE must decay into DM. If the interaction is consistent with the principles of thermodynamics, their temperatures will evolve according to

$\dot{T}/T = -3H(\partial p/\partial\rho)_n$, where n is the the number density of particles. Then, the temperature of the DM and the DE fluids will evolve differently due to the different time evolution of their energy densities. When a system is perturbed out of thermodynamic equilibrium it will react to restore it or it will evolve to achieve a new equilibrium [310]. Then, if both DM and DE are amenable to a phenomenological thermo-fluid description and follow the Le Châtelier–Braun principle, the transfer of energy-momentum from DE to DM will increase their temperature difference more slowly than if there were no interaction ($Q = 0$) or if it is transferred in the opposite direction, the temperature difference will increase faster [270]. Thus, both components, DM and DE, will stay closer to thermal equilibrium if energy transfers from DE to DM than otherwise.

Even if the DE field is non-thermal, i.e. it corresponds to a scalar field in a pure quantum state, a transfer of energy from DM to DE involves an uncompensated decrease of entropy. By contrast, a transfer in the opposite direction creates entropy by producing DM particles. The former process violates the second law of thermodynamics while the latter does not. This is also true if the DM particles are fermions and the DE is described as a scalar field. Due to the conservation of quantum numbers, DM decaying into DE would violate the second law while the inverse process would not. This latter process is similar to the production of particles in warm inflation [59] and the production of particles by the gravitational field acting on the quantum vacuum [268]. In section 7, we will discuss which is the direction of the energy flow that is favored by the observations. We will show that the data marginally favors a flow consistent with the second law of thermodynamics and is such that alleviates the coincidence problem.

2.8. The connection between modified gravity and interacting DM/DE

A DM/DE interaction is closely related to modified theories of gravity. One example is $f(R)$ gravity. In this theory matter is minimally coupled to gravity in the Jordan frame, while after carrying out a conformal transformation to the Einstein frame, the non-relativistic matter is universally coupled to a scalar field that can play the role of DE [119]. Interestingly, it was found that a general $f(R)$ gravity in the Jordan frame can be systematically and self-consistently constructed through conformal transformation in terms of the mass dilation rate function in the Einstein frame [170]. The mass dilation rate function marks the coupling strength between DE and DM (see detailed discussions in [170]). The new $f(R)$ model constructed in this way can generate a reasonable cosmic expansion. For this $f(R)$ cosmology, the requirement to avoid the instability in high curvature regime and to be consistent with CMB observations is exactly equivalent to the requirement of an energy flow from DE to DM in the interaction model to ensure the alleviation of the coincidence problem in the Einstein frame [119, 170]. This result shows the conformal equivalence between the $f(R)$ gravity in the Jordan frame and the interacting DM/DE model in the Einstein frame. Furthermore, this equivalence is also present at the linear perturbation level [171]. The $f(R)$ model constructed from the mass dilation rate can give rise to a matter dominated period and an effective DE equation of state in consistent with the cosmological observations [171, 172]. The equivalence of the Einstein and Jordan frames has also been discussed in [300]. In [95] it was argued that there exists a correspondence between the variables in the Jordan frame and those in the Einstein frame in scalar-tensor gravity and that the cosmological observables/relations (redshift, luminosity distance, temperature anisotropies) are frame-independent. Other discussions on the connection between modified gravity and interacting DM/DE can also be found, for example, in [207].

In addition to a conformal transformation, one can consider whether there are more general transformations with similar properties. These new transformations could provide more general couplings between matter and gravity through a scalar field. The question was first studied in [53] where a new class of transformations, called disformal transformations, were proposed. The idea behind such transformations is that matter is coupled to a metric which is not just a rescaling of the gravitational metric but it is stretched in a particular direction, given by the gradient of a scalar field. Disformal transformations can be motivated from brane world models and from massive gravity theories [74, 419]. Interactions between DM and DE allowing disformal couplings have also been studied in the background evolution, anisotropies in the cosmic microwave background and LSS [77, 211]. Recently the idea of the disformal transformation has also been extended to study more general theories of gravity such as the Horndeski theory [118, 204]. Similarly to the conformal transformation, in the disformal transformation, physics must be invariant and such cosmological disformal invariance exists [123]. All these results could provide further insight on how Cosmology can test gravity at the largest scales and provide evidence of generalized theories of gravity.

3. Background dynamics

In this section we will consider the evolution of a flat universe in DM/DE interacting models. The evolution of the main cosmological parameters will differ from that of the concordance model and their comparison with observations could, in principle, prove the existence of DM/DE interactions. To illustrate the background evolution we will choose a particle field description of the dark sectors. For the phenomenological fluid model, the discussions are more simplified and the readers can refer to [98, 133, 134, 414].

3.1. Attractor solutions of Friedmann models

The action describing the dynamics of a fermion DM field Υ coupled to a scalar DE field φ evolving within an expanding universe is

$$S = \int \mathrm{d}^4x\sqrt{-g}\Big(-\frac{R}{4} + \frac{1}{2}\partial_\mu\varphi\partial^\mu\varphi - V(\varphi) + \frac{\mathrm{i}}{2}\left[\bar{\Upsilon}\gamma^\mu\nabla_\mu\Upsilon - \bar{\Upsilon}\overleftarrow{\nabla}_\mu\gamma^\mu\Upsilon\right] - F(\varphi)\bar{\Upsilon}\Upsilon\Big). \quad (44)$$

The metric is the Friedmann–Robertson–Walker metric given by equation (1) with $K = 0$, R is the Ricci scalar, $V(\varphi)$ is the scalar field potential and $F(\varphi)$ is the interaction term. The Lagrangian is slightly more general than equation (25) since $F(\varphi)$ is an arbitrary function to be specified. From the action of equation (44) we can derive the equations that describe the background evolution of the universe

$$\ddot{\varphi} + 3H\dot{\varphi} + V' = -F'\bar{\Upsilon}\Upsilon, \tag{45}$$

$$H^2 = \frac{1}{3M_p^2}\left\{\frac{\dot{\varphi}^2}{2} + V(\varphi) + F(\varphi)\bar{\Upsilon}\Upsilon\right\}, \tag{46}$$

$$\dot{H} = -\frac{1}{2M_p^2}\{\dot{\varphi}^2 + F(\varphi)\bar{\Upsilon}\Upsilon\}, \tag{47}$$

where $M_p^2 = 1/8\pi G$ is the reduced Planck mass. Primes represent derivatives with respect to the scalar field φ. The fermion equation of motion can be exactly solved to describe the DM sector in terms of the scale factor as given by equation (35).

To construct analytic solutions we define W such that $H(t) = W(\varphi(t))$. This definition restricts the search of solutions to smooth and monotonic functions $\varphi(t)$ that are invertible; it does not solve the general case. Then, $\dot{H} = W_\varphi\dot{\varphi}$, where $W_\varphi \equiv \partial W/\partial\varphi$ and equation (47) can be rewritten as

$$-W_\varphi\ \dot{\varphi}\ 2M_p^2 = \dot{\varphi}^2 + F(\varphi)\frac{\bar{\Upsilon}_0\Upsilon_0}{a^3}. \tag{48}$$

Further, we choose $a(t)^{-3} = \sigma\ \dot{\varphi}^n\ J(\varphi)$, where σ is a real constant, n an integer and $J(\varphi)$ an arbitrary function of the scalar field. This expression is general enough to allow us to obtain a large class of exact solutions with interacting DM/DE; by choosing conveniently n and $J(\varphi)$ we can reduce the order of the equations of motion. Introducing this notation in equation (48) we obtain

$$\dot{\varphi}^{n-1} + \frac{[\dot{\varphi} + 2M_p^2 W_\varphi]}{F(\varphi)\bar{\Upsilon}_0\Upsilon_0\sigma\ J(\varphi)} = 0, \tag{49}$$

which can be solved as an algebraic equation for $\dot{\varphi}$ for each value of n. Let us consider two examples:

3.1.1. Example I. If we take $F(\varphi) = M - \beta\varphi$ and choose the de-Sitter solution ($\dot{a}/a = \text{const.} = H_0$) then equation (35) allows us to write equation (45) as

$$\ddot{\varphi} + 3H_0\dot{\varphi} + V' = \frac{\beta\bar{\Upsilon}_0\Upsilon_0}{a^3}. \tag{50}$$

that has the following solution

$$\varphi(t) = K_1 + K_2 e^{-3H_0 t} + K_3 e^{-\frac{3}{2}H_0 t}, \tag{51}$$

where K_1, K_2 and K_3 are constants.

For a power-law scale factor $a = K\,t^p$, with K and p positive constants, we have for $\varphi(t)$

$$\varphi(t) = Y_1 + Y_2\left[\frac{(\ln t)^2}{2} + Y_3 \ln t\right], \tag{52}$$

where Y_1, Y_2 and Y_3 are constants. This solution is clearly non-invertible and, therefore, outside the subset of solutions we are considering. Several other solutions have been obtained, though most of them turn out to be unphysical [269].

3.1.2. Example II. If we choose $n = 3$, $\sigma = 1$, $W(\varphi) = \mu^4/(\varphi M_P^2)$ and $J(\varphi) = -\varphi^2/(4\bar{\Upsilon}_0\Upsilon_0\mu^4 F(\varphi))$, where μ is a parameter with dimensions of mass, then

$$F(\varphi) = -C_1\frac{e^{(3\varphi^2/8M_p^2)}}{\varphi^4}, \quad V_3(\varphi) = \frac{3\mu^8}{4M_p^2\varphi^2}, \tag{53}$$

$$\varphi(t) = (6\mu^4 t)^{1/3}, \quad a(t) = \left(\frac{\bar{\Upsilon}_0\Upsilon_0 C_1}{2\mu^8}\right)^{1/3} e^{(6\mu^4 t)^{2/3}/8M_p^2}. \tag{54}$$

This solution corresponds to a massless fermionic DM interacting with DE. The interaction kernel $F(\varphi)$ is the product of an exponential and an inverse power-law; the coefficient C_1 measures the strength of the coupling. Notice that if $t > (2\sqrt{2}M_p^3/6\mu^4)$ the expansion is accelerated.

In this model, equations (45)–(47) can be solved analytically. The energy density, pressure and EoS parameter for DE are given by [269]

$$\rho_d(a) = \frac{\mu^8}{(32M_p^4)}\frac{1}{\ln^2(\gamma a)}(1 + 3\ln(\gamma a)), \tag{55}$$

$$p_d(a) = \frac{\mu^8}{(32M_p^4)}\frac{1}{(\ln(\gamma a))^2}(1 - 3\ln(\gamma a)), \tag{56}$$

$$w_d(a) = \frac{1 - 3\ln(\gamma a)}{1 + 3\ln(\gamma a)}, \tag{57}$$

where $\gamma = (2\mu^8/C_1\bar{\Upsilon}_0\Upsilon_0)^{1/3}$. For illustration, in figure 4 we plot the solution of equations (53)–(57) describing the evolution of the universe in the limit that baryons and radiation are not dynamically important. In the left panel we represent the fractional energy densities and in the right panel the deceleration and the EoS parameters. We also plotted the interaction term and the DM density and equation of state, respectively. Notice that DM and DE densities have similar amplitude today, at $a = 1$ when the deceleration parameter changes sign. This solution presents a transition from a decelerated to an accelerated expansion in agreement with observations.

The measured values of DM and DE energy densities from table 2 indicate that $P \sim O(10^{-7})$ and $\gamma \approx 2.06$. This gives the coupling constant $|C_1| \sim 10^{-17}$, i.e. the interaction is very weak [269].

This example shows that even with very simplifying assumptions, exact solutions can be found that display cosmologically viable DM and DE evolutions. The only requirement is that the coupling constant must be very small, an indication that, observationally, the model does not differ significantly from the concordance model while it retains all the conceptual advantages of a field description. Other studies on the dynamics of coupled quintessence can be found in [219, 342].

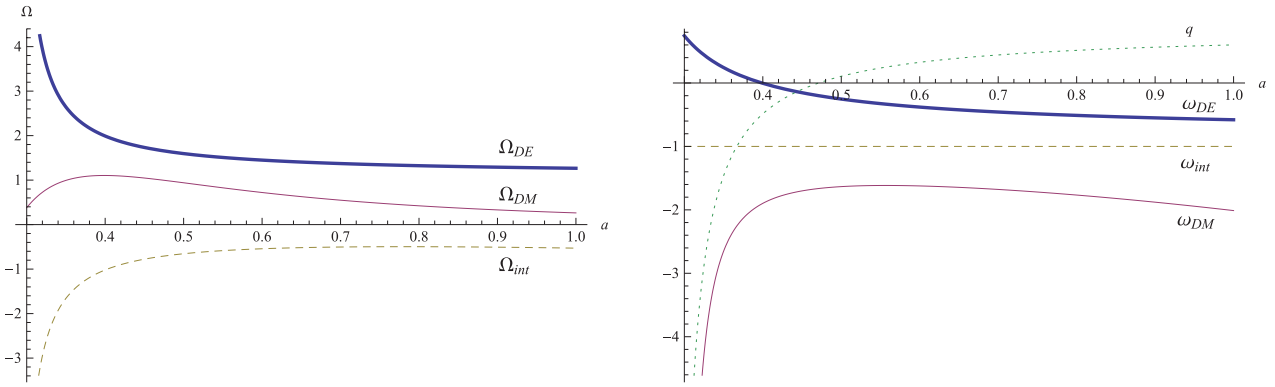

Figure 4. Density parameter Ω (left panel) and equation of state parameter ω and deceleration parameter (right panel) for the model given by equations (53)–(57). The interaction term has been explicitly separated.

3.2. Challenges for scaling cosmologies

The purpose of the interacting models is to generate cosmological solutions where the radiation epoch is followed by a period of matter domination and a subsequent accelerated expansion, as in the concordance model. To solve or alleviate the coincidence problem, an almost constant DM to DE ratio is also required. For the idea to be of interest, the final accelerating phase must be an attractor otherwise we would have a new coincidence problem. Such a sequence of cosmological eras: radiation, matter and DE dominated periods, poses a fundamental restriction to viable models. The canonical scalar-tensor model with an exponential scalar potential is ruled out since it does not lead to a matter dominated period [16] but even more general *k*-essence models have difficulties to generate viable cosmologies. As described in section 2.5, in these models, the Lagrangian density is $\mathcal{L} = p(X, \varphi)$, with $X = -\frac{1}{2}g^{\mu\nu}\partial_\mu\varphi\partial_\nu\varphi$. To obtain scaling solutions, it is necessary that $p(X, \varphi) = Xf(Y)$ where $Y = Xe^{\lambda\varphi}$ and $f(Y)$ is a generic function [298, 367].

For the above Lagrangian the equations of motion are

$$H^2 = \frac{8\pi G}{3}\left[X(f + 2f_1) + \rho_c + \rho_r\right], \tag{58}$$

$$\dot{H} = -4\pi G\left[2X(f + f_1) + \rho_c + \frac{4}{3}\rho_r\right], \tag{59}$$

$$\ddot{\varphi} = -3AH(f + f_1)\dot{\varphi} - \lambda X(1 - A(f + 2f_1)) - AQ\rho_c, \tag{60}$$

where $A = (f + 5f_1 + 2f_2)^{-1}$, $f_n = Y^n\frac{\partial^n f}{\partial Y^n}$ and Q is the interaction kernel given by

$$Q = -\frac{1}{\rho_c\sqrt{-g}}\frac{\partial\mathcal{L}_m}{\partial\varphi}, \tag{61}$$

where g is the determinant of the metric $g_{\mu\nu}$. The equations above can be simplified by introducing the dimensionless variables

$$x = \frac{\sqrt{4\pi G}\,\dot{\varphi}}{3H}, \quad y = \frac{\sqrt{8\pi G}\,e^{-\lambda\varphi/2}}{3H}, \quad z = \frac{\sqrt{8\pi G\rho_r}}{3H}, \tag{62}$$

$$\Omega_c = \frac{8\pi G\rho_c}{9H^2} = 1 - \Omega_\varphi - z^2, \quad \Omega_\varphi = x^2(f + 2f_1). \tag{63}$$

The corresponding equations have been analyzed in [25] where it was shown that a large class of coupled scalar field Lagrangins with scaling solutions do not give rise to a sufficiently long matter-dominated epoch before the onset of acceleration as to give rise to galaxies and LSS. As a result, DM/DE interacting models based on a scalar field description are strongly constrained at the background level. This reflects our lack of a solid physical foundation of the nature of DE. Particular examples of scalar field models that are not limited by the background evolution exist and are discussed in section 7, but are not generic. Therefore, in the next section we will particularize the study of perturbation theory to the phenomenological fluid models.

4. Perturbation theory

Models with non-minimally coupled DM and DE can successfully describe the accelerated expansion of the universe. Currently DE and DM have only been detected via their gravitational effects and any change in the DE density is conventionally attributed to its equation of state ω_d. This leads to an inevitable degeneracy between the signature of the interaction within the dark sector and other cosmological parameters. Since the coupling modifies the evolution of matter and radiation perturbations and the clustering properties of galaxies, to gain further insight we need to examine the evolution of density perturbations and test model predictions using the most recent data on CMB temperature anisotropies and large scale structure. Our purpose is to identify the unique signature of the interaction on the evolution of density perturbations in the linear and non-linear phases.

In this section we discuss linear perturbation theory. We present a systematic review on the first order perturbation equations, discuss the stability of their solutions and examine the signature of the interaction in the CMB temperature anisotropies. Finally, we study the growth of the matter density perturbations. Details can be found in [165, 167–169, 400]. Alternative formulations are described in [17, 37, 51, 52, 81, 100, 109, 144, 188, 209, 215, 217, 239, 241, 262, 284, 331, 368, 369, 374].

4.1. First order perturbation equations

The space-time element of equation (2) perturbed at first order reads

$$\begin{aligned} ds^2 = a^2(\tau)[&-(1+2\psi)d\tau^2 + 2\partial_i B d\tau dx^i \\ &+ (1+2\phi)\delta_{ij}dx^i dx^j + D_{ij}E dx^i dx^j], \end{aligned} \tag{64}$$

where τ is the conformal time defined by $d\tau = dt/a$, ψ, B, ϕ, E represent the scalar metric perturbations, a is the cosmic scale factor and $D_{ij} = (\partial_i\partial_j - \frac{1}{3}\delta_{ij}\nabla^2)$.

4.1.1. Energy-momentum balance. We work with the energy-momentum tensor $T^{\mu\nu} = \rho u^\mu u^\nu + p(g^{\mu\nu} + u^\mu u^\nu)$, for a two-component system consisting of DE and DM. The covariant energy-momentum transfer between DE and DM is given by $\nabla_\mu T_{(\lambda)}{}^{\mu\nu} = Q_{(\lambda)}{}^\nu$ where $Q_{(\lambda)}{}^\nu$ is a four vector governing the energy-momentum transfer between the different components [205]. The subindex λ refers to DM and DE respectively. For the whole system, DM plus DE, the energy and momentum are conserved, and the transfer vector satisfies $\sum_\lambda Q_{(\lambda)}{}^\nu = 0$.

The perturbed energy-momentum tensor reads,

$$\begin{aligned} \delta\nabla_\mu T^{\mu 0}_{(\lambda)} &= \frac{1}{a^2}\{-2[\rho'_\lambda + 3\mathcal{H}(p_\lambda+\rho_\lambda)]\psi + \delta\rho'_\lambda + (p_\lambda+\rho_\lambda)\theta_\lambda \\ &\quad + 3\mathcal{H}(\delta p_\lambda + \delta\rho_\lambda) + 3(p_\lambda+\rho_\lambda)\phi'\} = \delta Q^0_\lambda, \\ \partial_i\delta\nabla_\mu T^{\mu i}_{(\lambda)} &= \frac{1}{a^2}\{[p'_\lambda + \mathcal{H}(p_\lambda+\rho_\lambda)]\nabla^2 B + [(p'_\lambda+\rho'_\lambda) + 4\mathcal{H}(p_\lambda+\rho_\lambda)]\theta_\lambda \\ &\quad + (p_\lambda+\rho_\lambda)\nabla^2 B' + \nabla^2\delta p_\lambda + (p_\lambda+\rho_\lambda)\theta'_\lambda + (p_\lambda+\rho_\lambda)\nabla^2\psi\} \\ &= \partial_i\delta Q^i_{(\lambda)}, \end{aligned} \tag{65}$$

where $\theta = \nabla v$, v is the potential of the three velocity and primes denote derivatives with respect to the conformal time τ. At first order, the perturbed Einstein equations are

$$\begin{aligned} -4\pi G a^2\delta\rho &= \nabla^2\phi + 3\mathcal{H}(\mathcal{H}\psi - \phi') + \mathcal{H}\nabla^2 B - \frac{1}{6}[\nabla^2]^2 E, \\ -4\pi G a^2(\rho+p)\theta &= \mathcal{H}\nabla^2\psi - \nabla^2\phi' + 2\mathcal{H}^2\nabla^2 B - \frac{a''}{a}\nabla^2 B + \frac{1}{6}[\nabla^2]^2 E', \\ 8\pi G a^2\Pi^i_j &= -\partial^i\partial_j\psi - \partial^i\partial_j\phi + \frac{1}{2}\partial^i\partial_j E'' + \mathcal{H}\partial^i\partial_j E' \\ &\quad + \frac{1}{6}\partial^i\partial_j\nabla^2 E - 2\mathcal{H}\partial^i\partial_j B - \partial^i\partial_j B;, \end{aligned} \tag{66}$$

where $\delta\rho = \sum_\lambda \delta\rho_\lambda$ and $(p+\rho)\theta = \sum_\lambda (p_\lambda+\rho_\lambda)\theta_\lambda$ is the total energy density perturbation.

4.1.2. The general perturbation equations. Considering an infinitesimal transformation of the coordinates [205]

$$\tilde{x}^\mu = x^\mu + \delta x^\mu, \quad \delta x^0 = \xi^0(x^\mu), \quad \delta x^i = \partial^i\beta(x^\mu) + v^i_*(x^\mu) \tag{67}$$

where $\partial_i v^i_* = 0$. The perturbed quantities behave as

$$\begin{aligned} \tilde{\psi} &= \psi - \xi^{0\prime} - \frac{a'}{a}\xi^0, & \tilde{B} &= B + \xi^0 - \beta', \\ \tilde{\phi} &= \phi - \frac{1}{3}\nabla^2\beta - \frac{a'}{a}\xi^0, & \tilde{E} &= E - 2\beta \\ \tilde{v} &= v + \beta', & \tilde{\theta} &= \theta + \nabla^2\beta'. \end{aligned} \tag{68}$$

Inserting equation (68) in equation (65), we obtain

$$\delta\tilde{Q}^0 = \delta Q^0 - Q^{0\prime}\xi^0 + Q^0\xi^{0\prime}, \quad \delta\tilde{Q}_p = \delta Q_p + Q^0\beta', \tag{69}$$

where δQ_p denotes the potential of three vector δQ^i and verifies

$$\delta Q^i = \partial^i\delta Q_p + \delta Q^i_*, \tag{70}$$

with $\partial_i\delta Q^i_* = 0$. This is consistent with the results obtained using Lie derivatives,

$$\mathcal{L}_{\delta x}Q^\nu = \delta x^\sigma Q^\nu_{,\sigma} - Q^\sigma\delta x^\nu_{,\sigma}, \quad \delta\tilde{Q}^\nu = \delta Q^\nu - \mathcal{L}_{\delta x}Q^\nu, \tag{71}$$

which shows that Q^ν is covariant.

We expand metric perturbations in Fourier space by using scalar harmonics,

$$\begin{aligned} \tilde{\psi}Y^{(s)} &= (\psi - \xi^{0\prime} - \frac{a'}{a}\xi^0)Y^{(s)}, & \tilde{B}Y^{(s)}_i &= (B - k\xi^0 - \beta')Y^{(s)}_i, \\ \tilde{\phi}Y^{(s)} &= (\phi - \frac{1}{3}k\beta - \frac{a'}{a}\xi^0)Y^{(s)}, & \tilde{E}Y^{(s)}_{ij} &= (E + 2k\beta)Y^{(s)}_{ij}, \\ \tilde{\theta}Y^{(s)} &= (\theta + k\beta')Y^{(s)}, \end{aligned} \tag{72}$$

and the perturbed conservation equations of equation (65) read

$$\begin{aligned} &\delta'_\lambda + 3\mathcal{H}(\frac{\delta p_\lambda}{\delta\rho_\lambda} - \omega_\lambda)\delta_\lambda = -(1+\omega_\lambda)kv_\lambda - 3(1+\omega_\lambda)\phi' \\ &\quad + (2\psi - \delta_\lambda)\frac{a^2Q^0_\lambda}{\rho_\lambda} + \frac{a^2\delta Q^0_\lambda}{\rho_\lambda}, \\ &(v_\lambda + B)' + \mathcal{H}(1-3\omega_\lambda)(v_\lambda + B) = \frac{k}{1+\omega_\lambda}\frac{\delta p_\lambda}{\delta\rho_\lambda}\delta_\lambda - \frac{\omega'_\lambda}{1+\omega_\lambda}(v_\lambda + B) \\ &\quad + k\psi - \frac{a^2Q^0_\lambda}{\rho_\lambda}v_\lambda - \frac{\omega_\lambda a^2Q^0_\lambda}{(1+\omega_\lambda)\rho_\lambda}B + \frac{a^2\delta Q_{p\lambda}}{(1+\omega_\lambda)\rho_\lambda}. \end{aligned} \tag{73}$$

Introducing the gauge invariant quantities [205]

$$\begin{aligned} &\Psi = \psi - \frac{1}{k}\mathcal{H}\left(B + \frac{E'}{2k}\right) - \frac{1}{k}\left(B' + \frac{E''}{2k}\right), \quad \Phi = \phi + \frac{1}{6}E - \frac{1}{k}\mathcal{H}\left(B + \frac{E'}{2k}\right), \\ &\delta Q^{0I}_\lambda = \delta Q^0_\lambda - \frac{Q^{0\prime}_\lambda}{\mathcal{H}}\left(\phi + \frac{E}{6}\right) + Q^0_\lambda\left[\frac{1}{\mathcal{H}}\left(\phi + \frac{E}{6}\right)\right]', \quad V_\lambda = v_\lambda - \frac{E'}{2k}, \\ &\delta Q^I_{p\lambda} = \delta Q_{p\lambda} - Q^0_\lambda\frac{E'}{2k}, \qquad D_\lambda = \delta_\lambda - \frac{\rho'_\lambda}{\rho_\lambda\mathcal{H}}\left(\phi + \frac{E}{6}\right), \end{aligned} \tag{74}$$

we obtain the gauge invariant linear perturbation equations for the dark sector. D_λ is the gauge invariant density perturbation of DM or DE, and V_λ is the gauge invariant velocity perturbation for DM and DE respectively. For the DM they are

$$\begin{aligned} &D'_c + \left\{\left(\frac{a^2Q^0_c}{\rho_c\mathcal{H}}\right)' + \frac{\rho'_c}{\rho_c\mathcal{H}}\frac{a^2Q^0_c}{\rho_c}\right\}\Phi + \frac{a^2Q^0_c}{\rho_c}D_c + \frac{a^2Q^0_c}{\rho_c\mathcal{H}}\Phi' \\ &\quad = -kV_c + 2\Psi\frac{a^2Q^0_c}{\rho_c} + \frac{a^2\delta Q^{0I}_c}{\rho_c} + \frac{a^2Q^{0\prime}_c}{\rho_c\mathcal{H}}\Phi - \frac{a^2Q^0_c}{\rho_c}\left(\frac{\Phi}{\mathcal{H}}\right)', \\ &V'_c + \mathcal{H}V_c = k\Psi - \frac{a^2Q^0_c}{\rho_c}V_c + \frac{a^2\delta Q^I_{pc}}{\rho_c}, \end{aligned} \tag{75}$$

while for the DE we have

$$D_d' + \left\{\left(\frac{a^2Q_d^0}{\rho_d\mathcal{H}}\right)' - 3\omega_d' + 3(C_e^2-\omega_d)\frac{\rho_d'}{\rho_d} + \frac{\rho_d'}{\rho_d\mathcal{H}}\frac{a^2Q_d^0}{\rho_d}\right\}\Phi + \left\{3\mathcal{H}(C_e^2-\omega_d) + \frac{a^2Q_d^0}{\rho_d}\right\}D_d + \frac{a^2Q_d^0}{\rho_d\mathcal{H}}\Phi'$$
$$= -(1+\omega_d)kV_d + 3\mathcal{H}(C_e^2-C_a^2)\frac{\rho_d'}{\rho_d}\frac{V_d}{k} + 2\Psi\frac{a^2Q_d^0}{\rho_d} + \frac{a^2\delta Q_d^{0I}}{\rho_d} + \frac{a^2Q_d^{0'}}{\rho_d\mathcal{H}}\Phi - \frac{a^2Q_d^0}{\rho_d}\left(\frac{\Phi}{\mathcal{H}}\right)',$$
$$V_d' + \mathcal{H}(1-3\omega_d)V_d = \frac{kC_e^2}{1+\omega_d}D_d + \frac{kC_e^2}{1+\omega_d}\frac{\rho_d'}{\rho_d\mathcal{H}}\Phi - \frac{a^2Q_d^0}{\rho_d}V_d - (C_e^2-C_a^2)\frac{V_d}{1+\omega_d}\frac{\rho_d'}{\rho_d} - \frac{\omega_d'}{1+\omega_d}V_d + k\Psi + \frac{a^2\delta Q_{pd}^I}{(1+\omega_d)\rho_d}, \quad (76)$$

in these expressions we have introduced

$$\frac{\delta p_d}{\rho_d} = C_e^2\delta_d - (C_e^2-C_a^2)\frac{\rho_d'}{\rho_d}\frac{v_d+B}{k} \quad (77)$$

with C_e^2 is the effective sound speed of DE at the rest frame and C_a^2 is the adiabatic sound speed [370].

To alleviate the singular behavior caused by ω_d crossing -1, we substitute V_λ into U_λ in the above equations where

$$U_\lambda = (1+\omega_d)V_\lambda. \quad (78)$$

Thus we can rewrite equations (75) and (76) as

$$D_c' + \left\{\left(\frac{a^2Q_c^0}{\rho_c\mathcal{H}}\right)' + \frac{\rho_c'}{\rho_c\mathcal{H}}\frac{a^2Q_c^0}{\rho_c}\right\}\Phi + \frac{a^2Q_c^0}{\rho_c}D_c + \frac{a^2Q_c^0}{\rho_c\mathcal{H}}\Phi'$$
$$= -kU_c + 2\Psi\frac{a^2Q_c^0}{\rho_c} + \frac{a^2\delta Q_c^{0I}}{\rho_c} + \frac{a^2Q_c^{0'}}{\rho_c\mathcal{H}}\Phi - \frac{a^2Q_c^0}{\rho_c}\left(\frac{\Phi}{\mathcal{H}}\right)',$$
$$U_c' + \mathcal{H}U_c = k\Psi - \frac{a^2Q_c^0}{\rho_c}U_c + \frac{a^2\delta Q_{pc}^I}{\rho_c}, \quad (79)$$

$$D_d' + \left\{\left(\frac{a^2Q_d^0}{\rho_d\mathcal{H}}\right)' - 3\omega_d' + 3(C_e^2-\omega_d)\frac{\rho_d'}{\rho_d} + \frac{\rho_d'}{\rho_d\mathcal{H}}\frac{a^2Q_d^0}{\rho_d}\right\}\Phi$$
$$+\left\{3\mathcal{H}(C_e^2-\omega_d) + \frac{a^2Q_d^0}{\rho_d}\right\}D_d + \frac{a^2Q_d^0}{\rho_d\mathcal{H}}\Phi' = 3\mathcal{H}(C_e^2-C_a^2)\frac{\rho_d'}{\rho_d}\frac{U_d}{(1+\omega_d)k}$$
$$-kU_d + 2\Psi\frac{a^2Q_d^0}{\rho_d} + \frac{a^2\delta Q_d^{0I}}{\rho_d} + \frac{a^2Q_d^{0'}}{\rho_d\mathcal{H}}\Phi - \frac{a^2Q_d^0}{\rho_d}\left(\frac{\Phi}{\mathcal{H}}\right)', \quad (80)$$

$$U_d' + \mathcal{H}(1-3\omega_d)U_d = kC_e^2D_d + kC_e^2\frac{\rho_d'}{\rho_d\mathcal{H}}\Phi - (C_e^2-C_a^2)\frac{U_d}{1+\omega_d}\frac{\rho_d'}{\rho_d}$$
$$+(1+\omega_d)k\Psi - \frac{a^2Q_d^0}{\rho_d}U_d + \frac{a^2\delta Q_{pd}^I}{\rho_d}. \quad (81)$$

The quantity Φ is given by

$$\Phi = \frac{4\pi Ga^2\sum\rho_i\{D^i + 3\mathcal{H}U^i/k\}}{k^2 - 4\pi Ga^2\sum\rho_i'/\mathcal{H}}. \quad (82)$$

Equations (79) and (80) are the most generic form of the linear perturbation equations for the DM and the DE, regardless of the specific form of the interaction $Q_{(\lambda)}{}^{\nu}$. The transfer of energy-momentum between DM and DE has to be specified in a covariant form. In the next section we will specify $Q_{(\lambda)}{}^{\nu}$ for each particular coupling.

4.1.3. Covariant couplings. The four vector $Q_{(\lambda)}{}^{\nu}$ can be phenomenologically decomposed into two parts with respect to a given observer η with four velocity $U_{(\eta)}{}^{\mu}$,

$$Q_{(\lambda)}{}^{\mu} = Q_{(\lambda\eta)}U_{(\eta)}{}^{\mu} + F_{(\lambda\eta)}{}^{\mu}, \quad (83)$$

where $Q_{(\lambda\eta)} = -U_{(\eta)_\nu}Q_{(\lambda)}{}^{\nu}$ is the energy transfer rate of the λ component observed by λ' observer; $F_{(\lambda\eta)}{}^{\mu} = h_{(\eta)}{}^{\mu}{}_{\nu}Q_{(\lambda)}{}^{\nu}$ is the corresponding momentum transfer and h_ν^μ is the projection operator. In [169] it has been probed that such a decomposition of $Q_{(\lambda)}{}^{\nu}$ and its perturbed form are covariant. As discussed

in [169], we can specify the coupling vector $Q_{(\lambda)}{}^{\nu}$ in the comoving frame as

$$Q_{(\lambda)}{}^{\nu} = \left[\frac{Q_{(\lambda)}}{a}, 0, 0, 0\right]^{T} \tag{84}$$

where $Q_{(\lambda)}$ is the module of the four vector $Q_{(\lambda)}{}^{\nu}$. The perturbed form $\delta Q^{0}_{(\lambda)}$ can be uniquely determined from the background energy-momentum transfer $Q^{\mu}_{(\lambda)}$. From

$$Q_{(\lambda)}{}^{\mu} Q_{(\lambda)\mu} = g_{00}(Q_{(\lambda)}{}^{0})^{2} = -Q_{(\lambda)}{}^{2}, \tag{85}$$

where $Q_{(\lambda)} = aQ_{(\lambda)}{}^{0}$ is a scalar in the FRW space and the minus sign indicates that $Q_{(\lambda)}{}^{\mu}$ is time-like, we can obtain the form of the perturbed part of the energy-momentum transfer

$$\delta Q^{0}_{(\lambda)} = -\frac{\psi}{a} Q_{(\lambda)} + \frac{1}{a}\delta Q_{(\lambda)}. \tag{86}$$

The coupling vector defined by equation (83) is independent of the choice of observers. Although it is decomposed in two parts that depend on the observer η and its four velocity $U^{\mu}_{(\eta)}$, the decomposition cannot bring substantial physics since equation (83) is an identity. The perturbed forms, including the 0th component and the spatial component are also identities. The 0th component of the perturbed form can be uniquely determined by the background $Q^{\mu}_{(\lambda)}$. The spatial component of the perturbed energy-momentum transfer $\delta Q^{i}_{(\lambda)}$ is independent of the 0th component. It refers to the non-gravitational force and is composed of two parts,

$$\delta Q_{p\lambda} = \delta Q^{I}_{p\lambda}|_{t} + Q^{0}_{(\lambda)} v_{t}, \tag{87}$$

where $\delta Q_{p\lambda}$ is the potential of the perturbed energy-momentum transfer $\delta Q^{i}_{(\lambda)}$, $\delta Q^{I}_{p\lambda}|_{t}$ is the external non-gravitational force density and v_t is the average velocity of the energy transfer, that needs to be specified. In [370], v_t was allowed to follow the peculiar velocity of the DM or the DE respectively. In fact, $v_t = v_c$ or $v_t = v_d$ reproduce the results of [370]. In our analysis we will consider that there are no other interactions than gravity acting on the coupled DM/DE system; only the inertial drag effect due to the stationary energy transfer between DE and DM appears [346]. Thus, we set $v_t = 0$ and $\delta Q^{I}_{p\lambda}|_{t} = 0$, which leads to a vanishing perturbation, $\delta Q^{i} = 0$.

When constructing the four vector defined by equation (84), the module Q_λ can be chosen to be any combination of scalars in the FRW space, such as the energy density $\rho_{(\lambda)} = T_{(\lambda)}{}^{\mu\nu} U_{(\lambda)\mu} U_{(\lambda)}\nu$, expansion $H_{(\lambda)} = \frac{1}{3}\nabla_{\mu} U_{(\lambda)}{}^{\mu}$, or any other scalar function. Considering that Q_λ is independent of the observer so is the energy density as well as its perturbed form, we require H to be a global quantity invariant under change of observers. In a general phenomenological description, we can assume the DM/DE coupling is

$$Q_c = -Q_d = 3H(\xi_1\rho_c + \xi_2\rho_d). \tag{88}$$

The perturbed forms read

$$\delta Q_c = -\delta Q_d = 3H(\xi_1\delta\rho_c + \xi_2\delta\rho_d), \tag{89}$$

$$\delta Q^{0}_{c} = -\delta Q^{0}_{d} = -3H(\xi_1\rho_c + \xi_2\rho_d)\frac{\psi}{a} + 3H(\xi_1\delta\rho_c + \xi_2\delta\rho_d)\frac{1}{a}. \tag{90}$$

The gauge invariant quantities δQ^{0I}_{c} and δQ^{0I}_{d} in equations (79) and (80) are given by [167]

$$\frac{a^2\delta Q^{0I}_{c}}{\rho_c} = -3\mathcal{H}(\xi_1 + \xi_2/r)\Psi + 3\mathcal{H}\{\xi_1 D_c + \xi_2 D_d/r\} + 3\left(\xi_1\frac{\rho_c'}{\rho_c} + \frac{\xi_2}{r}\frac{\rho_d'}{\rho_d}\right)\Phi - \frac{a^2}{\rho_c}\frac{Q_c^{0'}}{\mathcal{H}}\Phi + \frac{a^2 Q^{0}_{c}}{\rho_c}\left[\frac{\Phi}{\mathcal{H}}\right]', \tag{91}$$

$$\frac{a^2\delta Q^{0I}_{d}}{\rho_d} = 3\mathcal{H}(\xi_1 r + \xi_2)\Psi - 3\mathcal{H}\{\xi_1 D_c r + \xi_2 D_d\} - 3\left(\xi_1 r\frac{\rho_c'}{\rho_c} + \frac{\rho_d'}{\rho_d}\xi_2\right)\Phi - \frac{a^2 Q^{0'}_{d}}{\rho_d}\Phi + \frac{a^2 Q^{0}_{d}}{\rho_d}\left[\frac{\Phi}{\mathcal{H}}\right]', \tag{92}$$

where as before $r = \rho_c/\rho_d$ is the DM to DE ratio.

4.1.4. Phenomenological gauge-invariant perturbation equations. Inserting the phenomenological interaction equations (88)–(92) into equations (79) and (80) and neglecting the spatial perturbations $\delta Q^{I}_{p\lambda} = 0$, we obtain the phenomenological general gauge-invariant perturbation equations for DM and DE, respectively,

$$\begin{aligned} D_c' &= -kU_c + 3\mathcal{H}\Psi(\xi_1 + \xi_2/r) - 3(\xi_1 + \xi_2/r)\Phi' \\ &\quad + 3\mathcal{H}\xi_2(D_d - D_c)/r, \\ U_c' &= -\mathcal{H}U_c + k\Psi - 3\mathcal{H}(\xi_1 + \xi_2/r)U_c, \end{aligned} \tag{93}$$

$$\begin{aligned} D_d' &= -3\mathcal{H}(C_e^2 - \omega_d)D_d + \{3\omega_d' - 9\mathcal{H}(\omega_d - C_e^2)(\xi_1 r + \xi_2 + 1 + \omega_d)\}\Phi \\ &\quad -9\mathcal{H}^2(C_e^2 - C_a^2)\frac{U_d}{k} + 3(\xi_1 r + \xi_2)\Phi' - 3\Psi\mathcal{H}(\xi_1 r + \xi_2) \\ &\quad -9\mathcal{H}^2(C_e^2 - C_a^2)(\xi_1 r + \xi_2)\frac{U_d}{(1+\omega_d)k} - kU_d + 3\mathcal{H}\xi_1 r(D_d - D_c), \\ U_d' &= -\mathcal{H}(1 - 3\omega_d)U_d - 3kC_e^2(\xi_1 r + \xi_2 + 1 + \omega_d)\Phi \\ &\quad + 3\mathcal{H}(C_e^2 - C_a^2)(\xi_1 r + \xi_2)\frac{U_d}{(1+\omega_d)} + 3(C_e^2 - C_a^2)\mathcal{H}U_d \\ &\quad + kC_e^2 D_d + (1 + \omega_d)k\Psi + 3\mathcal{H}(\xi_1 r + \xi_2)U_d. \end{aligned} \tag{94}$$

The general gauge invariant formalism fully removes the ambiguity of gauge choice. However, numerical solutions can be obtained after choosing a gauge without loosing generality (see section III of [205] for details). The results will be the same for different gauges if the gauge is fully fixed [169]. Following [165], in our subsequent discussion we will choose the conformal Newtonian gauge with adiabatic initial conditions.

4.2. Stability analysis

Models with a background evolution characterized by adiabatic initial conditions were studied in perturbation theory and found to have unstable growing modes when the interaction couplings were much larger than the gravitational strength [51]. In parallel, [370] the authors have considered models with an interacting

DE component and a constant equation of state; they found that perturbations were unstable for couplings proportional to the DM energy density; these models exhibited extremely rapid growth of DE fluctuations on superhorizon scales in the early universe. While this result would appear to rule out all couplings of the above form and with constant ω_d, the explicit examples in [370] did not include models where the interaction rate was proportional to the density of DE or the DE EoS varied with time that have been shown to have stable solutions [109, 165, 188, 400]. Also, the results of [370] do not rule out models with dynamical DE or DM or models where the coupling depends on elementary fields [111, 248], so the stability of the solutions have to be considered on the remaining cases.

In the above phenomenological gauge-invariant linear perturbation equations, $C_a^2 = \omega_d < 0$. However, it is not clear what expression should we have for C_e^2. In [370] it has been argued in favor of $C_e^2 = 1$. This is correct for scalar fields, but it is not obvious for other cases, especially for a fluid with a constant equation of state. From the stability point of view, the most dangerous possibility is $C_e^2 = 1 \neq C_a^2 = \omega_d < 0$ since the term in equation (94) can lead to a run away solution when the constant DE EoS is $\omega_d \simeq -1$. Hereafter, in equation (94) we will assume $C_e^2 = 1$, $C_a^2 = \omega_d$. Using the gauge-invariant quantity $\zeta = \phi - \mathcal{H}\delta\tau$ and letting $\zeta_c = \zeta_d = \zeta$, we obtain the adiabatic initial condition

$$\frac{D_c}{1 - \xi_1 - \xi_2/r} = \frac{D_d}{1 + \omega_d + \xi_1 r + \xi_2}. \tag{95}$$

The curvature perturbation given in equation (82) can be computed using the CMBFAST code [334]. First, let us consider the interaction proportional to the DM energy density, $\xi_2 = 0$, with an DE EoS verifying $\omega_d \neq -1$. If $\omega_d > -1$ is constant, we observe that $\xi_1 r$ exhibits a scaling behavior, which remains constant both at early and late times. This behavior is not changed when $\xi_2 \neq 0$.

The scaling behavior of $\xi_1 r$ influences the curvature perturbation Φ. When $\omega_d > -1$ and $\xi_1 \neq 0$, Φ blows up, what agrees with the result obtained in [370]. The instability starts at an earlier time when ω_d approaches -1 from above and it happens regardless of the value of ξ_2. Let us now demonstrate that this instability disappears when the constant EoS is $\omega_d < -1$. The study can be made analytic if in equation (94) we neglect all contributions except those terms that give rise to the instability. The approximate equations are

$$\begin{aligned} D_d' &\approx (-1 + \omega_d + \xi_1 r)3\mathcal{H}D_d - 9\mathcal{H}^2(1 - \omega_d)\left(1 + \frac{\xi_1 r + \xi_2}{1 + \omega_d}\right)\frac{U_d}{k}, \\ U_d' &\approx 2\left[1 + \frac{3}{1 + \omega_d}(\xi_1 r + \xi_2)\right]\mathcal{H}U_d + kD_d. \end{aligned} \tag{96}$$

If $\xi_1 \neq 0$ and $\xi_2 = 0$, assuming that $\xi_1 r \approx -\omega_d$, we can simplify the above equations to obtain

$$\begin{aligned} D_d' &\approx -3\mathcal{H}D_d - 9\mathcal{H}^2\frac{1 - \omega_d}{1 + \omega_d}\frac{U_d}{k}, \\ U_d' &\approx 2\frac{1 - 2\omega_d}{1 + \omega_d}\mathcal{H}U_d + kD_d. \end{aligned} \tag{97}$$

A second order differential equation for D_d is

$$D_d'' \approx \left(2\frac{\mathcal{H}'}{\mathcal{H}} - \frac{1 + 7\omega_d}{1 + \omega_d}\mathcal{H}\right)D_d' + 3(\mathcal{H}' - \mathcal{H}^2)D_d. \tag{98}$$

In the radiation dominated period, we have $\mathcal{H} \sim \tau^{-1}, \mathcal{H}' \sim -\tau^{-2}$, $(\mathcal{H}'/\mathcal{H}) \sim -\tau^{-1}$ and equation (98) can be approximated as $D_d'' \approx -3\frac{1 + 3\omega_d}{1 + \omega_d}\frac{D_d'}{\tau} - \frac{6}{\tau^2}D_d$, whose solution is $D_d \approx C_1\tau^{r_1} + C_2\tau^{r_2}$, where $r_1 = -\frac{1 + 4\omega_d - \sqrt{-5 - 4\omega_d + 10\omega_d^2}}{1 + \omega_d}$, $r_2 = -\frac{1 + 4\omega_d + \sqrt{-5 - 4\omega_d + 10\omega_d^2}}{1 + \omega_d}$. It is easy to check that when $\omega_d < -1$, both r_1 and r_2 are negative; this results in the decay of the perturbation of D_d. The solution is stable, regardless of the value of ξ_1.

To conclude, we have demonstrated that when the DE EoS is constant, $\omega_d > -1$ and the coupling is proportional to ρ_c ($\xi_1 \neq 0$) the curvature perturbation diverges; however, the divergence does not exist when $\omega_d < -1$. When the interaction is proportional to ρ_d ($\xi_2 \neq 0$), the solutions of the perturbation equations are stable in both cases, $\omega_d > -1$ and $\omega_d < -1$. Those terms in equation (96) that give rise to the unstable growth discussed above now reduce to

$$\begin{aligned} D_d' &\approx (-1 + \omega_d)3\mathcal{H}D_d - 9\mathcal{H}^2(1 - \omega_d)\left(1 + \frac{\xi_2}{1 + \omega_d}\right)\frac{U_d}{k}, \\ U_d' &\approx 2\left(1 + \frac{3\xi_2}{1 + \omega_d}\right)\mathcal{H}U_d + kD_d. \end{aligned} \tag{99}$$

We can rewrite the second order differential equation for D_d in the form

$$\begin{aligned} D_d'' = &\left[\left(-1 + 3\omega_d + \frac{6\xi_2}{1 + \omega_d}\right)\mathcal{H} + 2\frac{\mathcal{H}'}{\mathcal{H}}\right]D_d' \\ &+ 3(1 - \omega_d)\left[\mathcal{H}' + \mathcal{H}^2\left(-1 + \frac{3\xi_2}{1 + \omega_d}\right)\right]D_d, \end{aligned} \tag{100}$$

which, in the radiation dominated era, reduces to

$$\begin{aligned} D_d'' = &\left(-3 + 3\omega_d + \frac{6\xi_2}{1 + \omega_d}\right)\frac{D_d'}{\tau} \\ &+ 3(1 - \omega_d)\left(-2 + \frac{3\xi_2}{1 + \omega_d}\right)\frac{D_d}{\tau^2}. \end{aligned} \tag{101}$$

Introducing the auxiliary quantities $\Gamma = 3\omega_d^2 + \omega_d + 6\xi_2 - 2$ and $\Delta = 9\omega_d^4 + 30\omega_d^3 + 13\omega_d^2 + (-28 + 12\xi_2)\omega_d + 36\xi_2^2 + 12\xi_2 - 20$ [165], when $\Delta > 0$ we find

$$D_d \sim C_1\tau^{r_1} + C_2\tau^{r_2}, \tag{102}$$

$$r_1 = \frac{1}{2}\frac{\Gamma}{1 + \omega_d} + \frac{1}{2}\frac{\sqrt{\Delta}}{1 + \omega_d}, \qquad r_2 = \frac{1}{2}\frac{\Gamma}{1 + \omega_d} - \frac{1}{2}\frac{\sqrt{\Delta}}{1 + \omega_d}, \tag{103}$$

while, for $\Delta < 0$, it becomes

$$D_d \sim C_1\tau^{\frac{1}{2}\frac{\Gamma}{1+\omega_d}}\cos\frac{1}{2}\frac{\sqrt{|\Delta|}}{1 + \omega_d}\ln\tau + C_2\tau^{\frac{1}{2}\frac{\Gamma}{1+\omega_d}}\sin\frac{1}{2}\frac{\sqrt{|\Delta|}}{1 + \omega_d}\ln\tau. \tag{104}$$

It has been shown in [165] that Δ can be positive only in the vicinity of $\omega_d = -1$. When $\xi_2 \ll 1$ then $\Delta \ll 1$. The singularity occurs when $\omega_d = -1$ since it will lead to the divergence of r_1 that translates into a divergence in the density perturbation solution equation (102). When $\omega_d > -1$ and $\Delta > 0$, the blow-up in the density perturbation can also occur since $\Gamma/2(1+\omega_d)$ is also positive. But when ω_d grows further above -1, Δ will become negative and so does $\Gamma/2(1+\omega_d)$, which will lead to the convergent result of equation (104). When $\omega_d < -1$, $\Gamma/2(1+\omega_d)$ is always negative, the density perturbation will decay even when ω_d is close to -1 from below and Δ is small and positive.

In summary, when the interaction $\xi_2 \neq 0$, the system is stable for any constant $\omega_d < -1$. For $\omega_d > -1$, when the coupling is $\xi_2 \ll 1$, in the range of values of ω_d compatible with observations, the instability is also avoided. However, the system could become unstable in the observationally allowed range $\omega_d > -1$ when the interaction parameter is $\xi_2 \sim 1$.

The interaction kernel $Q = \xi_1\rho_m + \xi_2\rho_d$ was shown to be unstable when $\omega_d > -1$ is constant and $\xi_1 \neq 0$ [165], in agreement with [370]. For phantom case with constant EoS parameter, $\omega_d < -1$, the perturbation is stable regardless of the value of the coupling. These conclusions were confirmed by [190].

When the time dependence of the DE EoS is of the Chevallier–Polarski–Linder type [93, 235], the stability of the linear perturbation have also been studied [400] who found that the evolution of density perturbations at linear order is stable. Similar stability analysis for interacting scalar fields have been described by [109]. For field theory models (such as canonical bosons and fermions as DE and DM, respectively) the perturbations are also well defined, at least for a small range of parameters [111].

4.3. Cosmic microwave background temperature anisotropies

The formalism developed in section 4.1 can be used to study the evolution of matter and radiation perturbations that can then be tested against observations [264]. CMB temperature anisotropies provide a wealth of information that overshadows observables of the Hubble expansion. SNIa data are rather insensitive to the coupling between dark sectors [262, 263], while the integrated Sachs–Wolfe (ISW) component is a more sensitive probe [264, 415]. CMB observations are expected to break the degeneracy between the coupling and other cosmological parameters, such as ω_d and the DM abundance, providing tighter constraints on the interaction within the dark sector. Many interacting models have been studied in the literature. See for example [23, 110, 129, 133, 134, 157, 180, 244, 321, 322, 371, 381, 398–401] among others. In this section we will discuss the effect of the interaction in the pattern of CMB temperature anisotropies. The formalism reviewed here is mainly based on [167] and [169].

The temperature anisotropy power spectrum can be calculated by [318]

$$C_\ell = 4\pi \int \frac{\mathrm{d}k}{k} \mathcal{P}_\chi(k) |\Delta_\ell(k,\tau_0)|^2, \qquad (105)$$

where Δ_ℓ gives the transfer function for each ℓ, $\mathcal{P}_\chi$ is the primordial power spectrum and τ_0 is the conformal time at present. On large scales the transfer functions are

$$\Delta_\ell(k,\tau_0) = \Delta_\ell^{\mathrm{SW}}(k) + \Delta_\ell^{\mathrm{ISW}}(k), \qquad (106)$$

where $\Delta_\ell^{\mathrm{SW}}(k)$ is the contribution from the last scattering surface given by the ordinary Sachs–Wolfe (SW) effect and $\Delta_\ell^{\mathrm{ISW}}(k)$ is the contribution due to the change of the gravitational potential when photons passing through the universe on their way to the observer [318]. The ISW contribution can be written as

$$\Delta_\ell^{\mathrm{ISW}} = \int_{\tau_i}^{\tau_0} \mathrm{d}\tau j_\ell(k[\tau_0 - \tau]) \mathrm{e}^{\kappa(\tau_0)-\kappa(\tau)} [\Psi' - \Phi'], \qquad (107)$$

where j_ℓ is the spherical Bessel function and κ is the optical depth due to Thompson scattering. From Einstein equations, we obtain,

$$\Psi' - \Phi' = 2\mathcal{H}\left[\Phi + 4\pi G a^2 \sum_i U^i \rho^i / (\mathcal{H}k) + \mathcal{T}\right] - \mathcal{T}', \qquad (108)$$

where

$$\Phi' = -\mathcal{H}\Phi - \mathcal{H}\mathcal{T} - 4\pi G a^2 \sum_i U^i \rho^i / k,$$

$$\mathcal{T} = \frac{8\pi G a^2}{k^2} \{ p^\gamma \Pi^\gamma + p^\nu \Pi^\nu \}$$

and Π is the anisotropic stress of relativistic components which can be neglected in the following discussion.

In figure 5 we illustrate the effect of the DE EoS parameter ω_d and the fraction of DM, parametrized as the commonly used variable $\omega_{\mathrm{cdm}} = \Omega_c h^2$, on the CMB radiation power spectrum for a cosmological model without interaction. We shall see that the interaction also alters the height and location of the acoustic peaks and draughts, and this effect needs to be distinguished from that of other parameters. For comparison, in figure 6 we plot the CMB power spectrum of temperature anisotropies for different interaction models. Let us first concentrate on models with constant ω_d and a constant speed of sound. For simplicity, we limit our study to the three commonly studied phenomenological interaction kernels of table 3. In figure 6 we fixed the energy densities to the values given in table 2. Solid lines correspond to variations in the EoS parameter. Figure 6(a) shows that the power at low-ℓ increases with increasing value of ω_d, but the effect on the acoustic peaks is negligible. In figures 6(b)–(d) the variation is in the same direction but the effect of changing ω_d is smaller than when $\omega_d > -1$.

The effect of the interaction, represented in figure 6 by dashed lines, is more evident. The interaction changes the spectrum at low multipoles through its effect on the gravitational potentials and the ISW effect. When the coupling increases, the low-ℓ spectrum is further suppressed. When the interaction between dark sectors is proportional to the DM or total dark sector energy density, the low-ℓ spectrum is more sensitive to the change of the coupling than that of the DE EoS. The effects on the low multipoles due to the ISW effect and on the acoustic peaks are important since they could help

to break the degeneracy between the interaction, the DE EoS and other cosmological parameters as illustrated by figure 5.

The ISW effect has two components: early and late time effects. The early ISW effect occurs when the gravitational potentials evolve in time since matter–radiation equality to the moment when the radiation is no longer dynamically significant. Its contribution is largest around the first acoustic peak and below [184]. The late time ISW effect arises when the DE becomes important and the gravitational potentials decay. When a photon passes through a decaying potential well, it will have a net gain in energy. Consequently, the ISW effect can be used to probe the dynamical effect of the DE. This component has a significant contribution to the large scale CMB radiation power spectrum. Since galaxies trace the large scale gravitational field, cross-correlating matter templates constructed from galaxy catalogs with CMB temperature anisotropy maps can be used to isolate the ISW contribution [107, 113] and test the effect of the interaction [240, 264, 331, 398].

In the absence of interaction, the late ISW effect depends on the EoS parameter ω_d and sound speed C_e^2. For constant $C_e^2 \lesssim 1$ and $\omega_d > -1$, the spectrum of CMB temperature anisotropies on large scales is larger than in the concordance model [50, 391]. Increasing C_e^2 leads to further suppression of DM perturbations, increasing the contribution to the ISW effect [50]. However, when $\omega_d < -1$ the effect is the contrary, the contribution to the ISW effect increases as the sound speed of DE decreases [391].

The interplay between perturbations in the DE and DM and the ISW effect is very subtle and can not be disentangled easily from the radiation power spectrum. A more direct probe is to cross-correlate the late ISW effect to its source term, the time variation of the gravitational potential [391]. Both the power spectrum due to the late ISW effect and the cross-correlation with a matter template constructed from a galaxy catalog can be expressed in terms of quadratures [113]. The auto- and cross-correlation power spectra are given by

$$C_l^{gg} = 4\pi \int \frac{\mathrm{d}k}{k} \mathcal{P}_\chi(k) I_l^g(k) I_l^g(k) \tag{109}$$

$$C_l^{gI} = 4\pi \int \frac{\mathrm{d}k}{k} \mathcal{P}_\chi(k) I_l^g(k) \Delta_l^{\mathrm{ISW}}(k), \tag{110}$$

where the projected density of galaxies is given by $I_l^g(k) = \int \mathrm{d}z b_g(z) n(z) (D_c + D_b) j_l[k\chi(z)]$, where $n(z)$ is the number density of objects at a given redshift and $D_c(z), D_b(z)$ are the growth function of CDM and baryons respectively. Here $b_g(z)$ is the galaxy bias and $\chi(z)$ is the conformal distance, or equivalently the look-back time from the observer at redshift $z = 0$, $\chi(z) = \int_0^z \frac{\mathrm{d}z'}{H(z)} = \int_{\tau_i(z)}^{\tau_0} \mathrm{d}\tau = \tau_0 - \tau_i(z)$ (see section 1.2.4). We assume $b(z) \sim 1$ for simplicity and adopt the redshift distribution of the form [222] $n(z) = \frac{3}{2} A \frac{z^2}{z_0^3} \exp\left[-\left(\frac{z}{z_0}\right)^{3/2}\right]$, the normalization constant A is fixed by setting $\int n(z)\mathrm{d}z = 1$. This expression has a maximum near the median redshift $z_m = 1.4 z_0$. For illustrative purpose, we choose $z_m = 0.1$ and $z_m = 0.4$. The first value would correspond to a shallow survey like 2MASS [70] while the second would correspond to the SDSS photo-z galaxy sample [384] (see section 6 for details).

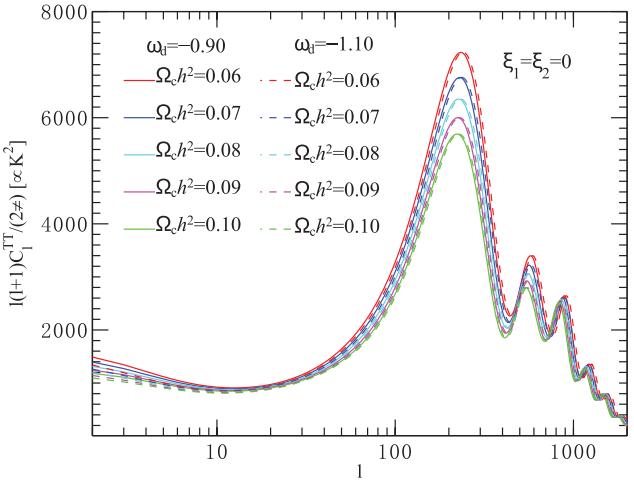

Figure 5. Variation of the CMB radiation power spectrum with cosmological parameters.

The late ISW effect is a promising tool to measure the EoS and sound speed of DE. Let us now analyze if it can provide useful evidence of the interaction. First, we will analyze the case of $\xi_1 \neq 0$, $\xi_2 = 0$ with constant EoS parameter $\omega_d < -1$ (model III in table 3) and sound speed $C_e^2 = 1$. The radiation power spectrum is given in figure 7(a). In the figure, the lower set of dashed lines correspond to the late ISW (LISW) and the upper set of dotted lines correspond to the early ISW (EISW) plus SW effect. Solid lines correspond to the total anisotropy. For this coupling the SW + EISW effect shows a larger variation than the LISW. The results show that larger the coupling bigger suppression of CMB anisotropies. This behavior can be expected since as shown in the figure 7(b) the potentials evolve more slowly when the interaction is larger. In figure 7(c) we illustrate the variation of the radiation power spectrum with sound speed. The figure shows that a smaller DE sound speed increases the LISW effect. The effect of the interaction in models IV is similar to model III and is not explicitly shown.

The results for model I (see table 3) are presented in figure 8. Lines in (a) and (c) follow the same conventions than figures 7(a) and (c). For this model the interaction does not modify the SW + EISW effect but it changes the LISW significantly. In this case, a positive coupling increases the amplitude of the LISW and a negative coupling decreases it compared with the uncoupled case. The behavior follows the evolution of the ISW source term shown in figure 8(b) that demonstrates how the change of the gravitational potential increases with increasing value of the coupling. In figure 8(c) we present the effect of the sound speed. When DM and DE interact, a variation on the sound speed from $C_e^2 = 1$ to $C_e^2 = 0.01$ does not lead to significant variations on the LISW. Finally, in model II with $C_e^2 = 1$ the effect of the interaction produces the same behavior as in model I.

Since the influence of the interaction in the LISW effect is relatively strong, it is interesting to discuss if the cross-correlation with templates constructed from the large scale matter distribution can measure how the potentials evolve

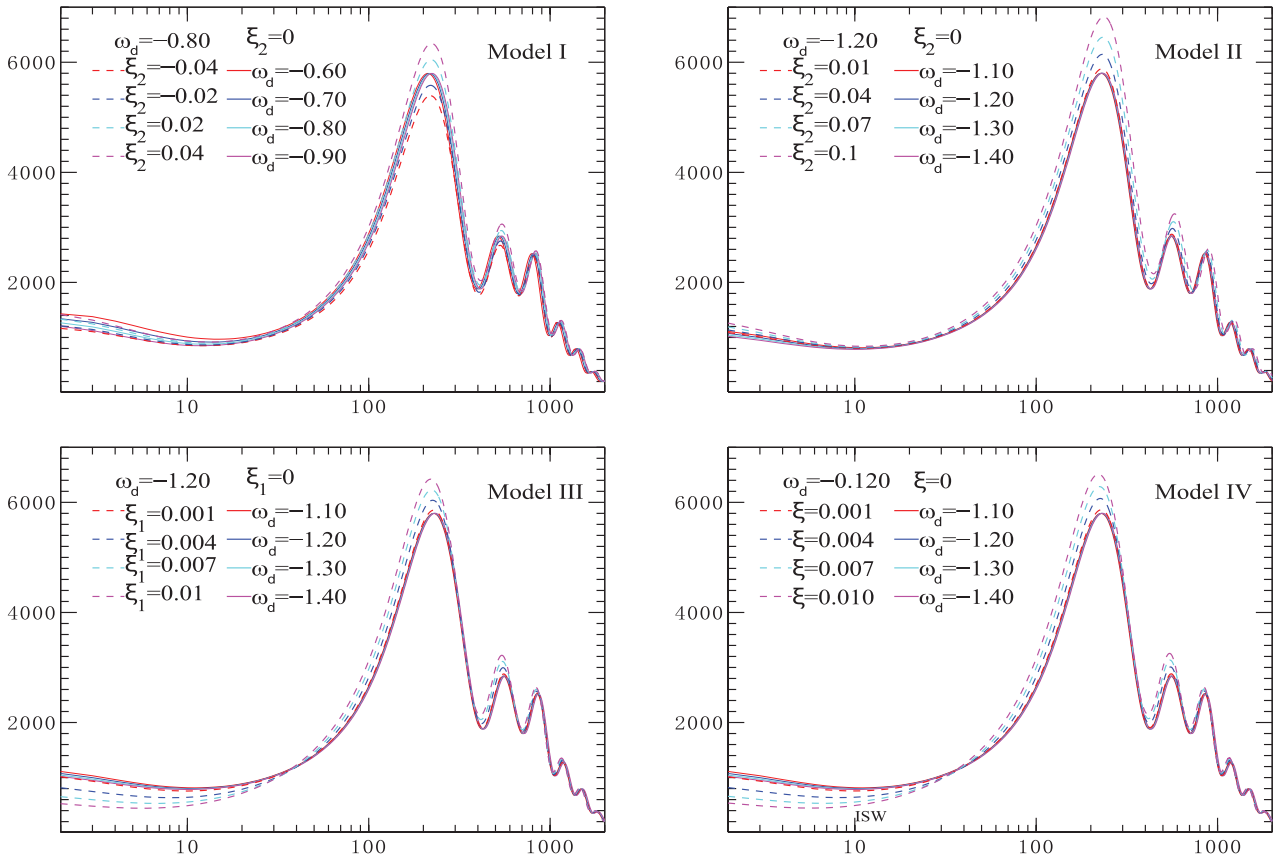

Figure 6. The CMB TT power spectrum for the phenomenological kernels given in table 3. Solid lines are for models without interactions between dark sectors. Dashed lines are for different strengths of interacting models.

with time. Progress in CMB and LSS surveys have enabled detections of the ISW-LSS cross correlation at $\sim 3\sigma$ level [11, 73, 80, 257]. The signal-to-noise ratio (S/N) can be further improved by a factor of a few for future all sky LSS surveys (see sections 6 and 8). The main advantage of cross-correlating temperature maps and matter density templates is that the primary CMB does not correlate with the LSS and does not bias the ISW measurement, it only contributes to the error bar. Then, using several traces of the matter distribution at different redshifts, it is possible to reconstruct the redshift evolution of the gravitational potential.

Although the ISW-LSS cross correlation is potentially powerful probe of the interaction between dark sectors, due to the low S/N of the current ISW-LSS measurements and the complexities of the theoretical interpretation (e.g. galaxy bias), we will not confront the model predictions against the existing ISW-LSS cross-correlation measurements. Instead, we will just calculate the expected cross-correlation signal between the ISW effect and galaxies given by equation (110) for some representative cases to show how the cross-correlation is modified due to the interaction. The results for model III are shown in figures 7(d) and 8(d). The top panels show the cross-correlation with two galactic templates of different depth and the low panels show the auto correlation power of the LISW traced by those templates. In both cases, a positive coupling decreases the auto-correlation and the cross-correlation spectra compared with the ΛCDM model while negative couplings increase them. The effect is more important for the shallow galaxy survey ($z_m = 0.1$) than for the deep one ($z_m = 0.4$).

Finally, the study of models with a variable DE EoS parameter have been discussed in [400]. DE perturbation are not longer negligible and contribute to the ISW effect. The effect on models based on a field theory description have also been discussed in [302].

4.4. Matter density perturbations

The interaction also modifies the evolution of matter density perturbations. If the DE couples to the DM, it must be dynamical and fluctuate in space and in time. In these models structure formation would be different than in the concordance model [28, 43, 154, 262, 364, 365], changing the growth index [81, 168, 242]. The collapse and subsequent dynamical equilibrium of clusters is modified compared to the concordance model [2, 3, 61]. Comparing virial masses with masses estimated from x-ray and weak lensing data of a large sample of clusters, [2, 3] found a small positive coupling in agreement with the results derived in [167, 169] from CMB data.

In this section we will analyze the effect of the interaction on the growth of DM density perturbations. First we restrict our attention to models with constant sound speed and constant DE EoS parameter. We will show that the effect of the interaction is larger than the effect of DE perturbations, providing another test of interacting models.

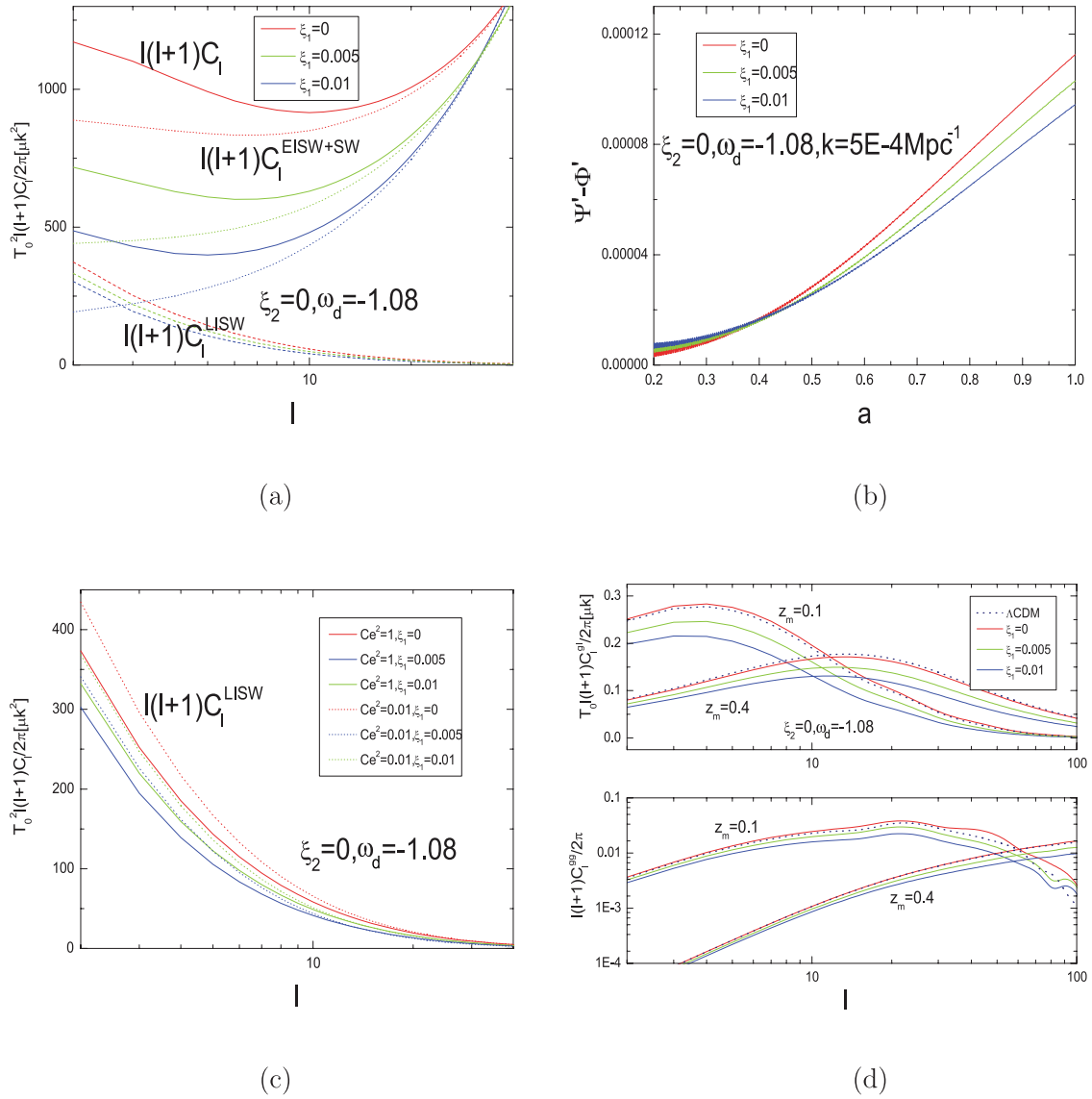

Figure 7. Different magnitudes for phenomenological fluid model III. (a) CMB radiation power spectra for small ℓ. (b) Evolution of the gravitational potentials. (c) Evolution of the integrated Sachs–Wolfe component. (d) Upper panel ISW and galaxy cross-spectra as given by equation (111); the lower panel shows the galaxy power spectra of equation (110).

Let us first derive the equations of evolution of DM density perturbations. From equation (74) and defining

$$\delta\rho_\lambda^I = \delta\rho_\lambda - \rho_\lambda'\frac{v_\lambda + B}{k}, \quad \delta p_\lambda^I = \delta p_\lambda - p_\lambda'\frac{v_\lambda + B}{k},$$
$$\Delta_\lambda = \delta_\lambda - \frac{\rho_\lambda'}{\rho_\lambda}\frac{v_\lambda + B}{k}, \quad V_\lambda = v_\lambda - \frac{E'}{2k}, \tag{111}$$

the perturbed Einstein equations equation (66) become

$$\Phi = 4\pi G\frac{a^2}{k^2}\sum_\lambda\left(\Delta_\lambda + \frac{a^2Q_\lambda^0}{\rho_\lambda}\frac{V_\lambda}{k}\right)\rho_\lambda,$$
$$k(\mathcal{H}\Psi - \Phi') = 4\pi G a^2\sum_\lambda(\rho_\lambda + p_\lambda)V_\lambda, \quad \Psi = -\Phi, \tag{112}$$

where we have neglected the pressure perturbation of DE, $\Pi_j^i = 0$. The gravitational potential is consistent with equation (82) when we combine equation (111) and equation (74) with equations (112) and (82).

Using the gauge invariant quantities of equation (111), we can obtain the linear perturbation equations for the DM,

$$\Delta_c' + \left[\frac{\rho_c'}{\rho_c}\frac{V_c}{k}\right]' = -kV_c - 3\Phi' + 2\Psi\frac{a^2Q_c^0}{\rho_c} - \Delta_c\frac{a^2Q_c^0}{\rho_c}$$
$$-\frac{\rho_c'}{\rho_c}\frac{V_c}{k}\frac{a^2Q_c^0}{\rho_c} + \frac{a^2\delta Q_c^{0I}}{\rho_c} + \frac{a^2Q_c^{0'}}{\rho_c\mathcal{H}}\Phi - \frac{a^2Q_c^0}{\rho_c}\left[\frac{\Phi}{\mathcal{H}}\right]', \tag{113}$$

$$V_c' = -\mathcal{H}V_c + k\Psi - \frac{a^2Q_c^0}{\rho_c}V_c + \frac{a^2\delta Q_{pc}^I}{\rho_c}. \tag{114}$$

Considering the pressure perturbation of DE equation (77), we obtain the gauge invariant form of DE perturbation equations [370]

$$\Delta_d' + \left[\frac{\rho_d'}{\rho_d}\frac{V_d}{k}\right]' + 3\mathcal{H}C_e^2\left(\Delta_d + \frac{\rho_d'}{\rho_d}\frac{V_d}{k}\right) - 3\mathcal{H}(C_e^2 - C_a^2)\frac{\rho_d'}{\rho_d}\frac{V_d}{k}$$
$$- 3\omega_d\mathcal{H}\left(\Delta_d + \frac{\rho_d'}{\rho_d}\frac{V_d}{k}\right) = -k(1+\omega_d)V_d - 3(1+\omega_d)\Phi' + 2\Psi\frac{a^2Q_d^0}{\rho_d}$$
$$-\left(\Delta_d + \frac{\rho_d'}{\rho_d}\frac{V_d}{k}\right)\frac{a^2Q_d^0}{\rho_d} + \frac{a^2\delta Q_d^{0I}}{\rho_d} + \frac{a^2Q_d^{0'}}{\rho_d\mathcal{H}}\Phi - \frac{a^2Q_d^0}{\rho_d}\left[\frac{\Phi}{\mathcal{H}}\right]', \tag{115}$$

$$V_d' + \mathcal{H}(1-3\omega_d)V_d = \frac{k}{1+\omega_d}\left[C_e^2\left(\Delta_d + \frac{\rho_d'}{\rho_d}\frac{V_d}{k}\right) - (C_e^2 - C_a^2)\frac{\rho_d'}{\rho_d}\frac{V_d}{k}\right]$$
$$- \frac{\omega_d'}{1+\omega_d}V_d + k\Psi - \frac{a^2Q_d^0}{\rho_d}V_d + \frac{a^2\delta Q_{pd}^I}{(1+\omega_d)\rho_d}. \tag{116}$$

In the subhorizon approximation $k \gg aH$, the above perturbation equations reduce to

$$\Delta_c' = -kV_c - \Delta_c\frac{a^2Q_c^0}{\rho_c} + \frac{a^2\delta Q_c^{0I}}{\rho_c},$$
$$V_c' = -\mathcal{H}V_c + k\Psi - \frac{a^2Q_c^0}{\rho_c}V_c + \frac{a^2\delta Q_{pc}^I}{\rho_c}; \tag{117}$$

$$\Delta_d' = 3\mathcal{H}(\omega_d - C_e^2)\Delta_d - k(1+\omega_d)V_d - \Delta_d\frac{a^2Q_d^0}{\rho_d} + \frac{a^2\delta Q_d^{0I}}{\rho_d},$$
$$V_d' + \mathcal{H}(1-3\omega_d)V_d = \frac{kC_e^2}{1+\omega_d}\Delta_d + \frac{C_a^2}{1+\omega_d}\frac{\rho_d'}{\rho_d}V_d + k\Psi - \frac{\omega_d'}{1+\omega_d}V_d - \frac{a^2Q_d^0}{\rho_d}V_d + \frac{a^2\delta Q_{pd}^I}{(1+\omega_d)\rho_d}. \tag{118}$$

Eliminating V_c, in the subhorizon approximation $k \gg aH$, we obtain the second order equation for the DM perturbation

$$\Delta_c'' = -\left(\mathcal{H} + \frac{2a^2Q_c^0}{\rho_c}\right)\Delta_c' + \left(-\Delta_c\frac{a^2Q_c^0}{\rho_c} + \frac{a^2\delta Q_c^{0I}}{\rho_c}\right)\left(\mathcal{H} + \frac{a^2Q_c^0}{\rho_c}\right)$$
$$-\Delta_c\left(\frac{a^2Q_c^0}{\rho_c}\right)' + \left(\frac{a^2\delta Q_c^{0I}}{\rho_c}\right)' - \frac{a^2k\delta Q_{pc}^I}{\rho_c} - k^2\Psi. \tag{119}$$

Similarly for the DE perturbation we have

$$\Delta_d'' = -3\mathcal{H}'C_e^2\Delta_d - \left(\frac{a^2Q_d^0}{\rho_d}\right)'\Delta_d + \left\{\mathcal{H}(1-3\omega_d) - \frac{\omega_d}{1+\omega_d}\frac{\rho_d'}{\rho_d} + \frac{a^2Q_d^0}{\rho_d}\right\}\times\left\{-3\mathcal{H}C_e^2 + 3\omega_d\mathcal{H} - \frac{a^2Q_d^0}{\rho_d}\right\}\Delta_d$$
$$-\left[\mathcal{H} + 3\mathcal{H}C_e^2 - 6\omega_d\mathcal{H} + \frac{2a^2Q_d^0}{\rho_d} - \frac{\omega_d}{1+\omega_d}\frac{\rho_d'}{\rho_d}\right]\Delta_d'$$
$$-k\left(\frac{a^2\delta Q_{pd}^I}{\rho_d}\right) - k^2C_e^2\Delta_d - k^2(1+\omega_d)\Psi + 3(\omega_d'\mathcal{H} + \omega_d\mathcal{H}')\Delta_d$$
$$+\frac{a^2\delta Q_d^{0I}}{\rho_d}\left[\mathcal{H}(1-3\omega_d) - \frac{\omega_d}{1+\omega_d}\frac{\rho_d'}{\rho_d} + \frac{a^2Q_d^0}{\rho_d}\right] + \left(\frac{a^2\delta Q_d^{0I}}{\rho_d}\right)'. \tag{120}$$

From the perturbed Einstein equation (112) we obtain the 'Poisson equation' in the subhorizon approximation,

$$-\frac{k^2}{a^2}\Psi = \frac{3}{2}H^2\{\Omega_c\,\Delta_c + (1-\Omega_c)\Delta_d\}, \tag{121}$$

which relates the matter inhomogeneities to the metric perturbations. Finally, using the results of section 4.1.3, we can obtain the perturbation equations for the dark sector with a constant DE EoS.

The stability of the growth function depends on the type of coupling and on whether ω_d is constant in time or not. When the interaction is proportional to the DM energy density ($\xi_2 = 0$) the growth of matter density perturbations is unstable. The unstable solution can disappear when ω_d varies with time. The growth is stable when the interaction is proportional to the energy density of DE ($\xi_1 = 0$). These results are consistent with the conclusions of the evolution of curvature perturbations on superhorizon scales in the early universe [165]. Hereafter we will restrict our analysis to the case $\xi_1 = 0$ since in this case all the solution are stable. We will consider adiabatic initial conditions at matter-radiation equality ($z = 3200$). We assume that the time derivatives of DM and DE perturbations are zero. To simplify the discussion, we restrict the analysis to a constant EoS parameter with $\omega_d < -1$ and to those scales of the matter power spectrum that have been measured, i.e. $k > 0.01h$ Mpc^{-1} [43]. Also, the DE sound speed, C_e^2, will be positive and smaller than unity. In figure 9 we plot the behavior of DE and

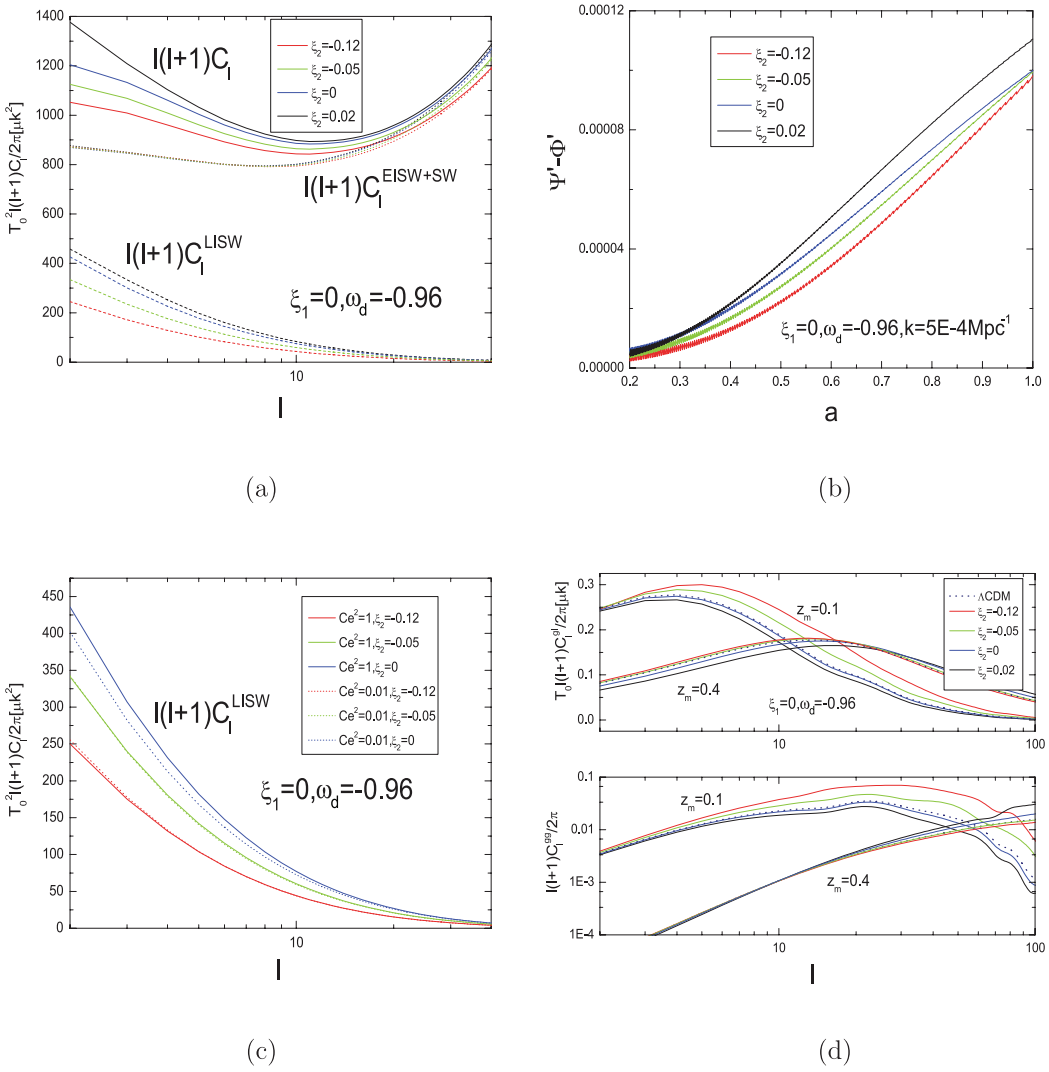

Figure 8. Same as in figure 7 but for model I.

DE perturbations for different effective sound speed, DE EoS parameter, wave number and coupling. The adiabatic initial conditions are $\delta_c/(1-\xi_1-\xi_2/r) = \delta_d/(1+\omega_d+\xi_1 r+\xi_2)$. Solid lines represent DM perturbations and dotted lines DE perturbations. The solutions largely overlap, except in the encircled region in panel (d).

In models without interaction, DE perturbations have an effect on the evolution of DM density pertubations, more important when the sound speed is $C_e^2 \sim 0$ and ω_d is significantly different from -1. Figure 9(a) illustrates this behavior: a smaller the value of C_e^2 corresponds to a larger growth of DE perturbation; larger the difference of ω_d from -1 larger the growth of DE perturbations. The effect is even more important on the DM perturbations. In figure 9(b) we illustrate the behavior for a constant sound speed. In this case, the DE perturbation grows larger when the difference of $\omega_d + 1$ from zero increases, consistent with [43]. However, when $C_e^2 \lesssim 1$ and $\omega_d \simeq -1$ the effect of DE is suppressed. Figure 9(c) illustrates that the effect of DE perturbations is smaller at large than at small scales. The previous results do not change qualitatively in the presence of an interaction as illustrated by figure 9(d). Only at very recent epochs, indicated in the figure by a red circle, there is an obvious difference due to the coupling.

An alternative probe of the evolution of DM perturbations is the growth index γ, related to the dimensionless growth rate $f = \mathrm{d}\ln\Delta_c/\mathrm{d}\ln a$ as $\gamma = \ln f/\ln\Omega_c$ (see section 6.2.1). This index is rather sensitive to cosmological parameters [299], the underline theory of gravity [142, 143] and a DM/DE coupling [43]. In figure 10 we plot this magnitude for model I with different values of the interaction parameter. Solid lines correspond to models with DE perturbations, while dotted lines correspond to models with a DE density homogeneously distributed. When there is no interaction and $\omega_d = \text{const.}$ the matter growth index deviates from the value of the concordance model more when there are DE density perturbations than when the DE is distributed homogeneously. The deviation is more important when ω_d differs significantly from -1 and when C_e^2 decreases. The difference in γ with and without DE perturbations can reach $\Delta\gamma = 0.03$. The differences between large and small scales in the subhorizon approximation, is not

as large as the effect of ω_d and C_e^2, in agreement with [43]. Detailed discussions on the matter growth index in the case of no interaction can be found in [168]. The effect of the interaction on the growth index is more important than the presence or absence of DE perturbations. For instance, if $\xi_2 \lesssim 10^{-2}$, value compatible with the expansion history of the universe [133, 164], the interaction dominates the variation on the growth index over the effect of DE perturbations. This result opens the possibility that future measurements of the growth factor could prove the existence of the interaction irrespectively of the DE distribution.

5. The DM/DE interaction beyond perturbation theory

5.1. Layzer–Irvine equation

In an expanding universe, the Layzer–Irvine equation describes how a collapsing system reaches a state of dynamical equilibrium [221, 275]. The final state will be altered if there exists a DM/DE interaction [2, 3, 61, 62, 120, 166, 277]. In this section we will derive the Layzer–Irvine equation in the presence of such an interaction. We start by redefining the perturbed gauge invariant couplings of equations (91) and (92) as [165, 167]

$$\frac{a^2\delta Q_c^{0I}}{\rho_c} \approx 3\mathcal{H}(\xi_1\Delta_c + \xi_2\Delta_d/r), \qquad \frac{a^2\delta Q_d^{0I}}{\rho_d} \approx -3\mathcal{H}(\xi_1\Delta_c r + \xi_2\Delta_d), \tag{122}$$

where $\Delta_c \approx \delta\rho_c/\rho_c = \delta_c$, $\Delta_d \approx \delta\rho_d/\rho_d = \delta_d$ and $r = \rho_c/\rho_d$. It is useful to rewrite equations (117) and (118) in real space

$$\begin{aligned}
&\Delta_c' + \nabla_{\bar{x}}\cdot V_c = 3\mathcal{H}\xi_2(\Delta_d - \Delta_c)/r,\\
&V_c' + \mathcal{H}V_c = -\nabla_{\bar{x}}\Psi - 3\mathcal{H}(\xi_1 + \xi_2/r)V_c;\\
&\Delta_d' + (1+\omega_d)\nabla_{\bar{x}}\cdot V_d = 3\mathcal{H}(\omega_d - C_e^2)\Delta_d + 3\mathcal{H}\xi_1 r(\Delta_d - \Delta_c),
\end{aligned} \tag{123}$$

$$\begin{aligned}
V_d' + \mathcal{H}V_d = &-\nabla_{\bar{x}}\Psi - \frac{C_e^2}{1+\omega_d}\nabla_{\bar{x}}\Delta_d - \frac{\omega_d'}{1+\omega_d}V_d,\\
&+ 3\mathcal{H}\left\{(\omega_d - C_a^2) + \frac{1+\omega_d - C_a^2}{1+\omega_d}(\xi_1 r + \xi_2)\right\}V_d;
\end{aligned} \tag{124}$$

where $\bar{x} = a^{-1}x$ and $\nabla_x = a^{-1}\nabla_{\bar{x}}$. Defining $\sigma_c = \delta\rho_c$, $\sigma_d = \delta\rho_d$, and assuming that the DE EoS is constant, we can rewrite equations (123) and (124) as

$$\begin{aligned}
&\dot{\sigma}_c + 3H\sigma_c + \nabla_x(\rho_c V_c) = 3H(\xi_1\sigma_c + \xi_2\sigma_d),\\
&\frac{\partial}{\partial t}(aV_c) = -\nabla_x(a\Psi) - 3H(\xi_1 + \xi_2/r)(aV_c);
\end{aligned} \tag{125}$$

$$\begin{aligned}
&\dot{\sigma}_d + 3H(1+C_e^2)\sigma_d + (1+\omega_d)\nabla_x(\rho_d V_d) = -3H(\xi_1\sigma_c + \xi_2\sigma_d),\\
&\frac{\partial}{\partial t}(aV_d) = -\nabla_x(a\Psi) - \frac{C_e^2}{1+\omega_d}\nabla_x\cdot(a\Delta_d),\\
&\qquad + 3H\left[(\omega_d - c_a^2) + \frac{1+\omega_d - c_a^2}{1+\omega_d}(\xi_1 r + \xi_2)\right](aV_d).
\end{aligned} \tag{126}$$

The dot denotes the derivative with respect to the coordinate time. The gravitational potential Ψ can be decomposed as $\Psi = \psi_c + \psi_d$, each component satisfying the following Poisson equation [252],

$$\nabla^2\psi_\lambda = 4\pi G(1+3\omega_\lambda)\sigma_\lambda. \tag{127}$$

The subscript $\lambda = (c, d)$ denotes DM and DE, respectively and σ_λ represents the inhomogeneous fluctuation field. In a homogeneous and isotropic background $\langle\psi_\lambda\rangle = 0$, since $\langle\sigma_\lambda\rangle = 0$. The corresponding gravitational potentials are [252]

$$\psi_c = -4\pi G\int \mathrm{d}V'\frac{\sigma_c}{|x-x'|}, \quad \psi_d = -4\pi G\int \mathrm{d}V'\frac{(1+3\omega_d)\sigma_d}{|x-x'|}. \tag{128}$$

For the DM, the rate of change of the peculiar velocity (equation (125)) can be recast as

$$\frac{\partial}{\partial t}(aV_c) = -\nabla_x(a\psi_c + a\psi_d) - 3H(\xi_1 + \xi_2/r)(aV_c). \tag{129}$$

Neglecting the influence of DE and the couplings, equation (129) represents the rate of change of the peculiar velocity of the DM particle in an expanding universe described by the Newton's law; this was the starting point of [221]. To derive the energy equation for the local inhomogeneities, we multiply equation (129) by $aV_c\rho_c\hat{\varepsilon}$ and integrate over the volume [221]. Here $\hat{\varepsilon} = a^3\mathrm{d}\bar{x}\wedge\mathrm{d}\bar{y}\wedge\mathrm{d}\bar{z}$ is the volume element which satisfies $\frac{\partial}{\partial t}\hat{\varepsilon} = 3H\hat{\varepsilon}$. Considering the continuity equation, the LHS of equation (129) can be multiplied by aV_m and integrated to yield

$$\frac{\partial}{\partial t}(a^2T_c) - a^2 3H(\xi_1 + \xi_2/r)T_c. \tag{130}$$

where $T_c = \frac{1}{2}\int V_c^2\rho_c\hat{\varepsilon}$ is the kinetic energy of DM associated with peculiar motions of DM particles.

The RHS of equation (129) can be transformed in a similar manner. Using partial integration, the potential part can be changed to

$$\begin{aligned}
-\int aV_c\nabla_x(a\psi_c + a\psi_d)\rho_c\hat{\varepsilon} = &\, a^2\int\nabla_x(\rho_c V_c)\psi_c\hat{\varepsilon}\\
&+ a^2\int\nabla_x(\rho_c V_c)\psi_d\hat{\varepsilon}.
\end{aligned} \tag{131}$$

Taking into account the first equation in (125), it can transformed to

$$\begin{aligned}
-\int aV_c\nabla_x(a\psi_c + a\psi_d)\rho_c\hat{\varepsilon} = &-a^2(\dot{U}_{cc} + HU_{cc}) - a^2\int\psi_d\frac{\partial}{\partial t}(\sigma_c\hat{\varepsilon})\\
&+ 3a^2H\{\xi_1 U_{cd} + \xi_2 U_{dc} + 2\xi_1 U_{cc} + 2\xi_2 U_{dd}\}
\end{aligned} \tag{132}$$

where $U_{cc} = \frac{1}{2}\int\sigma_c\psi_c\hat{\varepsilon}$, $U_{dc} = \int\sigma_d\psi_c\hat{\varepsilon}$, $U_{cd} = \int\sigma_c\psi_d\hat{\varepsilon}$, and $U_{dd} = \frac{1}{2}\int\sigma_d\psi_d\hat{\varepsilon}$.

The second term in the RHS of equation (129) can be rewritten as

$$-\int(aV_c)^2 3H(\xi_1 + \xi_2/r)\rho_c\hat{\varepsilon} = -a^2 6H(\xi_1 + \xi_2/r)T_c. \tag{133}$$

Combining equations (130), (132) and (133), one obtains

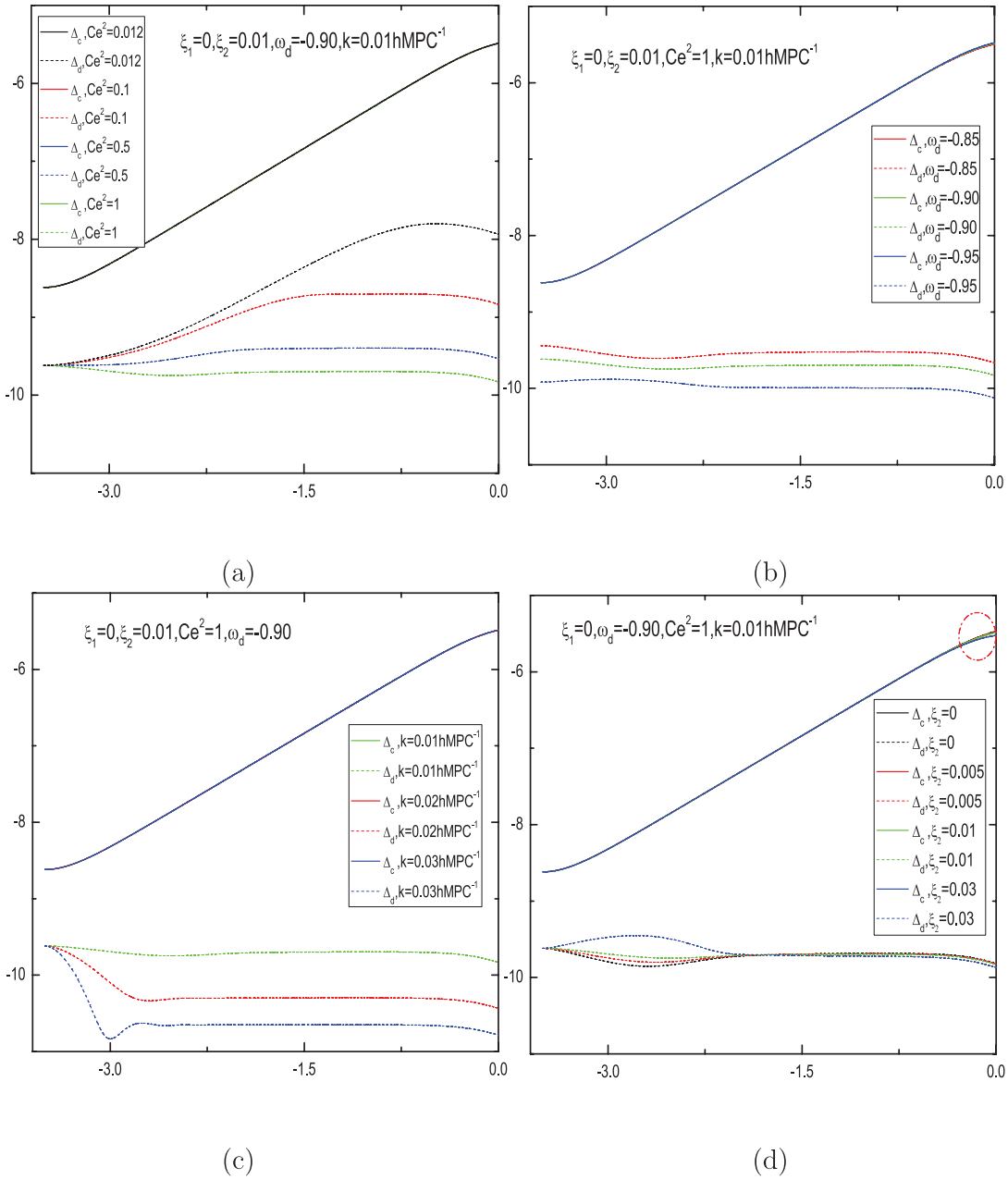

Figure 9. Behavior of DE and DE perturbations for different effective sound speed C_e, dark energy EoS parameter ω_d, wave number k and coupling. Solid lines represent DM perturbation and dotted lines DE perturbation.

$$\dot{T}_c + \dot{U}_{cc} + H(2T_c + U_{cc}) = -\int \psi_d \frac{\partial}{\partial t}(\sigma_c \hat{\varepsilon}) - 3H(\xi_1 + \xi_2/r)T_c, + 3H\{\xi_1 U_{cd} + \xi_2 U_{dc} + 2\xi_1 U_{cc} + 2\xi_2 U_{dd}\}. \quad (134)$$

This equation describes how the DM reaches a dynamical equilibrium in a collapsing system within an expanding universe. If the DE is distributed homogeneously then $\sigma_d = 0$ and equation (134) reduces to

$$\dot{T}_c + \dot{U}_{cc} + H(2T_c + U_{cc}) = -3H(\xi_1 + \xi_2/r)T_c + 6H\xi_1 U_{cc}. \quad (135)$$

For a system in equilibrium, $\dot{T}_c = \dot{U}_{cc} = 0$ and we obtain the virial condition $(2/3 + \xi_1 + \xi_2/r)T_c + (1/3 - 2\xi_1)U_{cc} = 0$ [2]. Neglecting the interaction $\bar{\xi}_1 = \bar{\xi}_2 = 0$, we reach the virial condition first derived by [221]. Let us remark that even when the DM is homogeneously distributed the coupling changes both the time required by the system to reach equilibrium and the equilibrium configuration itself [2].

Let us now consider the case when DE is not homogeneous. The rate of change of the peculiar velocity of DE is described by the second equation of equation (126). Multiplying both sides of this equation by $aV_d\rho_d\hat{\varepsilon}$ and integrating over the volume, on the LHS we have

$$\frac{\partial}{\partial t}(a^2 T_d) + 3a^2 H(\omega_d + \xi_1 r + \xi_2)T_d. \quad (136)$$

On the RHS the first term reads,

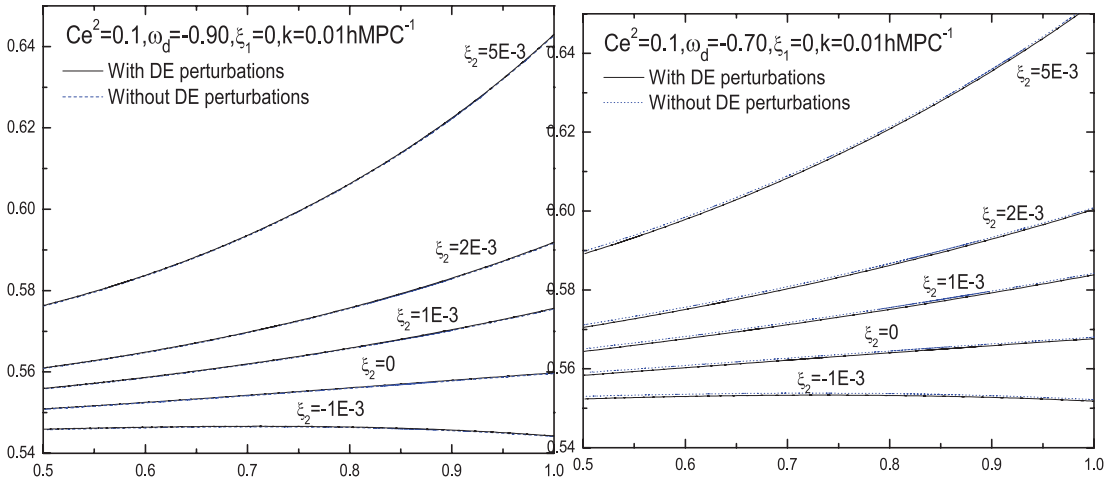

Figure 10. Growth index for interacting models. Solid lines are for the result with DE perturbation, while dotted lines are for the result without DE perturbation.

$$-\int aV_d\nabla_x(a\psi_c+a\psi_d)\rho_d\hat{\varepsilon}=-\frac{a^2}{1+\omega_d}(\dot{U}_{dd}+HU_{dd})$$
$$-\frac{a^2}{1+\omega_d}3H\{2(C_e^2+\xi_2)U_{dd}+2\xi_1U_{cc}+\xi_1U_{cd}+(C_e^2+\xi_2)U_{dc}\}$$
$$-\frac{a^2}{1+\omega_d}\int\psi_c\frac{\partial}{\partial t}(\sigma_d\hat{\varepsilon}). \tag{137}$$

For the remaining terms, we have

$$3H\left[(w-c_a^2)+\frac{1+w-C_a^2}{1+\omega_d}(\xi_1r+\xi_2)\right]\int(aV_d)^2\rho_d\hat{\varepsilon}$$
$$-\frac{c_e^2}{1+\omega_d}\int aV_d\nabla_x(a\Delta_d)\rho_d\hat{\varepsilon}$$
$$=6a^2H\left[(\omega_d-C_a^2)+\frac{1+\omega_d-c_a^2}{1+\omega_d}(\xi_1r+\xi_2)\right]T_d$$
$$-\frac{c_e^2}{1+\omega_d}a^2\int V_d\nabla_x(\sigma_d)\hat{\varepsilon}. \tag{138}$$

Combining equations (136)–(138), we arrive at

$$(1+\omega_d)\dot{T}_d+\dot{U}_{dd}+H[2(1+\omega_d)T_d+U_{dd}]=-3H\{2(C_e^2+\xi_2)U_{dd}+2\xi_1U_{cc}$$
$$+\xi_1U_{cd}+(C_e^2+\xi_2)U_{dc}\}-\int\psi_c\frac{\partial}{\partial t}(\sigma_d\hat{\varepsilon})-c_e^2\int V_d\nabla_x(\sigma_d)\hat{\varepsilon}$$
$$+3H\left[(1+\omega_d)(\omega_d-2C_a^2)+(1+\omega_d-2C_a^2)(\xi_1r+\xi_2)\right]T_d, \tag{139}$$

which describes how in an expanding universe collapsing DE perturbations reach dynamical equilibrium.

In the non-interacting case ($\xi_1=\xi_2=0$) when $C_e^2=0$ the DE would cluster just like CDM (compare (134) and (139)). Examples of DE models with this property were investigated in [112]. In the interacting case, the time and dynamics required by the DE and the DM to reach equilibrium in a collapsing system are different. This result was derived in linear theory. It would be more interesting to examine what occurs with the DE at the non-linear perturbation level to obtain a clearer picture of the dynamical evolution of the DE during the formalism of structure galactic halos and large scale structure.

5.2. Spherical collapse model

Let us now consider how the interaction between DE and DM affects the evolution of collapsing systems. The spherical collapse model is the simplest analytical model of structure formation. At the background level, the universe expands with the Hubble rate $H=\dot{a}/a$ and DE and DM satisfy the continuity equations (equations 12) and (13). A spherically symmetric region of radius R with energy density $\rho_\lambda^{cl}=\rho_\lambda+\sigma_\lambda$ (as before, $\lambda=(c,d)$ and cl indicates clustering), will eventually collapse due to its self-gravity provided that $\sigma_\lambda>0$. The equation of motion for the collapsing system is governed by Raychaudhuri equation.

$$\dot{\theta}=-\frac{1}{3}\theta^2-4\pi G\sum_\lambda(\rho_\lambda+3p_\lambda) \tag{140}$$

where $\theta=3(\dot{R}/R)$. Equation (140) can be written as,

$$\frac{\ddot{R}}{R}=-\frac{4\pi G}{3}\sum_\lambda(\rho_\lambda+3p_\lambda) \tag{141}$$

where R is the local expansion scale factor, to be distinguished from a the global (average) scale factor. Its evolution is determined by the matter inside the spherical volume and is not affected by the matter outside.

Assuming that the DE is homogeneously distributed ($\sigma_d=0$), the evolution of its energy density in an spherical volume is

$$\dot{\rho}_c^{cl} + 3\frac{\dot{R}}{R}\rho_c^{cl} = 3H(\xi_1\rho_c^{cl} + \xi_2\rho_d), \tag{142}$$

The Raychaudhuri equation applied to a spherical region has the form

$$\ddot{R} = -\frac{4\pi G}{3}[\rho_c^{cl} + (1+3\omega_d)\rho_d]R, \tag{143}$$

where ρ_d is the background DE energy density. Changing variables from time t to the scale factor a, we can write $\ddot{R} = (\dot{a})^2(\mathrm{d}^2R/\mathrm{d}a^2) + \ddot{a}(\mathrm{d}R/\mathrm{d}a)$ and change the Raychaudhuri equation to

$$2a^2\left(1+\frac{1}{r}\right)\frac{\mathrm{d}^2R}{\mathrm{d}a^2} - \frac{\mathrm{d}R}{\mathrm{d}a}\left[1+(3\omega_d+1)/r\right]a = -R\left[(3\omega_d+1)/r+\zeta\right], \tag{144}$$

where $\zeta = \rho_c^{cl}/\rho_c$. Therefore, we have

$$\frac{\mathrm{d}\zeta}{\mathrm{d}a} = \frac{3}{a}(1-\xi_2/r)\zeta - 3\frac{1}{R}\frac{\mathrm{d}R}{\mathrm{d}a}\zeta + \frac{3}{a}\xi_2/r. \tag{145}$$

In order to solve equations (144) and (145) we set the initial conditions $R \sim a$ and $dR/da = 1$ at matter-radiation equality, when we can consider that the spherical region is comoving with the background expansion. In the subhorizon limit, by neglecting DE inhomogeneities we can combine equations (144) and (145) and integrate the resulting equation from the initial moment $\zeta_i = \Delta_{ci} + 1$ till the spherical region collapses, at $R(a_{\rm coll}) \approx 0$ [168] to obtain the critical over density δ_c that determines which halos collapse. This linearly extrapolated density threshold will fix the abundances of collapsed halos at each redshift and mass scale.

If the DE distribution is not homogeneous, it will not fully trace the DM. Their four velocities will be different, $u^a_{(d)} \neq u^a_{(c)}$, and

$$u^a_{(d)} = \gamma(u^a_{(c)} + v^a_d) \tag{146}$$

where $\gamma = (1-v_d^2)^{-1/2}$ is Lorentz-boost factor and v^a_d is the relative velocity of DE fluid with respect to the DM rest frame. If the DE follows the DM distribution, $v^a_d = 0$. For non-comoving perfect fluids we have [364]

$$\begin{aligned} T^{ab}_{(c)} &= \rho_c u^a_{(c)} u^b_{(c)}, \\ T^{ab}_{(d)} &= \rho_d u^a_{(d)} u^b_{(d)} + p_d h^{ab}_{(d)}, \end{aligned} \tag{147}$$

where $h^{ab} = g^{ab} + u^a u^b$ is the projection operator. Inserting equation (146) into the second equation (147) and denoting $u^a_{(c)}$ by u^a, the energy momentum tensor for DE reads,

$$T^{ab}_{(d)} = \rho_d u^a u^b + p_d h^{ab} + 2u^a q^b_{(d)}, \tag{148}$$

where $q^a = (\rho_d + p_d)v^a_d$ is the energy-flux of DE seen in the DM rest frame. In the above equation, we neglect the second order terms in v^a_d and assume that the energy-flux velocity is much smaller than the speed of light $v^a_d \ll 1, \gamma \sim 1$. In the spherical model, we define the top-hat radius as the radius of the boundary of the DM halo. When the DE does not trace the DM it will not be bounded inside the top-hat radius and will be stretched outside the spherical region. If we assume that the DE leakage is still spherically symmetric, the Birkhoff theorem guarantees that in the spherical region the Raychaudhuri equation takes the same form as in (141). For the energy density conservation law we have

$$\nabla_a T^{ab}_{(\lambda)} = Q^b_{(\lambda)}, \tag{149}$$

where Q^b is the coupling vector and 'λ' denotes DE and DM respectively. The time-like part of the above equation, $u_b\nabla_a T^{ab}_{(\lambda)} = u_b Q^b_{(\lambda)}$, gives

$$\begin{aligned} &\dot{\rho}_c^{cl} + 3h\rho_c^{cl} = 3H(\xi_1\rho_c^{cl} + \xi_2\rho_d^{cl}), \\ &\dot{\rho}_d^{cl} + 3h(1+\omega_d)\rho_d^{cl} = -\vartheta(1+\omega_d)\rho_d^{cl} - 3H(\xi_1\rho_c^{cl} + \xi_2\rho_d^{cl}), \end{aligned} \tag{150}$$

where $\vartheta = \nabla_x v_d$. The external term incorporating ϑ in the DE density evolution corresponds to the energy loss caused by the leakage of DE out of the spherical region.

For the space-like part, $h^a_b\nabla_a T^{ab}_{(\lambda)} = h^a_b Q^b_{(\lambda)}$, only the DE has a non-zero spatial component and

$$\dot{q}^a_{(d)} + 4hq^a_{(d)} = 0, \tag{151}$$

where $q^a_{(d)}$ is the DE flux. Assuming that the energy and pressure are distributed homogeneously, we obtain

$$\dot{\vartheta} + h(1-3\omega_d)\vartheta = 3H(\xi_1\Gamma + \xi_2)\vartheta. \tag{152}$$

In this expression, $\Gamma = \rho_c^{cl}/\rho_d^{cl}$ is the ratio of the DM and DE density in the collapsed region. We kept only the linear terms of ϑ in equation (150). In equation (152), if ϑ vanishes initially, it will remain so during the subsequent evolution and the DE will fully trace the DM. However, in most cases, even at the linear level there is a small difference between v_d and v_c, so that the initial condition for ϑ is not zero. For illustration, we took the initial condition $\vartheta \sim k(v_d - v_c) \sim -5\times10^{-3}\delta_{ci}$, which is obtained from the prediction of linear equation with $k = 1\ \mathrm{Mpc}^{-1}$ at $z_i = 3200$. We have chosen $|\vartheta| \ll 1$; the negative sign indicates that at the initial moment DM expanded faster than that of DE. Taking $\vartheta \sim -10^{-3}\delta_{ci}$ did not change the results.

Defining $\zeta_c = \rho_c^{cl}/\rho_c$, $\zeta_d = \rho_d^{cl}/\rho_d$ and converting the time derivative from $\frac{\mathrm{d}}{\mathrm{d}t}$ to $\frac{\mathrm{d}}{\mathrm{d}a}$ we have the evolution of DM and DE in the spherical region described by

$$\begin{aligned} \vartheta' + \frac{R'}{R}(1-3\omega_d)\vartheta &= \frac{3}{a}(\xi_1\Gamma + \xi_2)\vartheta, \\ \zeta_c' &= \frac{3}{a}\{1-\xi_2/r\}\zeta_c - 3\frac{R'}{R}\zeta_c + \frac{3}{a}\xi_2\zeta_d/r, \\ \zeta_d' &= \frac{3}{a}(1+\omega_d+\xi_1 r)\zeta_d - 3(1+\omega_d) \\ &\quad\times\frac{R'}{R}\zeta_d - \frac{3}{a}\xi_1\zeta_c r - \vartheta(1+\omega_d)\zeta_d. \end{aligned} \tag{153}$$

When DE fully traces along DM, $\vartheta = 0$, only the last two equations are needed. The Raychaudhuri equation now becomes

$$\begin{aligned} &2a^2\left(1+\frac{1}{r}\right)R'' - R'\left[1+(3\omega_d+1)/r\right]a \\ &\quad = -R\left[(3\omega_d+1)\zeta_d/r + \zeta_c\right]. \end{aligned} \tag{154}$$

Taking for the spherical region of radius R the same initial conditions as above and adopting the adiabatic initial conditions:

$\Delta_{di} = (1+\omega_d)\Delta_{ci}$, $\zeta_{ci} = \Delta_{ci} + 1$ and $\zeta_{di} = \Delta_{di} + 1$, which lead to $\zeta_{di} = (1+\omega_d)\zeta_{ci} - \omega_d$, we can study the spherical collapse of both the DM and the DE. However, it is important to note that due to the coupling, ζ_d may be negative at some moment during the collapse which would be unphysical. To avoid reaching this point, we remove the coupling when ζ_d becomes negative. In this way, we guarantee $\zeta_d \geqslant 0$. In the linear evolution limit we assume the subhorizon approximation of the DM and DE perturbation equations to be valid. Even in this limit the DE and DM perturbations are coupled. Fortunately, the effect of DE perturbations is small compared with that of the DM [168]. Using the linear perturbation equations for DM and DE together with equations (153) and (154), in the spherical model with an inhomogeneous DE distribution we can obtain the linearly extrapolated density threshold $\delta_c(z) = \delta_c(z = z_{\rm coll})$ above which the structure collapses.

5.3. Press–Schechter formalism and galaxy cluster number counts

The variation of the cluster number counts with redshift has been studies as a promising tool to discriminate different DE models [7, 8, 76, 252, 254, 258, 349, 382, 395] and to test coupled quintessence models [242, 253, 259]. In these studies, DM and DE were assumed to be conserved separately at the background level; the models only included energy loss due to the DE inside a DM halo and mass conservation implied that the DM density evolved as $\rho_c \sim R^{-3}$. By contrast, in our study we will consider that the interaction within the dark sector exists at all scales.

Press and Schechter [301] designed a formalism to predict the number density of collapsed objects using the spherical collapse model. Although this formalism is a crude approximation and it is not precise enough to predict the exact number of clusters [189], it can be useful to understand how the interaction and the clustering of DE influence the threshold density of cluster collapse and, consequently, the cluster number counts as a function of mass and redshift.

In the Press–Schechter formalism, the comoving number density of collapsed DM halos of mass $[M, M + {\rm d}M]$ at redshift $[z, z + {\rm d}z]$ is [301]

$$\frac{{\rm d}n(M,z)}{{\rm d}M} = \sqrt{\frac{2}{\pi}}\frac{\rho_m}{3M^2}\frac{\delta_c}{\sigma}{\rm e}^{-\delta_c^2/2\sigma^2}\left[-\frac{R}{\sigma}\frac{{\rm d}\sigma}{{\rm d}R}\right], \qquad (155)$$

where $\rho_m = \rho_c + \rho_b$ is the comoving mean matter density at each particular redshift. In most cases, it is a constant and equals the present mean matter density, but this is not true when DE interacts with DM [242]. The quantity $\sigma = \sigma(R,z)$ represents the root mean square density fluctuation on a sphere of radius R. It has the explicit form [377],

$$\sigma(R,z) = \sigma_8\left(\frac{R}{8h^{-1}\,{\rm Mpc}}\right)^{-\epsilon(R)} D(z), \qquad (156)$$

where σ_8 has been evaluated on a sphere of radius $R = 8h^{-1}$ Mpc and $D(z)$ is the growth function defined by $D(z) = \delta_c(z)/\delta_c(0)$. The index ϵ is a function of the mass scale and the shape parameter Γ of the matter power spectrum [377],

$$\epsilon(R) = (0.3\Gamma + 0.2)\left[2.92 + \log_{10}\left(\frac{R}{8h^{-1}\,{\rm Mpc}}\right)\right]. \qquad (157)$$

To simplify, we will use the value of $\Gamma = 0.3$ throughout the analysis. The radius R at given M can be calculated by the relation [377],

$$R = 0.951h^{-1}\,{\rm Mpc}\left(\frac{M}{\Omega_m\, 10^{12}h^{-1}M_\odot}\right)^{1/3}, \qquad (158)$$

where the mass is given in $h^{-1}M_\odot$. The Press–Schechter formalism gives the comoving number density of halos, which can be compared with astronomical data. To this purpose, we calculate the all sky number of halos per unit of redshift

$$\frac{{\rm d}N}{{\rm d}z} = \int {\rm d}\,\Omega\,\frac{{\rm d}V}{{\rm d}z{\rm d}\,\Omega}\int n(M){\rm d}M, \qquad (159)$$

where the comoving volume element per unit redshift is ${\rm d}V/{\rm d}z{\rm d}\,\Omega = r^2(z)/H(z)$ and $r(z)$ is the comoving distance $r(z) = \int_0^z \frac{{\rm d}z'}{H(z)}$.

In the subsequent discussion we do not aim for a precise comparison with data, that would require computationally expensive N-body simulations, but to see in which direction the interaction modifies the cluster number counts. We will study the effect of a homogeneous and an inhomogeneous DE distribution. We will show that when the DE is distributed inhomogeneously, it plays an important role in the formation of structure.

5.3.1. Interaction proportional to the energy density of DE ($\xi_1 = 0, \xi_2 \neq 0$). When the interaction is proportional to the DE energy density, we have shown in section 4 that the curvature perturbation is always stable for both quintessence and phantom DE EoS. In figure 11 we present the results with a constant DE EoS with $\omega_d > -1$. Solid lines correspond to the case when the DE is distributed homogeneously. Figure 11(a) corresponds to $\xi_2 > 0$, i.e. DE decays into DM). In this case, the critical mass density decreases compared with the ΛCDM model; clusters collapse more rapidly than in the concordance model. When DM decays into DE, the threshold of collapse δ_c is higher than in the concordance model, so it is more difficult for an overdensity to collapse. The effect of the coupling is significant and changes cluster number counts. This can be seen in figures 11(b)–(d). For a positive coupling ($\xi_2 > 0$) cluster number counts are larger than in the ΛCDM model but the opposite is true when the coupling is negative ($\xi_2 < 0$).

When the DE is distributed inhomogeneously, we need to consider DE perturbations and their effect in structure formation. In figure 11 these results are shown as dotted lines. In this case, the critical threshold δ_c is slightly larger than the results without DE perturbations. The differences due to the effect of DE inhomogeneities is negligible compared with that of the interaction.

When the DE EoS is $\omega_d < -1$ and the DE distribution is homogeneous, the effect of the interaction on the evolution of critical threshold δ_c and the galaxy number counts is similar to when $\omega_d > -1$. However, when the DE clusters and $\omega_d < -1$,

the number counts are slightly larger than in the homogeneous case, although the differences are negligible, especially at low masses.

Compared with the effect of the interaction, the clustering properties of the DE have a negligible effect in the threshold of collapse δ_c and consequently also in cluster number counts. This is an indication that the fluctuation of DE field σ_d is small. In equation (139), a small value of σ_d leads to $U_{md} \sim U_{dm} \sim U_{dd} \sim T_d \to 0$, implying that the DE plays a very small role in the virialization of the structure. The small effect is a consequence of subhorizon DE perturbations being much smaller than those of the DM [168].

5.3.2. The interaction proportional to the energy density of DM ($\xi_1 > 0, \xi_2 = 0$). In this case, we will only consider stable perturbations, $\omega_d < -1$ since perturbations are unstable if $\omega_d > -1$ (see section 4). We also restrict the coupling to be positive to avoid having DE with a negative energy density at early times [164]. In figure 12 we present our results. Solid lines correspond to homogeneous and dotted lines to inhomogeneous DE distributions. The figure shows that the results for small couplings are similar to ΛCDM; figure 12(c) shows that larger positive coupling leads to higher number of clusters, as expected since δ_c and the ratio $\delta_c(z)/\sigma_8\, D(z)$ are smaller at high redshift for a larger (positive) ξ_1 than for the concordance model. The behavior is consistent with the case when the interaction is proportional to the DE.

When the DE clusters, we need to consider the effect of its perturbations. In this case δ_c is more suppressed at low redshift than in the case of homogeneous DE. The ratio $\delta_c(z)/\sigma_8\, D(z)$, shown in figure 12(b), is also smaller than in the case of homogeneous DE, leading to a larger number of clusters as shown in figure 12(c).

6. Observational tests

As discussed in section 3.2, general constraints on the form of the interaction can be obtained by imposing that at the background level the universe underwent a radiation and a matter dominated periods that lasted long enough as to allow the formation of CMB temperature anisotropies and the emergence of large scale structure, followed by the present period of accelerated expansion. Similar restrictions apply to models of modified gravity [27]. It is more informative to test theoretical predictions with observations. In models without interaction, the effects of DE are more significant at redshifts $z \leqslant 2$ [140], while the interaction extends the effect to larger redshifts and could even alter the sequence of cosmological eras. In this section we will summarize the magnitudes and data most commonly used to constraint DM/DE interacting models.

6.1. Data on the expansion history

Most models are usually too complex to be studied in detail and their viability is first established at the background level. Even at zero order one could expect significant differences on the Hubble expansion between DM/DE interacting models and the concordance model. In interacting models, the DM has an effective equation of state different from zero; the effect of the interaction is not equivalent to an EoS varying arbitrarily with time and the differences on the background evolution is usually first tested to verify the viability of any given model. In this section we will briefly summarize the most common observables, data sets used to this purpose and the constraints imposed on the models described in sections 2 and 3. In table 4 we list the acronyms of the current and future observational facilities that provide the most commonly used data sets.

6.1.1. Luminosity distance tests: constraints from supernovae. Supernovae type Ia (SN Ia) are still the most direct probe of the expansion and of the existence of DE. They are accurate standard candles [326] and have been used to establish that the universe is accelerating at present [281, 313]. By comparing their intrinsic luminosity to the measured flux one obtains a direct estimate of the physical distance to the object. Many SN samples such as ESSENCE [396] SDSS-II [200], CfA3 [178] union-2 [15] are publicly available and continue to be updated. The data tests models at $z \leqslant 1$, where most SNIa have been found. Nevertheless, future surveys will provide SNIa to higher redshifts, like the Wilson SN, the furtherest SNIa to date with a redshift $z = 1.914$, providing stronger constraints on model parameters. In figure 13 we represent the luminosity distances obtained from union-2 sample with their error bars. For comparison, we show the standard ΛCDM model with the cosmological parameters measured by the Planck Collaboration (see table 2) and two fluid models with the same cosmological parameters except an EoS and interaction parameters $\omega = -0.9$ and $\xi = 0.01, 0.1$ (see the definition in equation (14)). The differences between models are rather small, a clear indication of the difficulty of determining the interaction using only luminosity distances.

6.1.2. Angular diameter distance tests. Angular diameter distances, $D_{\rm A} = D_{\rm L}(1+z)^{-2}$, have also been used to constrain the rate of expansion. This distance is computed by measuring the angular size subtended by a standard ruler of known size. In models where the fraction of DE is negligible at recombination, the particle and sound horizons at last scattering [394] are such rulers. The pressure waves that propagate in the pre-recombination photo-baryon plasma imprint oscillations in both the matter and radiation power spectra. The angular scale subtended by the first acoustic peak in the radiation power spectrum has been used to determine the spatial flatness of the universe [184, 185]. The effect of this baryon acoustic oscillations (BAOs) of the matter power spectrum is to imprint a characteristic scale in the clustering of matter and galaxies, which appears in the galaxy correlation function as a localized peak at the sound horizon scale r_s. The angular scale of the comoving sound horizon is $r_s(z_*) = \int_{z_*}^{\infty} c_S\, H^{-1} {\rm d}z$ where $c_S(z)$ is the sound speed of the photon-baryon plasma. The CMB acoustic scale is $l_{\rm A} = \pi(1+z_*)D_{\rm A}(z_*)/r_s(z_*)$, but this distance prior is applicable only when the model in question is based on the standard FRW [214]. The interaction changes

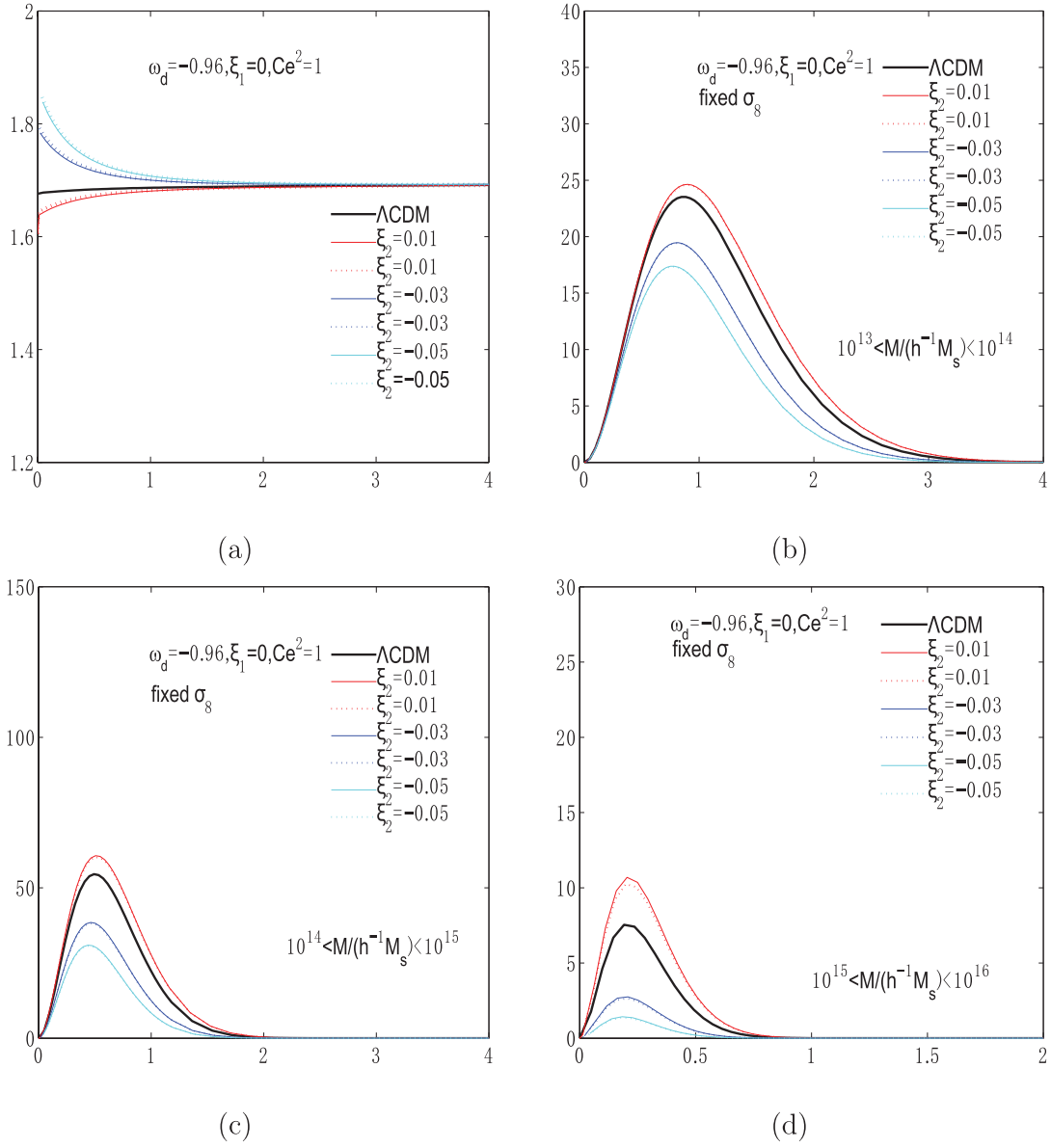

Figure 11. Cluster number counts for an interaction kernel $Q = \xi_2\rho_d$ and DE EoS with $\omega_d > -1$. Solid lines correspond to a DE distributed homogeneously and dotted lines to an inhomogeneous distribution.

the expansion history and the distance to the last scattering surface and the angular scale of the acoustic peaks and the application of the BAO scale to interacting DM/DE models is not straight-forward.

The Planck Collaboration has determined the sound horizon at the drag scale ($z_d = 1020$), assuming a ΛCDM cosmology. The scale relevant for the BAO which is slightly different from the decoupling of the photon-baryon plasma ($z_* = 1090$), is $r_{\rm drag} = 147.60 \pm 0.43$ Mpc [288, 292] (Notice that this magnitude is independent of the Hubble constant). This scale can be measured in the correlation function using galaxy surveys of large volume like the sloan digital sky survey (SDSS) [128]. Since the observed galaxy coordinates are angles and redshifts, the conversion of coordinate separations to comoving distances will depend on the angular diameter distance $d_{\rm A}(z)$ and the expansion rate $H(z)$. Errors on the two quantities are correlated, and in the existing galaxy surveys the best determined combination is approximately an average of the radial and angular dilation scale, $D_V(z)$, defined in [128] as $D_V = [(1+z)^2 D_{\rm A}^2 zc/H(z)]^{1/3}$. BAO data have been used by [169] to constrain DM/DE models. In figure 14 we represent the distance scale $r_{\rm drag}/D_V(z)$ obtained from different data sets: 2dFGRS [278], 6dFGRS [64, 66], SDSS-III [279, 323], SDSS MGS [317], BOSS 'low-z' and CMASS surveys [30, 90] and WiggleZ [65, 68, 198]. In addition, we represent the concordance LCDM model and two interacting DM/DE fluid models as in figure 13.

As an alternative to the sound horizon, the CMB shift parameter $R = \sqrt{\Omega_m}\int_0^{z_{\rm ls}} E(z')^{-1}{\rm d}z'$ has been used a standard ruler. In this expression $z_{\rm ls}$ is the redshift of the last scattering surface and $E(z)$ is given in equation (6). This parameter has been measure to be $R = 1.725 \pm 0.018$ [383] from WMAP [179, 214] and has been applied in the literature to test interacting models. [133, 134, 164, 248, 249].

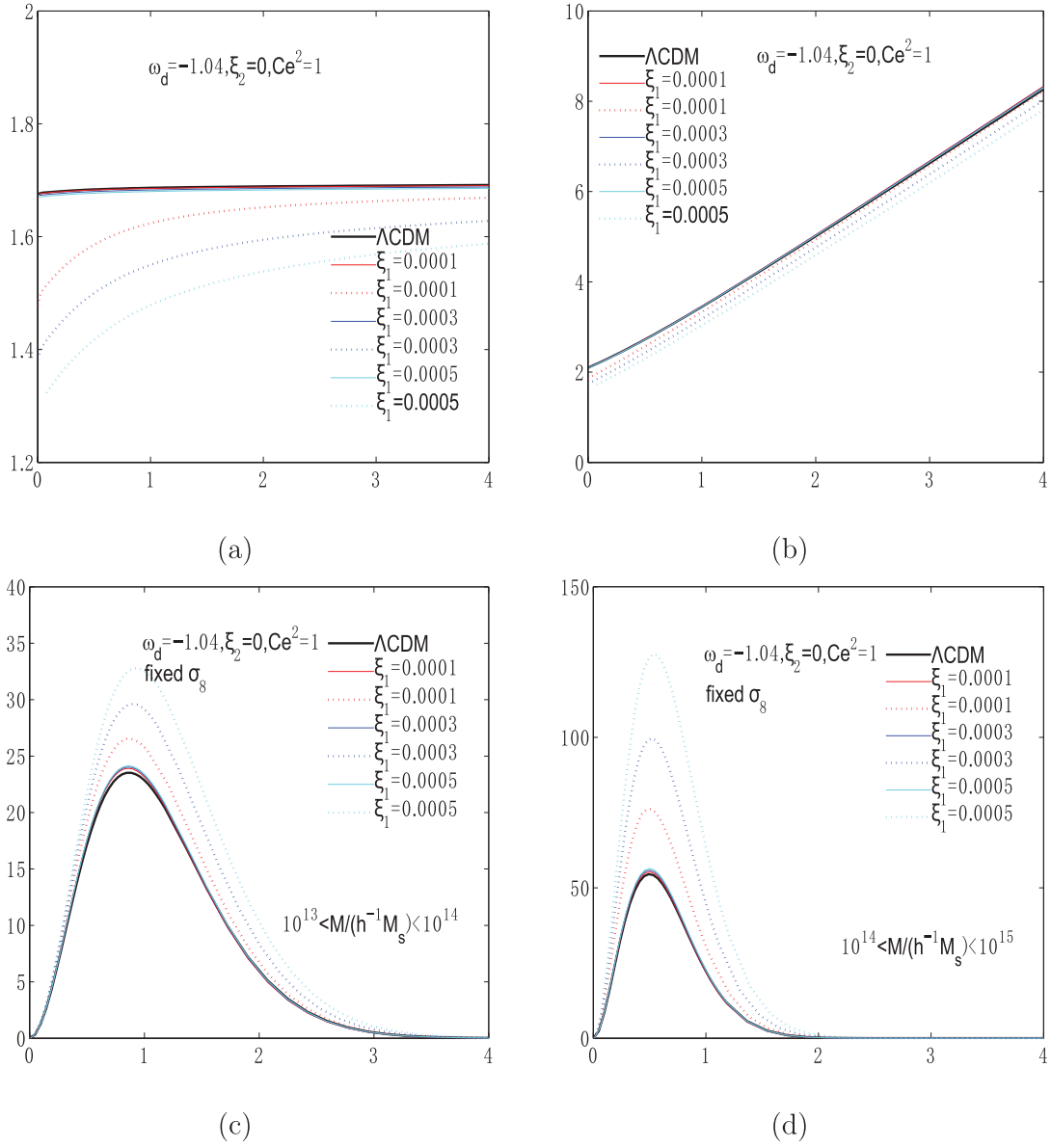

Figure 12. Cluster number counts with an interaction kernel $Q = \xi_1 \rho_c$. Solid lines correspond to a homogeneous DE distribution and dotted lines to the inhomogeneous case.

6.1.3. Expansion rate, look-back time and age. The interaction modifies the rate of expansion of the universe and changes the Hubble parameter and the age of astronomical objects as a function of redshift compared with the concordance model. Data on the Hubble expansion has been derived from the differential ages of old, passively evolving, galaxies [345] or from the spectra of red galaxies [353]. The data provide a measurement of the expansion rate of the universe in an almost model independent way [173]. A direct measurement of $H(z)$ was obtained by [145] using the 2-point correlation of sloan digital sky survey luminous red galaxies and taking the BAO peak position as a standard ruler in the radial direction and is independent of the BAO measurements of [279]. In [163] the age of a quasar at $z = 3.91$ was estimated to be $t_{\rm quasar} \leqslant 2.1$ Gyr and this value has been used to constrain cosmological models [138]. In [381] and [127] it was argued the age of this quasar favors the existence of an interaction. In figure 15 we represent the value of the Hubble expansion as a function of redshift measured from different data from BOSS [101, 260, 324] and WiggleZ [69]. These data has been compiled by [130] and [137] and are represented with triangles. Also included is data from [173] (diamonds) derived using SNIa, BAO data from figure 14 and expansion data from [373]. Lines show the prediction for the models of figure 13.

The look-back time (see section 1.2) can also be used to constrain models. In [190] and [345] the ages of 35 and 32 red galaxies are respectively given. For the age of the universe one can adopt $t_0^{\rm obs} = 13.73 \pm 0.12$ Gyr [213] from e.g. 5 years WMAP data, the seven year data [214] or else the most recent data from Planck, gives $t_0^{\rm obs} = 13.799 \pm 0.013$ Gyr

Table 4. Main current and planned observational facilities.

Acronym	Meaning & url address
2MASS	2-micron all sky survey www.ipac.caltech.edu/2mass
6dFGS	6-degree field galaxy survey www-wfau.roe.ac.uk/6dFGS
ACT	Atacama cosmology telescope www.princeton.edu/act/
BOSS	Baryon oscillation spectroscopic survey www.sdss3.org/surveys/boss.php
CMBPol	Cosmic microwave background polarization cmbpol.uchicago.edu/
COrE	Cosmic origins explorer www.core-mission.org/
CFHT	Canada–France–Hawaii telescope www.cfht.hawaii.edu/
DES	Dark energy survey www.darkenergysurvey.org/
eBOSS	Extended baryon oscillation spectroscopic survey eBOSS www.sdss.org/sdss-surveys/eboss/
Euclid	Euclid satellite, euclid consortium www.cosmos.esa.int/web/euclid/home
HETDEX	Hobby–Eberly telescope dark energy experiment http://hetdex.org/
JDEM	Joint dark energy mission http://jdem.lbl.gov/
J-PAS	Javalambre physics of the accelerating universe astronomical survey http://j-pas.org/
LSST	Large synoptic survey telescope www.lsst.org/lsst/
Pan-STARSS	Panoramic survey telescope and rapid response system www.ps1sc.org/
Planck	Planck satellite, Planck Collaboration www.cosmos.esa.int/web/planck/pla
PRISM	Polarized radiation imaging and spectroscopy mission www.prism-mission.org/
SDSS	Sloan digital sky survey www.sdss3.org/
SKA	Square kilometre array www.skatelescope.org/
SNAP	Super nova acceleration probe http://snap.lbl.gov/
SPT	South pole telescope https://pole.uchicago.edu/
WFIRST	Wide field infrared survey telescope http://wfirst.gsfc.nasa.gov/
WMAP	Wilkinson microwave anisotropy probe http://lambda.gsfc.nasa.gov/

[296] (actually, we cannot go that far in precision, considering the interaction, the above values being model dependent). Although this estimate for $t_0^{\rm obs}$ has been obtained assuming a ΛCDM universe, it does not introduce systematic errors in our calculation. Any such errors eventually introduced would be compensated by adjusting df, in equation (9). On the other hand, this estimate is in perfect agreement with other values, which are independent of the cosmological model, as for example $t_0^{\rm obs} = 12.6^{+3.4}_{-2.4}$ Gyr, obtained from globular cluster ages [216] and $t_0^{\rm obs} = 12.5 \pm 3.0$ Gyr, obtained from radioisotopes studies [92].

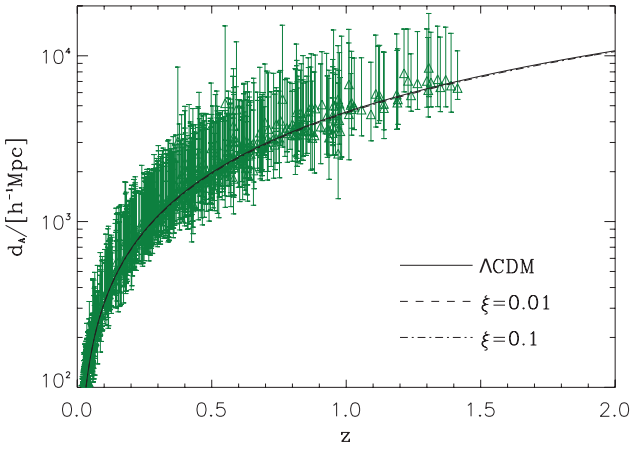

Figure 13. Luminosity distances derived from SNIa union 2 sample data. The sample can be downloaded from http://supernova.lbl.gov/Union/. As illustration, solid, dashed and dot–dashed lines represent the luminosity distance of the concordance model with the cosmological parameters measured by the Planck Collaboration and a fluid DM/DE model with $\omega = -0.9$ and different interaction parameter.

6.1.4. Cluster number counts. The cluster mass function and cluster redshift distribution probe the late time evolution of the universe and the associated DE effects (see section 5.3). These observables provide specific signatures of DM/DE interaction and the existence of DE inhomogeneities [45, 166]. Also, high resolution simulations of LSS formation show significant differences in the mass function between DM/DE models and Λ CDM [357]. Cluster counts are exponentially sensitive to the properties of the DE but their effectiveness relies in obtaining good estimators of the cluster mass. They could be used to constrain the properties of DE if the evolution in the relationship between observable quantities and the cluster mass can be calibrated [234]. Cluster surveys such as those of DES, SPT, WFirst, Euclid or e-Rosita, detecting about 10^4 clusters out to redshifts $z = 2$ would provide enough statistics to constrain/measure $\Omega_{\rm DE}$, $w_{\rm DE}$ with 3% and 6% accuracy [233]. The dependence of cluster abundances and DM/DE coupling has been studied in [166, 242] who found that increasing the coupling reduces significantly the cluster number counts, and that DE inhomogeneities increases cluster abundances. Wiggles in cluster number counts were shown to be a specific signature of coupled DE models. The interaction can significantly enhance the probability to observe very massive clusters at redshifts $z \geqslant 1.4$, that are very unlikely in the concordance model [41].

Observationally, cluster counts from the Planck Collaboration show the data is not in full agreement with the concordance model. In 2013, the Planck Collaboration described a tension between the constraints on Ω_m and σ_8 from cluster counts and those from the primary CMB in the concordance model [291], result confirmed by the analysis of the latest data [297]. At present, it is unclear if the tension arises from low-level systematics in the data or is an indication of new physics;

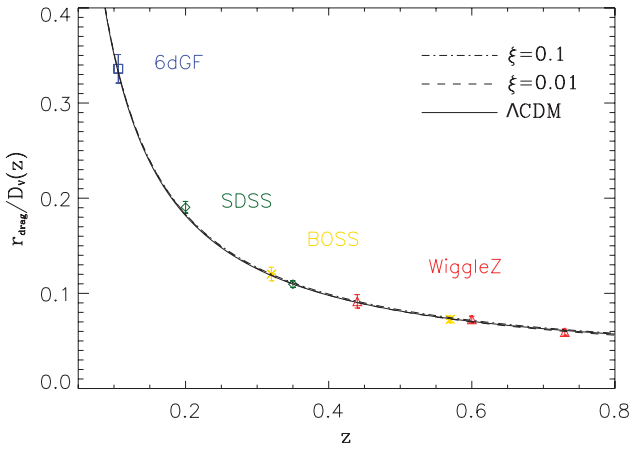

Figure 14. Ratio of the BAO drag scale to the angle-averaged dilation scale $D_V(z)$. The 6dFGS data is from [64] (blue), the SDSS from [279, 317] (green), the BOSS from [30] (gold) and WiggleZ from [198] (red). Like in figure 13 solid, dashed and dot–dashed lines corresponds to the theoretical prediction of the concordance model and the interacting DM/DE model IV for different interaction parameters.

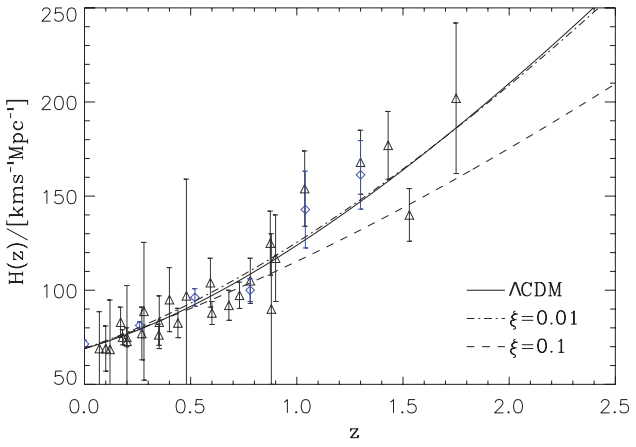

Figure 15. Hubble factor as a function of redshift. The data has been taken from [173, 260], [101] and [324] from the baryon oscillation spectroscopic survey data release 7, 9 and 11, respectively, [69] (at $z = 0.44, 0.6, 0.73$) using data from WiggleZ DE Survey. Black triangles correspond to the data from the compilation of [130] and [137] while diamonds are given in [173]. Lines correspond to model predictions and follow the same conventions as in figure 13.

unstable DM models help to ease the tension [60] and could be more easily accommodated in interacting quintessence models.

6.1.5. The Sandage–Loeb test. The Sandage–Loeb test provides a direct measurement of the expansion of the universe by measuring the redshift drift of extra-galactic sources. The test was first proposed in [327] and it was shown to be feasible using the spectra of distant quasars at the redshift interval $z = [2, 5]$ [237]. Measuring the redshift drift of quasar spectra would be useful to determine the cosmic expansion history on a redshift interval where other DE probes are unable to provide useful information [108]. The data would be helpful to break the degeneracy between the values of Ω_m and H_0 existing in BAO, SNIa and CMB data [147], to constrain the equation of state parameter of DE and, consequently, also constrain any possible DM/DE interactions at those redshifts [148]. Monte Carlo simulations of data taken with high resolution spectrographs using ~ 40 m telescopes have been carried out to show how these observations would constrain DM/DE interactions [149]. As we indicate in section 8.1.3 this test could be within reach of the forthcoming generation of observational facilities.

6.1.6. Equivalence principle tests. The interaction between DM and DE produces a violation of the equivalence principle between baryons and DM. The DE modifies the gravity felt by the DM particles. At Newtonian scales, the interaction simply renormalizes Newton gravitational constant for the DM [115, 262]. The skewness of the large scale structure is a probe of gravitational clustering [273] and can be used to probe violations of the equivalence principle [24]. Moreover, if the DE couples only to DM and not to baryons, as requested by the constraints as imposed by local gravity measurements, the baryon fluctuations develop a constant, scale-independent, large-scale bias which is in principle directly observable [26].

6.2. Constraints from large scale structure

The growth rate of large scale structure is another very sensitive probe of the evolution of the gravitational potential. The transition from a matter dominated universe to a period of accelerated expansion freezes the growth of matter density perturbations [44, 274]. The interaction modifies the scale-invariant Harrison–Zel'dovich matter power spectrum [162, 410] adding power at large scales [126] and leading to a mismatch between the CMB-inferred amplitude of the fluctuations, late-time measurements of σ_8 [41, 218] and galaxy rotation curves [42].

6.2.1. The growth rate of matter density perturbations. In the concordance model, the vacuum energy is homogeneously distributed within the horizon and only perturbations in the matter fluid are considered. If DE perturbations exist, they affect the evolution of matter perturbations through the gravitational field and are themselves affected by the interaction. The dimensionless growth rate is defined as $f = \mathrm{d}\ln\Delta_c/\mathrm{d}\ln a$ where Δ_c is the growth factor as discussed in section 4, it is customary to express in terms of the growth index as $f(\Omega_m) \simeq \Omega_m^{\gamma(\Omega_m)}$ [275]. In most models of DE, structure formation stops when the accelerated expansion begins. By contrast, the coupling of DE to DM can induce the growth of perturbations even in the accelerated regime [26, 262]. Depending on the parameters, the growth may be much faster than in a standard matter-dominated era. Then, the growth index γ probes the nature of DE and can discriminate between models [127, 168, 236, 329, 366]. Data on the product $f(z)\,\sigma_8(z)$ of the growth rate $f(z)$ of matter density perturbations and the redshift-dependent rms fluctuation of the linear matter density field σ_8 has been compiled by [46]. This estimator is (almost) model independent [350]. The Euclid satellite is expected to measure the growth factor within 1 to 2.5% accuracy for each of 14 redshift bins in the interval of redshifts $[0.5 - 2]$ [29]

(see section 8.2.2). A model independent test to probe possible departures from the concordance model at perturbation level was proposed in [256] and found that if the data on the growth factor was free of systematics, it was in conflict with the concordance model.

There are also effects at high redshifts. Due to the interaction the growth rate of matter density perturbations during the radiation dominated regime is slower compared to non-interacting models with the same ratio of DM to DE today. This effect introduces a damping on the power spectrum at small scales proportional to the strength of the interaction similar to the effect generated by ultra relativistic neutrinos [262]. The interaction also shifts matter-radiation equality to larger scales [126].

In figure 16 we present a compilation of growth factor data from different surveys, measured in units of the amplitude of the matter power spectrum at $8h^{-1}$ Mpc, σ_8 [64, 101, 181, 198, 243, 260, 363]. The different lines correspond to the concordance model and a DM/DE interacting fluid model with EoS parameter $\omega_d = -1.1$. The interaction parameters are given in the figure.

6.2.2. Redshift space distortions. The growth of LSS induces galaxy peculiar velocities, i.e. coherent flows of galaxies towards matter overdensities. When redshifts are used to map galaxy positions, the reconstructed spatial distribution of objects is distorted in the radial direction, effect known as redshift space distortions (RSD). On large scales galaxies trace the linear growth of cosmological structures enhancing the amplitude of the 2-point correlation function; on small scales virialized structures are elongated along the line of sight. The amplitude of the former effect is directly proportional to the logarithmic growth rate of density fluctuations $f_m(z) = \mathrm{d}\ln\delta(a)/\mathrm{d}\ln a$ [160, 193]. The recent RSD measurements [67, 238, 324] indicate values smaller than the ΛCDM prediction. Analysis of the BOSS sample using RSD has yielded the tightest constraints to date on the growth rate of structure [309]. In [250] the cross-correlation between galaxies and galaxy groups was used to measure RSD as a probe of the growth rate of cosmological structure.

6.2.3. The Alcock–Paczynski test. Alcock and Paczynski (A–P) test expresses the idea that if one assumes the wrong cosmological model to convert redshift measurements to distances, an intrinsically spherical object or pattern comoving with the Hubble flow will appear ellipsoidal [14]. The distortion is proportional to $D_A(z)$ and $H(z)$. The BAO is an example of the A–P test but with an object of a known size [201]. The test is partially degenerate due to the apparent ellipticity of clustering caused by RSD. Although the two effects have a different dependence with scale, with a sufficient large volume one could expect to separate them [246].

6.3. Constraints from CMB temperature anisotropies

The cosmic microwave background is the main source of information on the physics of the early universe. The different time evolution of the gravitational potentials in interacting models induces several effects that change the radiation power spectrum with respect to the concordance model. Baryons and DM evolve differently, affecting the ratio between the odd and even peaks [22]. The change of the potential modifies the lensing B-mode contribution [21]. The sound speed of gravitational waves is also modified and it affects the amplitude of the primordial B-mode [307]. The damping tail of the radiation power spectrum varies, providing a measurement of the abundance of DE at different redshifts [83, 308]. Comparing models with data requires to follow the evolution of all energy density components by solving the perturbation equations from some early time [18, 23, 261, 263].

CMB temperature anisotropies have been measured by several experiments out to $\ell = 3000$ [58, 287, 344, 354]. Earlier studies on DM/DE interaction used WMAP, and additionally other data sets on CMB temperature anisotropies, to set upper limits on the strength of the DM/DE coupling [110, 111, 144, 167, 169, 170, 261, 263, 283, 321, 369, 371, 398] or to constrain the cross-section of DM/DE interactions [401]. More recently, Planck CMB data have been used to constrain interacting models with different kernels discussed in the literature: $Q = H\xi_1\rho_c$ [110, 372], $Q = H\xi_2\rho_d$ [72, 110, 404, 405, 406], $Q = H(\xi_1\rho_c + \xi_2\rho_d)$ [110, 135, 302]. Other couplings have also been discussed; [322] has shown that the data provides a moderate Bayesian evidence in favor of an interacting vacuum model. Nevertheless, since CMB temperature anisotropy data probes the DM density at the time of last scattering, i.e. at redshift $z \sim 1100$ while the interaction preferentially modifies the evolution between the last scattering surface and today, the data is degenerate with respect to $\Omega_c h^2$ and the interaction rate and complementary data sets are required to break the degeneracy such as baryon acoustic oscillations, supernova data, the growth of matter density perturbations and the ISW discussed below [102, 166, 371, 400].

Data on temperature anisotropies, covariance matrices, window functions likelihoods and many other resources are publicly available[5]. As an illustration, in figure 17 we plot the radiation power spectrum measured by the Planck Collaboration (red and green) [292] and the south pole telescope [354] (blue). For comparison, we also superpose the model predictions for the concordance ΛCDM model and the interacting DM/DE fluid model. In model I the EoS parameter is $\omega = -0.9$ when the kernel is proportional to the DE density and $\omega = -1.1$ when it is proportional to the DM density.

6.3.1. The ISW effect. The decay of the gravitational potential affects the low-multipoles of the radiation power spectrum by generating ISW temperature anisotropies [184, 208, 318]. These anisotropies are generated by evolving gravitational potential at the onset of the accelerated expansion and change with the interaction [167, 170]. The contribution to the radiation power spectrum due to the evolution of the gravitational potential at low redshifts is given by equation (109). The ISW effect at low redshifts is generated by local structures, the spatial pattern of ISW anisotropies will correlate with

[5] All data products can be downloaded from http://lambda.gsfc.nasa.gov/product/

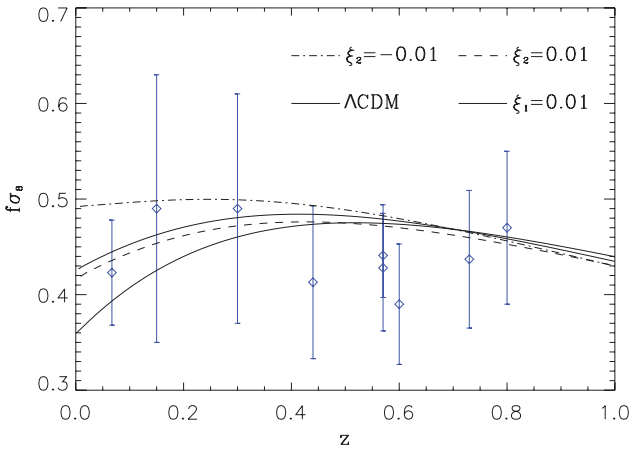

Figure 16. Growth factor data in units of σ_8, obtained from different surveys: 6dF [64] ($z = 0.067$), [181] ($z = 0.15$), SDSS DR7 [260] ($z = 0.3$) and SDSS DR9, [101] ($z = 0.57$) and VIPERS [363] ($z = 0.8$). Lines correspond to the concordance model and a DM/DE interacting fluid model with EoS parameter $\omega_d = -1.1$ with different interaction parameters.

the distribution of the large scale structure and the cross-correlation with a template of the matter distribution is given by equations (109) and (110) [113]. Several groups looked for evidence of ISW effect by cross-correlating the WMAP data with templates built from different catalogs [73, 257]. The ISW signal at the position of superclusters is larger than expected in the ΛCDM model [158]. An update of these earlier results have been carried out by the Planck Collaboration that reported a $\sim 4\sigma$ detection of the ISW effect [290] and confirmed the previously mentioned ISW anomaly. Since the DM/DE interaction damps the growing mode of the Newtonian potential faster compared to models with no interaction, it enhances the ISW effect [151]. Comparison of the fraction of DE measured in CMB temperature maps with the fraction obtained from the ISW effect would provide a direct evidence of DM/DE interaction [264]. The Planck Collaboration constrained the vacuum energy density to be $0.49 < \Omega_\Lambda < 0.78$ at the 68% confidence level compatible with the concordance model but also in agreement with interaction models with $\xi \leqslant 0.01$ [264]. Similar constraints but on a different coupling were obtained by [240, 331, 398].

6.3.2. Constraints from peculiar velocities. The interaction does not only change the time evolution of the gravitational potentials. It also changes the potentials themselves [262]. Since the gravitational potential gives rise to peculiar motions, the interaction, in turn, will modulate peculiar velocities of baryons and their effect on the CMB temperature anisotropies. The correlation of spatial variations in the distribution of galaxy luminosities with the peculiar velocity field has been shown to be a powerful test of gravity and dark energy theories on cosmological scales [132]. In addition, while in the concordance model baryons trace the DM distribution in the linear regime, in DM/DE interacting models baryons do not follow DM as closely due to the DE inertial drag on the DM [166]. Peculiar velocities modify temperature fluctuations on the CMB at small scales via the conventional Kinetic Sunyaev–Zel'dovich (kSZ) effect [355] generated by the ionized gas in the diffuse intergalactic medium and in the potential wells of galaxy clusters. Large scale flows have been detected in WMAP [195, 196] and Planck [36] data, the pairwise velocity dispersion of the unresolved cluster population has been measured [161] and the kSZ radiation power spectrum has been constrained using the data on CMB temperature anisotropies [150, 293]. In [402] it was determined that peculiar velocities could be between five times smaller and two times larger than in the concordance model and showed that peculiar velocities could provide constraints stronger than those derived from the ISW effect. The evidence of interaction between dark sectors in the kSZ observations were discussed in [402].

6.4. Gravitational lensing

The effect of lensing is to remap the CMB fluctuations. The effect is parameterized in terms of the lensing potential φ [226],

$$\varphi(\hat{n}) = -2\int_0^{\varsigma_{\rm rec}} \mathrm{d}\varsigma \frac{\varsigma_{\rm rec}-\varsigma}{\varsigma_{\rm rec}\,\varsigma}\Psi(\varsigma\hat{n};\tau_0-\tau), \qquad (160)$$

itself a function of a gravitational potential Ψ. The observed anisotropy in direction $\hat{n}$ is the unlensed (primordial) anisotropy in the direction $\hat{n}+\nabla\varphi(\hat{n})$; ς is the conformal distance, τ the conformal time, τ_0 the conformal time at present and the integration is carried out up to recombination. This expression assumes that the universe is spatially flat. The lensing potential power spectrum probes the matter power spectrum up to recombination [10]. It is also sensitive to the growth index [348]. The *Planck* satellite has measured the lensing potential using data on temperature and polarization anisotropies with a statistical significance of 40σ and has released an estimate of the lensing potential over approximately 70% of the sky, in band powers for the multipole range $40 \leqslant \ell \leqslant 400$ and with an associated likelihood for cosmological parameter constraints [295]. The data reveals some tension with the concordance ΛCDM model: the lensing amplitude is $A_{\rm L} = 1.22 \pm 0.10$, which is in 2σ tension with the amplitude of the CMB spectrum reconstructed from lensing deflection angle spectrum, $A_{\rm L}^{\phi\phi} = 0.95 \pm 0.04$ while both quantities should be unity in the concordance model. In [186] it was argued that some models whose effective Newton gravitational constant is larger than that in ΛCDM could explain the discrepancy. However, in order to lens the CMB anisotropy, the growth of matter density perturbation needs to be enhanced, giving a value of σ_8 larger than the measured value. A full non-linear study of gravitational lensing on different cosmological models is still lacking. In [88, 265] the impact of the DM/DE coupling on weak lensing statistics was analyzed by constructing realistic simulated weak-lensing maps using ray-tracing techniques through a suite of N-body cosmological simulations. Model-independent constraints on the growth function of structure and the evolution of the DE density can be obtained from the reconstruction through lensing tomography [183] and further information can be obtained from the power spectra and cross-correlation measurements of the weak gravitational lensing

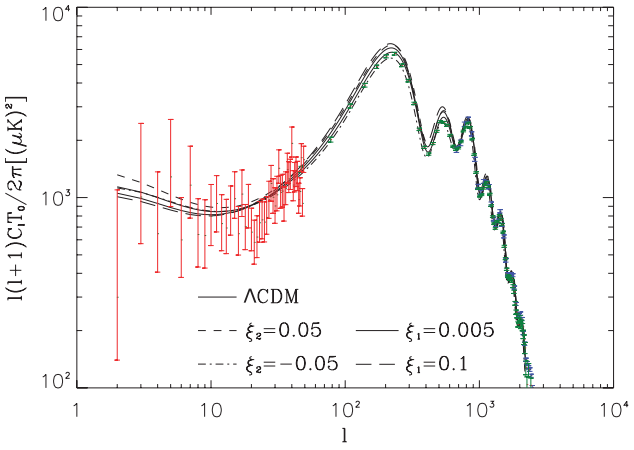

Figure 17. Radiation power spectrum from Planck (low multipoles red and high multipoles in green) and the south pole telescope (blue). Planck data can be downloaded from the Planck legacy archive www.cosmos.esa.int/web/planck/pla and the latest compilation of SPT data (as of May 2014) can be downloaded from http://pole.uchicago.edu/public/data/story12/index.html. Lines correspond to the theoretical model predictions for the concordance ΛCDM model and the interacting DM/DE fluid model. In this case, the EoS parameter is $\omega_d = -0.9$ when $\xi_2 \neq 0$ and $\omega_d = -1.1$ when $\xi_1 \neq 0$.

in the CMB and from the cosmic shearing of faint galaxies images [182].

6.5. Model selection statistics

The data sets described above are not exclusively tests of interacting DE models. Fitting data to the model predictions to determine/constrain its parameters is not sufficient to establish the validity of the model. The concordance model requires only the energy density associated to the cosmological constant to explain the current period of accelerated expansion. Interacting DE models require at least two additional parameters: the DE EoS and the DM/DE coupling constant. Further improvement on the available data sets will help as to constrain/measure the cosmological parameters with higher accuracy. Equally important is the inference problem of deciding what set of parameters is needed to explain any given data, known as model selection [231]. Adding extra parameters necessarily improves the fit to the data at the expense of reducing the predictive power of the model [230]. The purpose of model selection statistics is to address whether the improved fit favors the introduction of extra parameters. The most commonly used criteria are the Akaike information criterion (AIC) [12] and the Bayesian information criterion (BIC) [333]. If $\hat{\mathcal{L}}(\theta)$ is the maximum of a likelihood function of a model of θ parameters, N the number of data points and k the number of parameters to be estimated from the data, then

$$AIC = 2k - 2\ln\hat{\mathcal{L}}(\theta); \qquad BIC = -2\ln\hat{\mathcal{L}}(\theta) + k\ln N. \tag{161}$$

Information criteria penalize the introduction of new parameters that do not significantly improve the quality of the fit. For instance, if adding an extra parameter reduces the BIC by 2–6 units, the data shows a positive evidence in favor of the new parameter being required to explain the data; if the decrement is 6–10, the evidence is called strong and if it is larger than 10, very strong [230]. The BIC generally penalizes the number of parameters more strongly than the AIC, although it depends on the number of data points N and parameters k.

7. Observational constraints on specific models

Determining the properties of interacting DE/DM models requires the use of all the available observational data, combining different probing techniques described in section 6 and has been extensively considered in the literature [16, 20, 52, 134, 248]. Comparisons with the CMB data using WMAP and Planck results have also been carried out [110, 261, 263, 321]. Further constraints, relying on cluster properties [2, 3] as well as structure formation [166], age constraints and other properties [5, 343, 372, 381] have also been discussed.

In this section, we will review the constraints that observations have imposed on some specific models. Since the data is constantly evolving, not all the models have been tested using the most recent data.

We will first go over the constraints obtained by using the observational data on the universe expansion history. Those data are not only obtained from distance based methods such as the SN data, but also obtained based on time-dependent observables for instance the age estimates of galaxies. We will combine four fundamental observables including the new 182 Gold SNIa samples [315], the shift parameter of the CMB given by the three-year WMAP observations [383], the BAO measurement from the SDSS [128] and age estimates of 35 galaxies provided in [328, 345] to perform the joint systematic analysis of the coupling between dark sectors.

Furthermore we will review the constraints on the interacting DE models by employing the data from the CMB temperature anisotropies together with some other external data described as follows:

(i) CMB temperature anisotropies: From the 2013 Planck data release we use the high-ℓ TT likelihood, which includes measurements up to a maximum multipole $\ell_{\rm max} = 2500$, combined with the low-ℓ TT likelihood, which includes measurements in the range $\ell = 2$–49 [286, 293] (figure 17). We also include the polarization measurements from WMAP 9 yr [58], in particular the the low-ℓ ($\ell < 32$) TE, EE and BB likelihoods.

(ii) BAO: We combine the results from three data sets of BAO: the 6DF at redshift $z = 0.106$ [64], the SDSS DR7 at redshift $z = 0.35$ [266] and the SDSS DR9 at $z = 0.57$ [30] (figure 14)

(iii) SNIa data: The supernova cosmology project (SCP) union 2.1 compilation [358] with 580 measured luminosity distances (figure 13)

(iv) Hubble constant data: Finally we also include the Hubble constant $H_0 = 73.8 \pm 2.4$ km s^{-1} Mpc^{-1}, measured by [316]. This value is in tension with the result of the Planck Collaboration [286, 292], so the constraints derived using H_0 could be shifted slightly if a different value is used.

We will limit the study to models with $\Omega_k = 0$; our numerical calculations have been performed using the CMBEASY [124] and CAMB [224] codes. We modified the codes to include the effect of the DM/DE coupling at the background and perturbation level. To compare the theoretical predictions with observations, we perform Monte Carlo Markov Chain (MCMC), using a modified version of the CosmoMC program [225, 226].

7.1. Constraints on the phenomenological interaction from the universe expansion history

In this section we examine different phenomenological interaction models between DE and DM by performing statistical joint analysis with observational data arising from the 182 Gold type Ia SN samples, the shift parameter of the CMB given by the three-year WMAP observations, the BAO measurement from the SDSS and age estimates of 35 galaxies. We compare the compatibility of these data sets. Especially we find that including the time-dependent observable, we can add sensitivity of measurement and give complementary results for the fitting. The complementary effect of adding the time observable was also noticed by using the lookback time data from [285]. Detailed analysis of our result can be found in [133].

We do not specify any special model for DE, but consider as an example the commonly used DE EoS parametrization $\omega_d(z) = w_0 + \frac{w_1 z}{(1+z)^2}$. After employing the MCMC method to explore the parameter space, we obtain the constraints on the model parameters in the table 5 when the coupling between DE and DM is taken proportional to energy densities of DM, DE and total dark sectors (T), respectively. For the chosen EoS, the priors on the model parameters are $-10 < w_0 < 10$, $-15 < w_1 < 15, 0 < \Omega_m < 0.8, -1 < \xi_i < 1$.

In [133] it was argued that adding the age constraint, the coupling between DE and DM tends to be a small positive value which gives more compatibility among different data sets. We will see below that this result is consistent with the constraints obtained by using the CMB temperature anisotropies and other external observations.

7.2. Field description of the interaction between DE and DM

In section 2 we presented a field description of DM, DE and their interaction. In figure 18 we present the results of the likelihood analysis for a DE described as an scalar field with an exponential potential $V(\varphi) = Ae^{-\lambda\varphi/M_{pl}}$ and an interaction of the linear type: $F(\varphi) = M - \beta\varphi$ (see section 2.5). The influence of the fermionic mass M and the Yukawa coupling β is degenerate and both parameters can not be fit simultaneously. Let us define $\varrho = \beta/M$ to represent the amplitude of the Yukawa coupling in units of the fermionic mass. Only this parameter will be constrained by the observations. This approach has the advantage of decreasing one degree of freedom. The cosmological parameters have similar values to those in the concordance model. The constraint is much weaker on the parameter of the DE self-interaction potential λ. For Planck data alone the likelihood of interaction parameter r is almost symmetric around zero. Adding low redshift data, λ tends to its lower limit, while r breaks the symmetry around zero. Including BAO, SNIa and H_0, a null interaction is disfavored and the likelihood of ϱ shows a preference for negative values.

Furthermore it was found [111] that if we can determine the scalar potential parameter λ, for example if we have a theoretical model to fix it as a large value, we observe that the Yukawa interaction between DE and DM can be preferred by the cosmological data. This shows that the field description of the interaction between DE and DM is compatible with observations. In addition, the best fit value of the cosmological parameter that we have obtained helps to alleviate the coincidence problem, since there will be more time for the DM and DE energy densities to become comparable. This will be discussed further at the end of this section.

Discussions on how to break the degeneracy of the model parameters when the DE is described as a k-essence scalar field can be found in [248]. For more general discussion on the constraints of the non-minimally coupled k-essence DE models, readers are referred to [294].

7.3. Phenomenological description of the interaction between DE and DM

The phenomenological description of the interaction between dark sectors was introduced in section 2 and the linear perturbation theory of the model was discussed in section 4. For the sake of simplicity in our subsequent discussion, we will review only models with a DE EoS parameter $\omega_d = \text{const.}$. The results for a variable EoS have been reported in [302, 400]. We restrict our analysis to the models that satisfy the stability condition (section 4.2). The interaction kernels were summarized in table 3.

The results of the MCMC analysis using different data sets are shown in figure 19. When the coupling is proportional to the energy density of the DE, the data constrain the value of the interaction parameter to be in the range $-0.3 \leqslant \xi_2 \leqslant 0.1$. When the coupling is proportional to the energy density of the DM or the total energy density of the dark sector, the constraint is much tighter and the coupling are positive at the 68% confidence level (CL). Including additional data tightens the constraints on the cosmological parameters compared with the CMB data alone. Results for different models can be found in [2, 3, 23, 61, 110, 129, 133, 134, 157, 167, 169, 180, 228, 229, 244, 255, 321, 322, 371, 381, 398–401, 407]. The conclusion of these analyses is that they are in agreement with those obtained from temperature anisotropies of the CMB by [294]. Evidence of the existence of interaction but with a low CL was given in [322].

7.4. High redshift evidence for interacting DE

The effect of a dynamical DE component and of a DM/DE interaction is easier to be established at high redshift. Recently, the analysis of BOSS data presented evidence against the concordance model by measuring the BAO in the

Table 5. Parameters at 68.3% confidence level.

Coupling	EoS	w_0	w_1	Ω_m	$\xi/\xi_1/\xi_2$
T	ω_d	$-1.50^{+0.31}_{-0.30}$	$3.90^{+2.09}_{-2.31}$	$0.26^{+0.02}_{-0.02}$	$0.01^{+0.03}_{-0.03}$
DM	ω_d	$-1.50^{+0.32}_{-0.31}$	$3.91^{+2.12}_{-2.34}$	$0.25^{+0.02}_{-0.02}$	$0.01^{+0.04}_{-0.04}$
DE	ω_d	$-1.49^{+0.31}_{-0.30}$	$3.78^{+2.13}_{-2.39}$	$0.26^{+0.02}_{-0.02}$	$0.05^{+0.06}_{-0.10}$

redshift range $2.1 \leqslant z \leqslant 3.5$ from the correlation function of the Lyα forest from high redshift quasars [121]. Their result indicates a 1.8σ deviation (from *Planck* + WMAP) and 1.6σ deviation (from ACT/SPT) from ΛCDM at $z = 2.34$. While the statistical evidence is still not significant, if confirmed, this result cannot be explained by a dynamical DE component. An interacting DE appears as a simple and efficient solution to explain the BOSS result. If DE and DM interact and the former transfers energy to the latter, as required to alleviate the coincidence problem (see section 2.7) and indicated by the data [110], it would explain the value of the Hubble parameter, $H(z = 2.34) = 222 \pm 7$ km s^{-1} Mpc^{-1}, smaller than the expected value in ΛCDM [135]. Let us now briefly summarize which of the models given in table 3 can explain better the BOSS result.

Let us consider a universe filled only with DM, DE and baryons. We can use the Hubble parameter obtained from the Friedmann equation and compare it with the value obtained by the BOSS collaboration for different sets of cosmological parameters. We can also compare the constraints for $H(z = 2.34)$ and $D_A(z = 2.34)$ given by the BOSS experiment with constraints from CMB adjusted data using ΛCDM and the interaction model. To carry out this analysis we need to establish first the evolution with redshift of the energy densities of each component, specially DE and DM since due to the interaction they are not independently conserved. For the models I and II, they behave as [164]

$$\rho_d = (1+z)^{3(-1+\omega_d+\xi_2)}\rho_d^0,$$
$$\rho_c = (1+z)^3\left\{\frac{\xi_2\left[1-(1+z)^{3(\xi_2+\omega_d)}\right]\rho_d^0}{\xi_2+\omega_d}+\rho_c^0\right\}. \qquad (162)$$

The baryonic density is given by the usual expression $\rho_b = \rho_b^0(1+z)^3$. For the model III, the evolution is

$$\rho_d = (1+z)^{3(1+\omega_d)}\left(\rho_d^0+\frac{\xi_1\rho_c^0}{\xi_1+\omega_d}\right)-\frac{\xi_1}{\xi_1+\omega_d}(1+z)^{3(1-\xi_1)}\rho_c^0,$$
$$\rho_c = \rho_c^0(1+z)^{3(1-\xi_1)}. \qquad (163)$$

From these solutions, it is easy to establish that when the energy is transferred from the DE to the DM, the energy density of the DM is always smaller than what it would have been in the standard ΛCDM model. Since ρ_c is the dominant component at redshifts $z \geqslant 1$ and it is smaller than in the concordance model, so it would be the Hubble parameter, as indicated by the BOSS data.

To make the previous statement more quantitative we took two sets of values for the cosmological parameters $\Omega_d^0, \Omega_c^0, \Omega_b^0$ and H_0: (1) the values used by BOSS collaboration, obtained from the Planck Collaboration analysis of the ΛCDM model and listed in table 6, and (2) the values derived by [110] by fitting DM/DE interacting fluid models to the *Planck*, BAO, SNIa and H_0 indicated above. Using both data sets, the Hubble parameter at $z = 2.34$ has been computed using equations (163) and (162) for the cosmological models listed in table 3. The results are shown in figure 20. The right panel corresponds to the cosmological parameters of the BOSS collaboration and the left panel to those of [110]. The figure shows the measured value $H(z = 2.34)$ and its 1σ and 2σ contours. In both panels, the ΛCDM model that corresponds to the case of no interaction is always outside the 1σ CL. While still not statistically significant, it does show that the data prefers an DM/DE interacting model with positive interaction. Further improvements on the data could help to establish the existence of an interaction.

7.5. The coincidence problem

One motivation to study interacting DM/DE models is to alleviate the coincidence problem. The DM/DE ratio r in the ΛCDM model is of order unity only at the present time, requiring a fine-tuning on the initial conditions at the Planck scale of 90 orders of magnitude (see section 1.3.2). Let us examine if when interacting DE models are compared with observations, the goal can be satisfied. We will concentrate on the analysis of the phenomenological fluid model. The results shown in figure 19 suggest that a positive coupling is compatible with the data. Positive values work in the direction of solving the cosmological coincidence problem [164, 167] and similar conclusions have also been reached for the field description of the DE [111]. Let us particularize our analysis for fluid models. In section 2.1.1 we demonstrated that model IV solves the coincidence problem since the DM/DE ratio evolves from an unstable attractor r_s^+ to a stable one r_s^- (see equation (16)). When the coupling is $0 < \xi \ll 1$, the ratios behave asymptotically as

$$r_s^+ \sim \frac{1}{\xi} \quad \text{and} \quad r_s^- \sim \xi, \qquad (164)$$

i.e. the ratios depend on the coupling constant ξ and do not depend on the initial conditions at the Planck scale. This solution of the coincidence problem is illustrated in figure 21. Purple solid lines represent the evolution of the energy densities in units of the critical energy density today, ρ_{cr}^0, with different initial conditions. The density contrast r at present is different for different initial conditions but all the curves are bounded by the two attractors solutions r_s^+ and r_s^-. In this particular case we fixed $\xi = 10^{-4}$ and $\omega_d = -1.05$. During the whole thermal history of the universe, the DM to DE ratio takes values within the range $10^{-4} < r < 10^4$; it changes much less than in the ΛCDM model, thus the cosmological coincidence problem is greatly alleviated.

8. Current and future observational prospects

The discovery that the expansion of the universe is accelerating has led to a large observational effort to understand its origin.

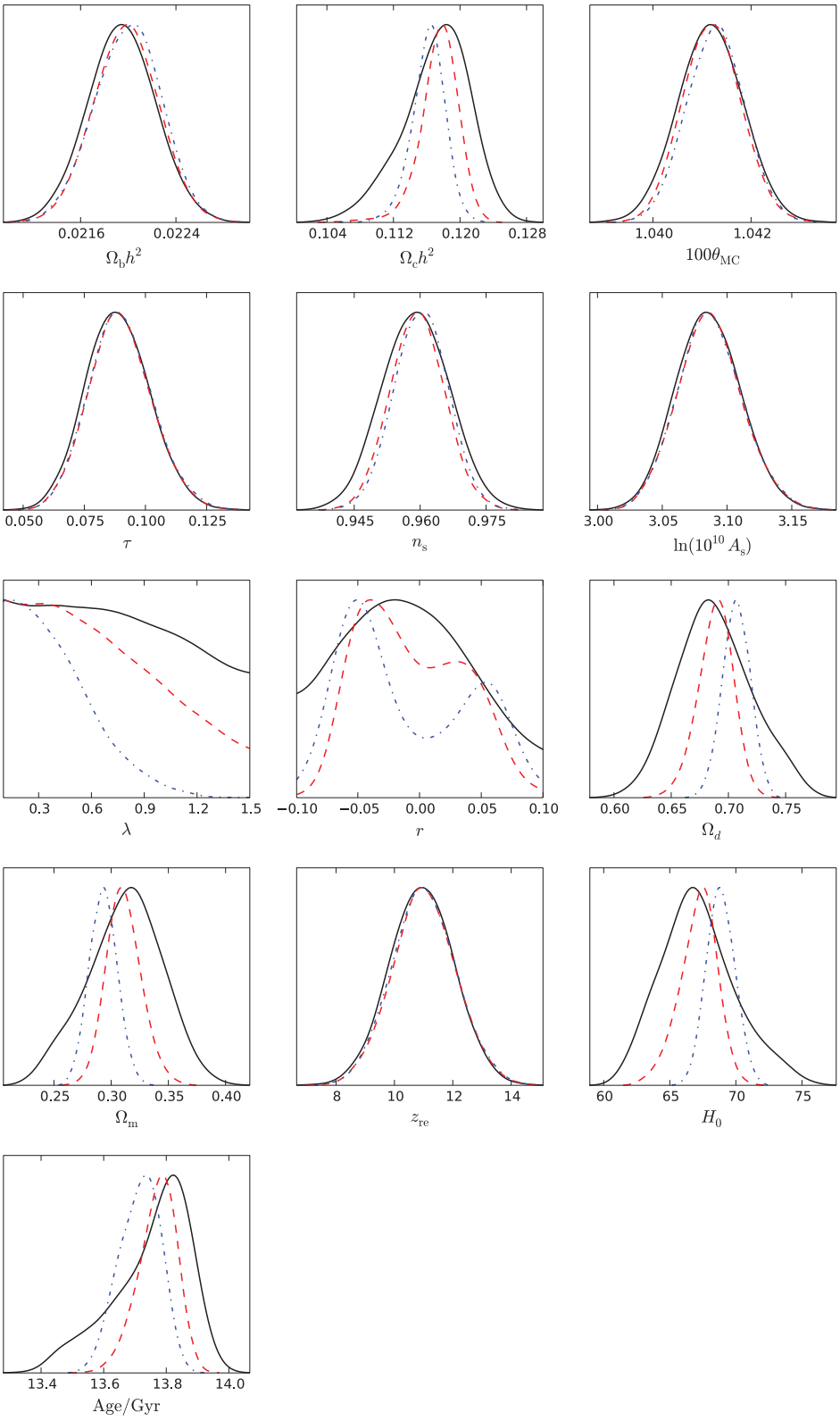

Figure 18. Marginalized likelihoods for the parameters of the Yukawa model. The black solid lines correspond to the Planck constraints, the red dashed lines correspond to Planck + BAO and the blue dot–dashed lines correspond to Planck + BAO + SNIa + H_0.

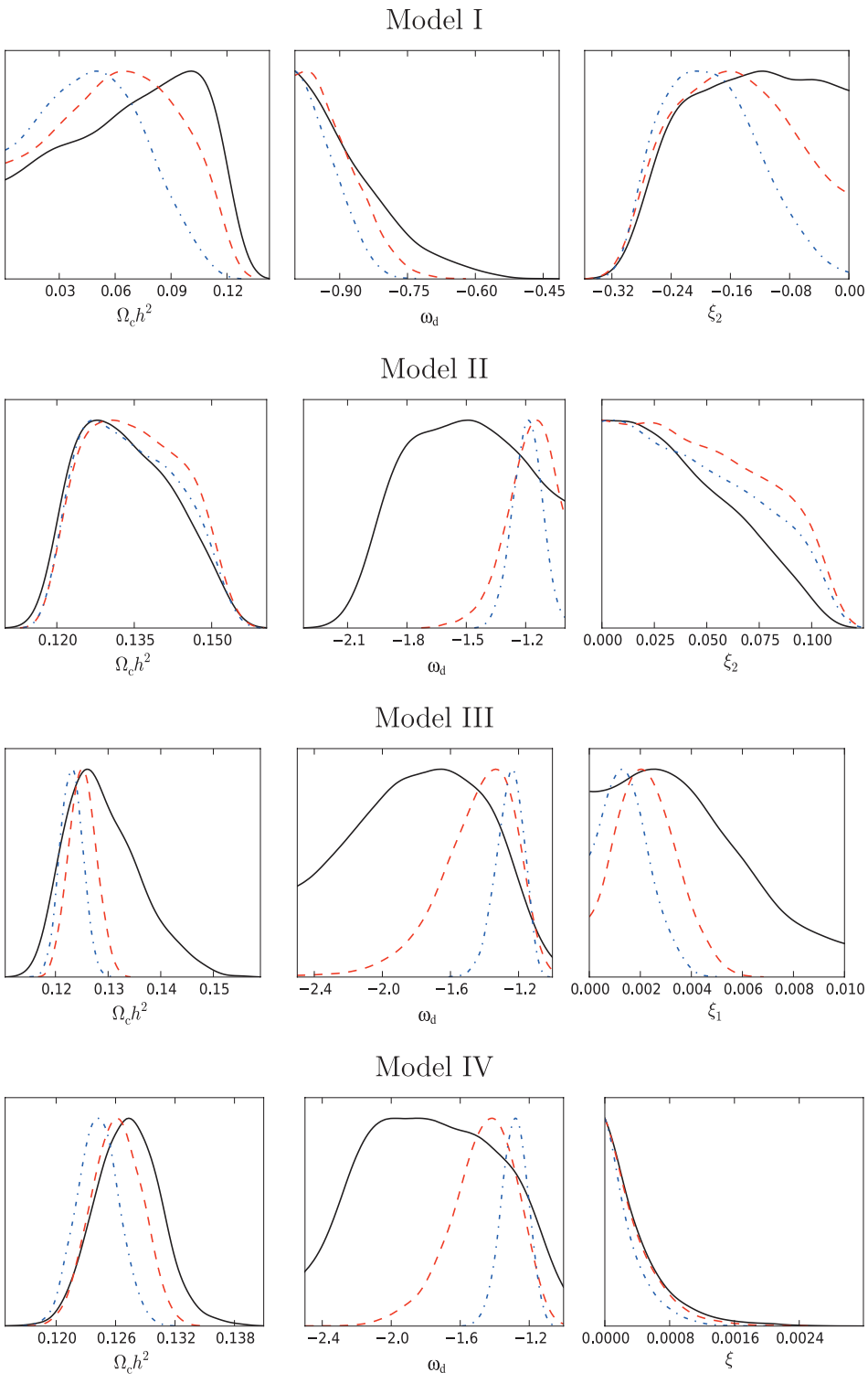

Figure 19. Marginalized likelihoods for the parameters describing interacting fluid models of table 3. Black solid lines correspond to the constraints from Planck data alone, red dashed lines to Planck + BAO and blue dot–dashed lines to Planck + BAO + SNIa + H_0.

New facilities are being designed and built aiming to measure the expansion history and the growth of structure in the universe with increasing precision out to greater redshifts. Since the interaction changes the expansion history of the universe, the evolution of matter and radiation density perturbations, peculiar velocities and gravitational fields, these new facilities will not only test the current period of accelerated expansion but also constrain the nature of the interaction. Observations of SNIa, BAOs, gravitational lensing, redshift-space distortions and the growth of cosmic structure probe the evolution of the universe at $z \leqslant 2-3$. In parallel, the physics of DM/DE interactions at recombination can be probed by the CMB radiation power spectrum while the ISW effect and lensing pattern of the CMB sky are sensitive to the growth of matter at lower redshifts.

The DE task force (DETF) was established to advise the different U.S. funding agencies on future DE research. Their report categorized different experimental approaches by introducing a quantitative 'figure of merit' that is sensitive to the properties of DE, including its evolution with time [13]. Using this figure of merit, they evaluated ongoing and future DE studies based on observations of baryon acoustic oscillations, galaxy clusters, supernova and weak lensing. The DETF categorized the different experiments by their different degree of development. Stage I referred to the discovery experiments, stage II to the on-going experiments at that time when the report was elaborated (circa 2006), stage III was defined as the next generation that are currently in full operation. They also looked forward to a stage IV generation of more capable experiments. Examples of stage II surveys are the Canada–France–Hawaii telescope (CFHT) legacy survey, with observations of SNIa [105] and weak lensing [176] and that ended in 2009, the ESSENCE [396] and SDSS-II [139] supernova surveys and BAO measurements from the SDSS [128, 266, 280]. While new observations continue to be expanded and improved with more recent instruments, the CHFT Lensing survey remains the largest weak lensing survey to date.

In this section we will briefly review projects that are currently operating or under construction (stage III and IV). All of these facilities share the common feature of surveying wide areas to collect large samples of galaxies, clusters, and/or supernovae and they will help clarify the nature of the interaction between dark sectors. Acronyms were given in table 4. More details can be found in [390].

8.1. Ground based observations

The existing and planned ground based DE experiments collect data on SNIa, galaxy clustering and gravitational lensing. Wide-field imaging is used to measure weak gravitational lensing and clustering of galaxies in bins of photometrically estimated redshifts and wide-field spectroscopy, to map the clustering of galaxies, quasars and the Ly-α forest and measure distances and expansion rates with BAO and the history of structure growth with redshift-space distortions (RSD). type Ia supernovae are searched to determine the distance-redshift relation.

8.1.1. Stage III: 6dFGS, BOSS, HETDEX, pan-STARRS, WiggleZ. The 6-degree field galaxy survey (6dFGS) has mapped the nearby universe over $\sim$17 000 deg^2 of the southern sky with galactic latitude $|b| > 10^0$. The median redshift of the survey is $z = 0.053$. It is the largest redshift survey of the nearby universe, reaching out to $z \sim 0.15$. The survey data includes images, spectra, photometry, redshifts and a peculiar velocity survey of a subsample of 15 000 galaxies. The final release of redshift data is given in [191].

The baryon oscillation spectroscopic survey (BOSS) is currently the largest spectroscopic redshift survey worldwide, mapping 10^4 deg^2 up to $z = 0.7$. BOSS is the largest of the four surveys that comprise SDSS-III and has been in operation for 5 years since 2009. Its goals are to measure angular diameter distance and expansion rate using BAO, using 1.5 million galaxies [30]. Using Ly-α lines towards a dense grid of high-redshift quasars, it has pioneered a method to measure BAO at redshifts $z = [2, 3.5]$. The analysis of SDSS Data Release 9 has provided a measurement of the BAO scale at $z \sim 2.5$ with a precision of 2–3% [79, 347]. This survey will be followed by the extended BOSS (eBOSS) that will be operating for six years and will extend the BOSS survey to higher redshifts.

Table 6. Cosmological parameters used by the BOSS collaboration [121].

Parameter	Bestfit	σ
h	0.706	0.032
$\Omega_c^0 h^2$	0.143	0.003
Ω_d^0	0.714	0.020
$\Omega_b^0 h^2$	0.02207	0.00033

Similar to BOSS, the Hobby–Eberly telescope DE experiment (HETDEX) at the Austin McDonald observatory has the goal of providing percent-level constraints on the Hubble parameter and angular diameter distance on the redshift range $z = [1.9, 3.5]$ by using a combination of BAO and power spectrum shape information. It will be achieved by surveying 0.8 million $Ly-\alpha$ emitting galaxies on a field of view of 420 deg^2 [177].

The panoramic survey telescope and rapid response system (Pan-STARRS) describes a facility with a cosmological survey among its major goals. The final goal is to use four coordinated telescopes to carry out survey of the full sky above DEC $= -45°$ [251] that will go a factor $\sim$10 deeper than the SDSS imaging survey. The survey will provide data on high redshift SN, galaxy clustering and gravitational lensing. For that purpose, in addition to the wide survey, an ultra-deep field of 1200 deg^2 will be observed down to magnitude 27 in the g band with photometric redshifts to measure the growth galaxy clustering. Data from this facility has already been used to constrain the equation of state parameter [412].

The WiggleZ DE survey is a large-scale redshift survey carried out at the Anglo-Australian telescope and is now complete. It has measured redshifts for $\sim$240 000 galaxies over 1000 deg^2 in the sky. It combines measurements of cosmic distance using BAO with measurements of the growth of structure from redshift-space distortions out to redshift $z = 1$ [198].

8.1.2. CMB experiments: ACT, SPT. The Atacama cosmology telescope (ACT) operates at 148, 218 and 277 GHz with full-width at half maximum angular resolutions of $(1.4', 1.0', 0.9')$ [359]. ACT observes the sky by scanning the telescope in azimuth at a constant elevation of 50.5° as the sky moves across the field of view in time, resulting in a stripe-shaped observation area. The collaboration has released two observed areas of 850 deg^2 and 280 deg^2 [125]. Sky maps, analysis software, data products and model templates are available through NASA legacy archive for microwave background data analysis (LAMBDA).

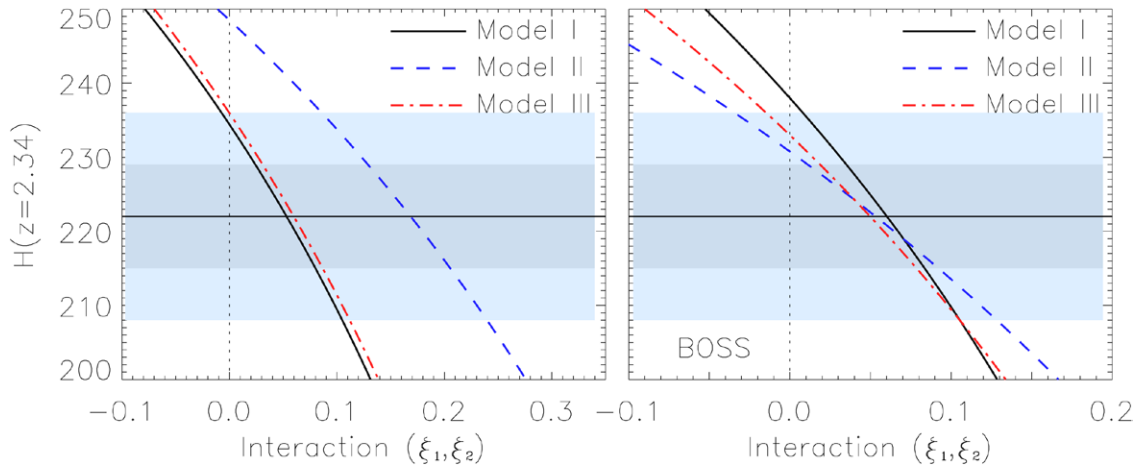

Figure 20. Hubble function at redshift $z = 2.34$ as a function of the interaction parameters ξ_1, ξ_2 for models III and I, II, respectively. In the left panel we used the cosmological parameters from tables V, XI and XII of [110]. In the right panel, labeled BOSS, the cosmological parameters are those of table 6. The horizontal line corresponds to the BOSS measured value $H(2.34) = 222 \pm 7$ km s^{-1} Mpc^{-1} with the shaded areas representing 1σ and 2σ CL.

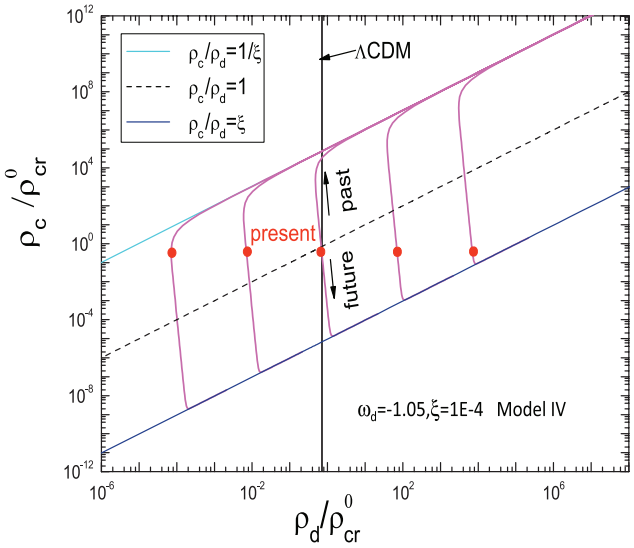

Figure 21. ρ_c^0 is the critical energy density today. The attractor solutions of r do not depend on the initial conditions at the early time of the universe. The purple lines represent the density evolution of cosmological model with different initial conditions. Solid circles represent the density contrast r today. Values change with the initial conditions but they are bounded in two attractor solutions $r_s^- \sim \xi$, $r_s^+ \sim 1/\xi$ in $\rho_c - \rho_d$ plane.

The south pole telescope (SPT) is a 10 m telescope designed to map primary and secondary anisotropies in the CMB, currently operating at 95, 150, 220 GHz with a resolution with resolution $(1.7, 1.2, 1.0)'$. The noise levels are 18 μK at 150 GHz and $\sim\sqrt{2}$ larger for the other two channels [150]. It has observed a region of 2540 deg^2. Data in the three frequencies were used to produce a radiation power spectra covering the multipole range $2000 < \ell < 11\,000$. At present is the most precise measurement of the radiation power spectrum at $\ell > 2,500$ at those frequencies; at those angular scales the signal is dominated by the SZ effect and is not so relevant to constrain models of DM/DE interaction.

A polarization-sensitive receiver have been installed on the SPT; data at 95 and 150 GHz has provided a measurement of the B-mode polarization power spectrum from an area of 100 deg^2, spanning the range $300 \leqslant \ell \leqslant 2300$. The resulting power spectra was consistent with the spectrum arising from the gravitational lensing of E-mode polarization [199].

8.1.3. Stage IV: DES, eBOSS, JPAS, LSST, SKA, WFMOS, BINGO. The DE survey (DES) is a wide-field imaging and supernova survey on the Blanco 4 m telecope at Cerro Tololo (Chile) using the DE camera. It has started operations and it will continue for five years. The DE spectroscopic survey instrument (DESI) is a wide field spectroscopic instrument intended to start in 2018 and operate also for 5 years in the nearly twin Mayall telescope at Kitt peak (Arizona). DESI will obtain spectra and redshifts for at least 18 million emission-line galaxies, 4 million luminous red galaxies and 3 million quasi-stellar objects, to probe the effects of DE on the expansion history BAO and measure the gravitational growth history through RSD. The resulting 3D galaxy maps at redshift $z < 2$ and Ly-α forest at $z > 2$ are expected to provide the distance scale in 35 redshift bins with a one-percent precision [223]. The imaging survey will detect 300 million galaxies, with approximately 200 million WL shape measurements, almost a two-order of magnitude improvement over the CFHTLens Weak Lensing survey.

Approved as a major cosmology survey in SDSS-IV (2014–2020), eBOSS will capitalize on this premier facility with spectroscopy on a massive sample of galaxies and quasars in the relatively uncharted redshift range that lies between the BOSS galaxy sample and the BOSS Ly-α sample. Compared with BOSS, this new survey will focus on a smaller patch of 7500 deg^2 but it will reach higher magnitudes. It will measure both the distance-redshift relation and the evolution of the Hubble parameter using different density tracers; the clustering of luminous red galaxies (LGRs) and emission line galaxies (ELGs), quasars and Ly-α systems to probe the BAO scale in the redshift ranges [0.6, 0.8], [1, 2.2] and [2.2, 3.5] respectively and it will achieve 1–2% accuracy in distance measurements from BAOs between $0.6 < z < 2.5$.

The Javalambre physics of the accelerating universe astronomical survey (JPAS) is a new astronomical facility dedicated to mapping the observable universe in 56 colors [55]. The starting date for this multi-purpose astrophysical survey is 2015. In five years, JPAS will cover $\sim$8000 deg^2 using a system of 54 narrow band and 2 broad-band filters in the range 300–1000 nm. The filter system was optimized to accurately measure photometric redshifts for galaxies up to $z \sim 1$. The main instruments are a 2.5 m telescope located at El Pico del Buitre (Teruel, Spain) and a 1.2 Giga-pixel camera. The main goals of the survey are to measure angular and radial components of BAO from the galaxy clustering, determine the evolution of the cosmic volume from cluster counts and luminosity distances from SNIa. The filter system will permit to determine the redshifts of the observed supernovae. The camera is not optimized to measure galaxy elipticities so weak lensing studies would require ellipticity measurements obtained from other surveys. The JPAS telescope will measure BAO from high redshift quasars to achieve a better precision than BOSS [55], open the possibility of using the test described in section 7.4 to disproof the concordance model.

The large synoptic survey telescope (LSST) is a wide-field, ground-based telescope, designed to image $\sim$20 000 deg^2 in six optical bands from 320 nm to 1050 nm. The telescope will be located on Cerro Pachón (Chile) and it will operate for a decade allowing to detect galaxies to redshifts well beyond unity. Its science goals are to measure weak and strong gravitational lensing, BAO, SNIa and the spatial density, distribution, and masses of galaxy clusters as a function of redshift. Its first light is expected on 2019.

The square kilometre array (SKA) is a radio-facility which is scheduled to begin construction in 2018. The HI galaxy redshift survey can provide us with accurate redshifts (using the 21 cm line) of millions of sources over a wide range of redshifts, making it an ideal redshift survey for cosmological studies [6, 38, 78, 135, 202, 303, 330, 411]. Although technically challenging, the SKA could measure the expansion rate of the universe in real time by observing the neutral hydrogen (HI) signal of galaxies at two different epochs [117, 203].

Wide-field multi-object spectrograph (WFMOS) is a camera specially devoted to galaxy surveys. It will be mounted atop the 8.2 m Subaru telescope on Mauna Kea (Hawaii). One of the science goals of the WFMOS camera is high precision measurements of BAO. The WFMOS DE survey comprises two parts: a 2000 deg^2 survey of two million galaxies at redshifts $z < 1.3$ and a high redshift survey of about half a million Lyman break galaxies (LBGs) at redshifts $2.5 < z < 3.5$ that would probe distances and the Hubble rate beyond $z = 2$ (see [47] for more details).

BINGO is a radio telescope designed to detect BAO at radio frequencies by measuring the distribution of neutral hydrogen at cosmological distances using a technique called intensity mapping. The telescope will be located in an abandon mine in Northern Uruguay. It will operate in the range [0.96, 1.26] GHz to observe the redshifted 21 cm Hydrogen line. It will consist of a two-mirror compact range design with a 40 m diameter primary and it will have no moving parts to provide an excellent polarization performance and very low side-lobe levels (for details see [48]).

8.1.4. Stage IV: CMB experiments. Currently, the interest on CMB ground experiments is centered on polarization. For a cosmic variance limited experiment polarization alone places stronger constraints on cosmological parameters than CMB temperature [141]. Experiments like SPTpol [199] and Quixote [146] are currently taken data aiming to characterize the polarization of the CMB and of the Galactic and extragalactic sources. CMB experiments devoted to measuring polarization from the ground are also being proposed; the scientific capabilities of a CMB polarization experiment like CMB-S4 in combination with low redshift data would be able to constrain the DE EoS and DM annihilation rate among other parameters [1, 397].

8.2. Space based surveys

Satellite surveys usually require a dedicated facility and, consequently, are more expensive than those carried out from the ground. Their significant advantage is that, by observing outside the atmosphere, the data usually contains a lower level of systematic errors.

8.2.1. Stage III: WMAP, Planck. The Wilkinson microwave anisotropy probe (WMAP) was a satellite mission devoted to measure CMB temperature fluctuations at frequencies operating between 23 and 94 GHz. Launched on June 30, 2001 and operated for 9 years up to the end of September 2010. The main results and data products of the nine years of operation are described in [58]. The final 9yr data released was soon followed by those of the Planck Collaboration. The Planck satellite observed the microwave and sub-millimeter sky from August 12th, 2009 to Oct 23rd, 2013 in nine frequencies between 30 and 857 GHz, with angular resolution between 33' and 5'. This satellite measured the temperature–temperature, temperature-E mode and E mode–E mode power spectra up to $\ell \sim 2000$ [287] and derived the CMB lensing potential [289]. Temperature maps, a catalog of Sunyaev–Zeldovich (SZ) clusters and likelihood codes to assess cosmological models against the Planck data [286, 292] and other data products can be downloaded from the Planck Legacy Archive (see table 4).

8.2.2. Stage IV: eRosita, Euclid and WFIRST. The extended Röntgen survey with an imaging telescope array (eROSITA) is a x-ray satellite expected to be launched at the end of 2017. It will perform the first imaging all-sky survey in energy range 0.3–10 keV [247] to detect $\sim 10^5$ galaxy clusters out to redshifts $z > 1$. In the soft x-ray band (0.5–2 keV), it will be about 20 times more sensitive than the ROSAT all sky survey, while in the hard band (2–10 keV) it will provide the first ever true imaging survey of the sky at those energies.

Euclid is a European space agency DE satellite mission scheduled for launch in 2020. This mission is designed to perform two surveys: a wide 15 000 deg^2 survey in the optical and near-infrared and a deep survey on 40 deg^2 two magnitudes deeper. Euclid will map the extra-galactic sky

with the resolution of the Hubble space telescope, with optical and near-infrared (NIR) imaging and NIR spectroscopy. Photometric redshifts for the galaxies in the wide survey will be provided from ground photometry and from the NIR survey. In addition, 50 million spectroscopic redshifts will be obtained. Euclid data will allow to measure the expansion history and the growth of structure with great precision. A detailed quantitative forecast of Euclid performance has been discussed in [220]. The data will allow to constrain many different cosmological models; when the growth factor is parametrized as $f_g = \Omega_m(z)^\gamma$ the value $\gamma \simeq 0.545$ corresponds to the ΛCDM model and Euclid will measure this parameter with a precision of $\Delta\gamma = 0.03$ [174]. Forecasts for other magnitudes such as the bias, DE sound speed and the RSD are given in [29].

The wide field infrared survey telescope (WFIRST) is an american satellite mission that is currently being reviewed and expected to be launch in 2023. This mission updates and expands earlier proposed missions like the super nova acceleration probe (SNAP) and the joint DE mission (JDEM). Like Euclid, one of its primary science goals is to determine the properties of DE and in many respects complements EUCLID. WFIRST strategy is to construct a narrow and deep galaxy redshift survey of 2000 deg^2. Both satellites will measure the redshift for a similar number of galaxies and will obtain a comparable precision for the BAO derived angular diameter distances and Hubble constant redshift evolution [352]. Additionally, the measured fluctuations of the cosmic infrared background could probe angular diameter distances at redshift $z \sim 10$ [197].

Many synergies will come from cross-correlating data from different observations For instance, Euclid, WFIRST and SKA have similar scientific aims but will carry observations at different wavelengths. Euclid and WFIRST probe the low redshift universe, through weak lensing and galaxy clustering measurements. The SKA has the potential to probe a higher redshift regime and a different range in scales of the matter power spectrum, which are linear scales rather than the quasi-non-linear scales probed by Euclid and WFIRST. The combination of different observations will be particularly sensitive to signatures of modified gravity. Cross-correlation of different data sets will help to control systematics for the primary science. The SKA, WFIRST and Euclid will be commissioned on similar timescales offering an exciting opportunity to exploit synergies between these facilities. [202]

8.2.3. CMB experiments: CMBpol, COrE, PRISM. The cosmic origins explorer (COrE) is a Stage IV full-sky, microwave-band satellite proposed to ESA within Cosmic Vision 2015–2025. COrE will provide maps of the microwave sky in polarization and temperature in 15 frequency bands, ranging from 45 GHz to 795 GHz, with angular resolutions from 23′ at 45 GHz and 1.3′ at 795 GHz, with sensitivities roughly 10 to 30 times better than Planck [35].

The polarized radiation imaging and spectroscopy mission (PRISM) is a large-class mission proposed to ESA in May 2013 to survey the CMB sky both intensity and polarization. The mission will detect approximately 10^6 clusters using the thermal SZ effect and a peculiar velocity survey using the kinetic SZ effect that comprises our entire Hubble volume [31]. NASA is carrying similar efforts through the primordial polarization program definition team (PPPDT) that converge towards a satellite dedicated to the study of CMB polarization (CMBPol) [49].

Combing these complementary ground based and space based observations, we would hopefully achieve a better understanding of the nature of DM, DE and the interaction within the dark sectors.

Conclusions

In principle an interaction must exist between any two fields provided some symmetry prevents it. In the case of DM and DE no such symmetry is known; this is why a non-gravitational coupling between these two main components of the cosmic energy budget should be expected on general grounds. Thus far the observational evidence favoring the interaction is a bit more than marginal as the ΛCDM model is, as we write, consistent with the data. Nevertheless, if the coupling is such that DE decays into DM, then the coincidence problem that afflicts the said model gets alleviated and possibly solved. By contrast, if the coupling occurs in the opposite sense (i.e., $Q<0$), this problem is worsened and the second law of thermodynamics very likely violated.

Only observation can provide us with a conclusive answer. It is to be expected that the wealth of data to come from present and planned experiments (summarized in section 8) will establish whether the coupling exist, its strength, and in what sense it proceeds. Optimistically, it will tell us which interacting model has been chosen by nature.

Acknowledgments

We thank S Tsujikawa for comments and suggestions. EA wishes to thank FAPESP and CNPq (Brazil) for support and AA Costa, E Ferreira and R Landim for discussions and suggestions. FAB acknowledges financial support from grant FIS2012-30926 (MINECO/FEDER) and the 'Programa de Profesores Visitantes Severo Ochoa' of the Instituto de Astrofísica de Canarias. BW would like to acknowledge the support by National Basic Research Program of China (973 Program 2013CB834900) and National Natural Science Foundation of China and he wishes to thank J H He and X D Xu for helpful discussions.

References

[1] Abazajian K N *et al* 2015 *Astropart. Phys.* **63** 66
[2] Abdalla E, Abramo L R, Sodre L and Wang B 2009 *Phys. Lett.* B **673** 107
[3] Abdalla E, Abramo L R and Souza J 2010 *Phys. Rev.* D **82** 023508
[4] Abdalla E, Graef L L and Wang B 2013 *Phys. Lett.* B **726** 786
[5] Abdalla E and Wang B 2007 *Phys. Lett.* B **651** 89

[6] Abdalla F *et al* 2014 Cosmology from HI galaxy surveys with the SKA *Proc. Advancing Astrophysics with the Square Kilometre Array (AASKA14) (Giardini Naxos, Italy, 9–13 June, 2014)* (arXiv:1501.04035)
[7] Abramo L R, Batista R C, Liberto L and Rosenfeld R 2007 *J. Cosmol. Astropart. Phys.* JCAP11(2007)012
[8] Abramo L R, Batista R C, Liberto L and Rosenfeld R 2009 *J. Cosmol. Astropart. Phys.* JCAP07(2009)011
[9] Abramo L R and Finelli F 2003 *Phys. Lett.* B **575** 165
[10] Acquaviva V and Baccigalupi C 2006 *Phys. Rev.* D **74** 103510
[11] Afshordi N, Loh Y S and Strauss M 2004 *Phys. Rev.* D **69** 083524
[12] Akaike H 1974 *Ann. Stat.* **19** 46
[13] Albrecth A *et al* 2006 Report of the dark energy task force (arXiv: astro-ph/0609591)
[14] Alcock A and Paczynski B 1979 *Nature* **281** 358
[15] Amanullah R *et al* 2010 *Astrophys. J.* **716** 712
[16] Amendola L 2000 *Phys. Rev.* D **62** 043511
[17] Amendola L 2003 *Astrophys. J.* **583** L53
[18] Amendola L 2004 *Phys. Rev.* D **69** 103524
[19] Amendola L, Baldi M and Wetterich C 2008 *Phys. Rev.* D **78** 023015
[20] Amendola L, Campos G C and Rosenfeld R 2007 *Phys. Rev.* D **75** 083506
[21] Amendola L, Castro T, Marra V and Quartin M 2014 *Mon. Not. R. Astron. Soc.* **449** 2845
[22] Amendola L, Pettorino V, Quercellini C and Vollmer A 2012 *Phys. Rev.* D **85** 103008
[23] Amendola L and Quercellini C 2003 *Phys. Rev.* D **68** 023514
[24] Amendola L and Quercellini C 2004 *Phys. Rev. Lett.* **92** 181102
[25] Amendola L, Quartin M, Tsujikawa S and Waga I 2006 *Phys. Rev.* D **74** 023525
[26] Amendola L and Tocchini-Valentini D 2002 *Phys. Rev.* D **66** 043528
[27] Amendola L and Tsujikawa S 2008 *Phys. Lett.* B **660** 125
[28] Amendola L, Tsujikawa S and Sami M 2006 *Phys. Lett.* B **632** 155
[29] Amendola L *et al* 2013 *Living Rev. Relativ.* **16** 6
[30] Anderson L *et al* 2014 *Mon. Not. R. Astron. Soc.* **441** 24
[31] André P *et al* 2014 *J. Cosmol. Astropart. Phys.* JCAP02(2014)006
[32] Armendariz-Picon C, Mukhanov V F and Steinhardt P J 2001 *Phys. Rev.* D **63** 103510
[33] Armendariz-Picon C, Damour T and Mukhanov V 1999 *Phys. Lett.* B **458** 209
[34] Armendariz-Picon C 2007 *J. Cosmol. Astropart. Phys.* JCAP07(2007)007
[35] Armitage-Caplan C 2011 COrE (cosmic origins explorer) a white paper (arXiv:1102.2181)
[36] Atrio-Barandela F *et al* 2015 *Astrophys. J.* **810** 143
[37] Aviles A and Cervantes-Cota J L 2011 *Phys. Rev.* D **84** 083515
[38] Bacon D *et al* 2014 Synergy between the large synoptic survey telescope and the square kilometre array *Proc. Advancing Astrophysics with the Square Kilometre Array (AASKA14) (Giardini Naxos, Italy, 9–13 June, 2014)* (arXiv:1501.03977)
[39] Bak D and Rey S-J 2000 *Class. Quantum Grav.* **17** L83
[40] Baldi M 2012 *Mon. Not. R. Astron. Soc.* **420** 430
[41] Baldi M and Pettorino V 2011 *Mon. Not. R. Astron. Soc.* **412** L1
[42] Baldi M and Salucci P 2012 *J. Cosmol. Astropart. Phys.* JCAP02(2012)014
[43] Ballesteros G and Riotto A 2008 *Phys. Lett.* B **668** 171
[44] Barrow J D and Saich P 1993 *Mon. Not. R. Astron. Soc.* **262** 717
[45] Basilakos S, Plionis M and Lima J A S 2010 *Phys. Rev.* D **82** 083517
[46] Basilakos S, Nesseris S and Perivolaropoulos L 2013 *Phys. Rev.* D **87** 123529
[47] Bassett B A *et al* 2005 *Astron. Geophys.* **46** 526
[48] Battye R A *et al* . 2013 *Mon. Not. R. Astron. Soc.* **434** 1239
[49] Baumann D *et al* 2009 *CMBPol Mission Concept Study* (*AIP Conf. Proc.* vol 1141) (Melville, NY: American Institute of Physics) p 3 (arXiv:0811.3911)
[50] Bean R and Dore O 2004 *Phys. Rev.* D **69** 083503
[51] Bean R, Flanagan E E and Trodden M 2008 *Phys. Rev.* D **78** 023009
[52] Bean R, Flanagan E E, Laszlo I and Trodden M 2008 *Phys. Rev.* D **78** 123514
[53] Bekenstein J D 1993 *Phys. Rev.* D **48** 3641
[54] Bekenstein J D 1994 *Phys. Rev.* D **49** 1912
[55] Benitez N *et al* 2014 J-PAS: the javalambre-physics of the accelerated universe astrophysical survey (arXiv:1403.5237)
[56] Bento M C, Bertolami O and Sen A A 2002 *Phys. Rev.* D **66** 043507
[57] Bento M C, Bertolami O and Sen A A 2004 *Phys. Rev.* D **70** 083519
[58] Bennett C L *et al* 2013 *Astrophys. J. Suppl.* **208** 20
[59] Berera A 1995 *Phys. Rev. Lett.* **75** 3218
[60] Berezhiani Z, Dolgov A D and Tkachev I I 2015 *Phys. Rev.* D **92** 061303
[61] Bertolami O, Pedro F G and Delliou M L 2007 *Phys. Lett.* B **654** 165
[62] Bertolami O, Pedro F G and Delliou M L 2011 *Gen. Relativ. Grav.* **44** 1073
[63] Bertone G, Hooper D and Silk J 2005 *Phys. Rept.* **405** 279
[64] Beutler F *et al* 2011 *Mon. Not. R. Astron. Soc.* **444** 3501
[65] Beutler F, Blake C, Koda J, Marin F A, Seo H-J, Cuesta A J and Schneider D P 2016 *Mon. Not. R. Astron. Soc.* **455** 3230
[66] Beutler F *et al* 2012 *Mon. Not. R. Astron. Soc.* **423** 3430
[67] Beutler F *et al* 2014 *Mon. Not. R. Astron. Soc.* **443** 1065
[68] Blake C *et al* 2011 *Mon. Not. R. Astron. Soc.* **415** 2876
[69] Blake C *et al* 2012 *Mon. Not. R. Astron. Soc.* **425** 405
[70] Bilicki M, Jarrett T H, Peacock J A, Cluver M E and Steward L 2014 *Astrophys. J. Suppl.* **210** 9
[71] Bond J R, Efstathiou G and Silk J 1980 *Phys. Rev. Lett.* **45** 1980
[72] Bolotin Y L, Kostenko A, Lemets O and Yerokhin D 2015 *Int. J. Mod. Phys.* D **24** 1530007
[73] Boughn S P and Crittenden R G 2004 *Nature* **427** 45
[74] Brax P, Burrage C and Davis A C 2012 *J. Cosmol. Astropart. Phys.* JCAP12(2012)016
[75] Brax P and Martin J 2006 *J. Cosmol. Astropart. Phys.* JCAP11(2006)008
[76] Brax P, Rosenfeld R and Steer D A 2010 *J. Cosmol. Astropart. Phys.* JCAP08(2010)033
[77] van de Bruck C and Morrice J 2015 *J. Cosmol. Astropart. Phys.* JCAP04(2015)036
[78] Bull P *et al* 2015 *Pos AASKA* **14** 024
[79] Busca N G *et al* 2013 *Astron. Astrophys.* **552** 96
[80] Cabre A *et al* 2007 *Mon. Not. R. Astron. Soc.* **381** 1347
[81] Caldera-Cabral G, Maartens R and Schaefer B M 2009 *J. Cosmol. Astropart. Phys.* JCAP07(2009)027
[82] Caldera-Cabral G, Maartens R and Ureña-López L A 2009 *Phys. Rev.* D **79** 063518
[83] Calabrese E, Huterer D, Linder E V, Melchiorri A and Pagano L 2011 *Phys. Rev.* D **83** 123504
[84] Caldwell R R, Dave R and Steinhardt P J 1998 *Phys. Rev. Lett.* **80** 1582
[85] del Campo S, Herrera R and Pavón D 2006 *Phys. Rev.* D **74** 023501
[86] del Campo S, Herrera R and Pavón D 2015 *Phys. Rev.* D **91** 123539

[87] Capozziello S, Cardone V F, Funaro M and Andreon S 2004 *Phys. Rev.* D **70** 123501
[88] Carbone C, Baldi M, Pettorino V and Baccigalupi C 2013 *J. Cosmol. Astropart. Phys.* JCAP9(2013)4
[89] Carvalho F C, Alcaniz J S, Lima J A S and Silva R 2006 *Phys. Rev. Lett.* **97** 081301
[90] Carvalho G C, Bernui A, Benetti M, Carvalho J C and Alcaniz J S 2016 *Phys. Rev.* D **93** 023530
[91] Cataldo M, Cruz N, del Campo S and Lepe S 2001 *Phys. Lett.* B **509** 138
[92] Cayrel R *et al* 2001 *Nature* **409** 691
[93] Chevallier M and Polarski D 2001 *Int. J. Mod. Phys.* D **10** 213
[94] Chiba T 2003 *Phys. Lett.* B **575** 1
[95] Chiba T and Yamaguchi M 2013 *J. Cosmol. Astropart. Phys.* JCAP10(2013)040
[96] Chimento L P 2004 *Phys. Rev.* D **69** 123517
[97] Chimento L P, Jakubi A S and Pavón D 2000 *Phys. Rev.* D **62** 063508
[98] Chimento L P, Jakubi A S, Pavón D and Zimdahl W 2003 *Phys. Rev.* D **67** 083513
[99] Chimento L P 2010 *Phys. Rev.* D **81** 043525
[100] Chongchitnan S 2009 *Phys. Rev.* D **79** 043522
[101] Chuang C H *et al* 2013 *Mon. Not. R. Astron. Soc.* **433** 3539
[102] Clemson T, Koyama K, Zhao G-B, Maartens R and Valiviita J 2012 *Phys. Rev.* D **85** 043007
[103] Cohen A G, Kaplan D B and Nelson A E 1999 *Phys. Rev. Lett.* **82** 4971
[104] Cole S *et al* 2005 *Mon. Not. R. Astron. Soc.* **362** 505
[105] Conley A *et al* 2011 *Astrophys. J. Suppl.* **192** 1
[106] Contaldi C R, Hoekstra H and Lewis A 2003 *Phys. Rev. Lett.* **90** 221303
[107] Cooray A 2002 *Phys. Rev.* D **65** 103510
[108] Corasaniti P S, Huterer D and Melchiorri A 2007 *Phys. Rev.* D **75** 062001
[109] Corasaniti P S 2008 *Phys. Rev.* D **78** 083538
[110] Costa A A, Xu X D, Wang B, Ferreira E G M and Abdalla E 2014 *Phys. Rev.* D **89** 103531
[111] Costa A A, Olivari L C and Abdalla E 2015 *Phys. Rev.* D **92** 103501
[112] Creminelli P, Amico G, Norena J, Senatore L and Vernizzi F 2010 *J. Cosmol. Astropart. Phys.* JCAP03(2010)027
[113] Crittenden R G and Turok N 1996 *Phys. Rev. Lett.* **76** 575
[114] Cui J-L, Yin L, Wang L-F, Li Y-H and Zhang X 2015 *J. Cosmol. Astropart. Phys.* JCAP09(2015)024
[115] Damour T, Gibbons G W and Gundlach C 1990 *Phys. Rev. Lett.* **64** 123
[116] Das C R, Laperashvil L V, Nielsen H B and Tureanu A 2011 *Phys. Rev.* D **84** 063510
[117] Darling J 2012 *Astrophys. J. Lett.* **761** L26
[118] Deffayet C, Gao X, Steer D A and Zahariade G 2011 *Phys. Rev.* D **84** 064039
[119] De Felice A and Tsujikawa S 2010 *Living Rev. Rel.* **13** 3
[120] Delliou M L, Marcondes R J F, Neto G B and Abdalla E 2015 *Mon. Not. R. Astron. Soc.* **453** 2
[121] Delubac T *et al* 2015 *Astron. Astrophys.* **574** A59
[122] Dodelson S and Widrow L M 1994 *Phys. Rev. Lett.* **72** 17
[123] Domenech G, Naruko A and Sasaki M 2015 *J. Cosmol. Astropart. Phys.* JCAP10(2015)067
[124] Doran M 2005 *J. Cosmol. Astropart. Phys.* JCAP05(2005)011
[125] Dünner R *et al* 2013 *Astrophys. J.* **762** 10
[126] Durán I, Atrio-Barandela F and Pavón D 2012 *J. Cosmol. Astropart. Phys.* JCAP04(2012)008
[127] Durán I and Pavón D 2011 *Phys. Rev.* D **83** 023504
[128] Eisenstein D J *et al* 2005 *Astroph. J.* **633** 560
[129] Fabris J, Fraga B, Pinto-Neto N and Zimdahl W 2010 *J. Cosmol. Astropart. Phys.* JCAP04(2010)008
[130] Farooq O and Ratra B 2013 *Astrophys. J. Lett.* **766** L7
[131] Feinstein A 2002 *Phys. Rev.* D **66** 063511
[132] Feix M, Nusser A and Branchini E 2015 *Phys. Rev. Lett.* **115** 011301
[133] Feng C, Wang B, Abdalla E and Su R K 2007 *Phys. Lett.* B **665** 111
[134] Feng C, Wang B, Gong Y G and Su R-K 2007 *J. Cosmol. Astropart. Phys.* JCAP09(2007)005
[135] Ferreira E, Quentin J, Costa A A, Abdalla E and Wang B 2014 New evidence for interacting dark energy from BOSS (arXiv:1412:2777)
[136] Fischler W and Susskind L 1998 Holography and cosmology (arXiv: hep-th/9806039)
[137] Font-Ribera A *et al* 2014 *J. Cosmol. Astropart. Phys.* JCAP05(2014)027
[138] Friaça A C S, Alcaniz J S and Lima J A S 2005 *Mon. Not. R. Astron. Soc.* **362** 1295
[139] Frieman J A *et al* 2008 *Astron. J.* **135** 338
[140] Frieman J A, Turner M and Huterer D 2008 *Ann. Rev. Astron. Astrophys.* **46** 385
[141] Galli S *et al* 2014 *Phys. Rev.* D **90** 063504
[142] Gannouji R, Moraes B and Polarski D 2009 *J. Cosmol. Astropart. Phys.* JCAP02(2009)034
[143] Gannouji R and Polarski D 2008 *J. Cosmol. Astropart. Phys.* JCAP05(2008)018
[144] Gavela M B, Hernandez D, Lopez Honorez L, Mena O and Rigolin S 2009 *J. Cosmol. Astropart. Phys.* JCAP7(2009)34
[145] Gaztañaga E *et al* 2009 *Mon. Not. R. Astron. Soc.* **399** 1663
[146] Genova-Santos R *et al* 2015 The QUIJOTE experiment: project overview and first results *Highlights of Spanish Astrophysics VIII, Proc. XI Scientific Meeting of the Spanish Astronomical Society (Teruel, Spain, 8–12 September 2014)* (arXiv:1504.03514)
[147] Geng J-J, Zhang J-F and Zhang X 2014 *J. Cosmol. Astropart. Phys.* JCAP07(2014)006
[148] Geng J-J, Zhang J-F and Zhang X 2014 *J. Cosmol. Astropart. Phys.* JCAP12(2014)018
[149] Geng J-J, Li Y-H, Zhang J-F and Zhang X 2015 *Eur. Phys. J.* C **75** 356
[150] George E M 2015 *Astrophys. J.* **799** 177
[151] Giannantonio T *et al* 2008 *Phys. Rev.* D **77** 123520
[152] Gong Y, Wang B and Zhang Y-Z 2005 *Phys. Rev.* D **72** 043510
[153] Gong Y, Wang B and Zhang Y-Z 2006 *Phys. Lett.* B **636** 286
[154] Gong Y G 2008 *Phys. Rev.* D **78** 123010
[155] Gross D J, Harvey J A, Martinec E and Rohm R 1985 *Phys. Rev. Lett.* **54** 502
[156] Guberina B, Horvat R and Nikolic H 2005 *Phys. Rev.* D **72** 125011
[157] Guo Z K, Ohta N and Tsujikawa S 2007 *Phys. Rev.* D **76** 023508
[158] Granett B R, Neyrinck M C and Szapudi I 2008 *Astrophys. J.* **683** L99
[159] Hagiwara K *et al* 2002 *Phys. Rev.* D **66** 010001
[160] Hamilton A J S 1992 *Astrophys. J. Lett.* **385** L5
[161] Hand N 2012 *Phys. Rev. Lett.* **109** 041101
[162] Harrison E R 1970 *Phys. Rev.* D **1** 2726
[163] Hasinger G, Schartel N and Komossa S 2002 *Astrophys. J. Lett.* **573** L77
[164] He J H and Wang B 2008 *J. Cosmol. Astropart. Phys.* JCAP06(2008)010
[165] He J H, Wang B and Abdalla E 2009 *Phys. Lett.* B **671** 139
[166] He J H, Wang B, Abdalla E and Pavón D 2010 *J. Cosmol. Astropart. Phys.* JCAP12(2010)022
[167] He J H, Wang B and Zhang P J 2009 *Phys. Rev.* D **80** 063530
[168] He J H, Wang B and Jing Y P 2009 *J. Cosmol. Astropart. Phys.* JCAP07(2009)030
[169] He J H, Wang B and Abdalla E 2011 *Phys. Rev.* D **83** 063515
[170] He J H, Wang B and Abdalla E 2011 *Phys. Rev.* D **84** 123526

[171] He J H and Wang B 2012 Modeling $f(R)$ gravity in terms of mass dilation rate (arXiv:1203.2766)
[172] He J H and Wang B 2013 *Phys. Rev.* D **87** 023508
[173] Heavens A F, Jiménez R and Verde L 2014 *Phys. Rev. Lett.* **113** 1302
[174] Heavens A F, Kitching T D and Verde L 2007 *Mon. Not. R. Astron. Soc.* **380** 1029
[175] Herrera R, Pavón D and Zimdahl W 2004 *Gen. Relativ. Grav.* **36** 2161
[176] Heymans C *et al* 2012 *Mon. Not. R. Astron. Soc.* **427** 146
[177] Hill G J *et al* 2008 *Panoramic Views of the Universe* (*Astronomical Society of the Pacific Conf. Series* vol 399) (San Francisco, CA: Astronomical Society of the Pacific) p 115
[178] Hicken M *et al* 2009 *Astrophys. J.* **700** 331
[179] Hinshaw G *et al* 2007 *Astrophys. J. Suppl.* **170** 288
[180] Hornorez L, Reid B, Mena O, Verde L and Jimenez R 2010 *J. Cosmol. Astropart. Phys.* JCAP09(2010)029
[181] Howlett C *et al* 2015 *Mon. Not. R. Astron. Soc.* **449** 848
[182] Hu W 2002 *Phys. Rev.* D **65** 023003
[183] Hu W 2002 *Phys. Rev.* D **66** 083515
[184] Hu W and Sugiyama N 1995 *Phys. Rev.* D **44** 489
[185] Hu W and White M 1996 *Astrophys. J.* **471** 30
[186] Hu B and Raveri M 2015 *Phys. Rev.* D **91** 123515
[187] Huang Q-G and Li M 2004 *J. Cosmol. Astropart. Phys.* JCAP08(2004)013
[188] Jackson B M, Taylor A and Berera A 2009 *Phys. Rev.* D **79** 043526
[189] Jenlins A *et al* 2001 *Mon. Not. R. Astron. Soc.* **321** 372
[190] Jimenez R, Verde L, Treu T and Stern D 2003 *Astrophys. J.* **593** 622
[191] Jones D H *et al* 2004 *Mon. Not. R. Astron. Soc.* **355** 747
[192] Joyce A, Jain B, Khoury J and Trodden M 2015 *Phys. Rep.* **568** 1
[193] Kaiser N 1987 *Mon. Not. R. Astron. Soc.* **227** 1
[194] Kamenschik A Y, Moschella U and Pasquier V 2001 *Phys. Lett.* B **511** 265
[195] Kashlinsky A *et al* 2008 *Astrophys. J.* **686** L49
[196] Kashlinsky A *et al* 2010 *Astrophys. J.* **712** L81
[197] Kashlinsky A *et al* 2015 *Astrophys. J. Lett.* **813** L12
[198] Kazin E A 2014 *Mon. Not. R. Astron. Soc.* **441** 3524
[199] Keisler R 2015 *Astrophys. J.* **807** 151
[200] Kessler R *et al* 2009 *Astrophys. J. Supp.* **185** 32
[201] Kim A G *et al* 2015 *Astropart. Phys.* **63** 2
[202] Kitching T D *et al* 2015 Euclid & SKA synergies (arXiv:1501.03978)
[203] Klöckner H R *et al* 2015 Real time cosmology—a direct measure of the expansion rate of the universe *Proc. Advancing Astrophysics with the Square Kilometre Array (AASKA14) (Giardini Naxos, Italy, 9–13 June, 2014)* (arXiv:1501.03822)
[204] Kobayashi T, Yamaguchi M and Yokoyama J 2011 *Prog. Theor. Phys.* **126** 511
[205] Kodama H and Sasaki M 1984 *Prog. Theor. Phys. Suppl.* **78** 1
[206] Kodama Y, Yonetoku D, Murakami T and Tanabe S 2008 *Mon. Not. R. Astron. Soc.* **391** L1
[207] Kofinas G, Papantonopoulos E and Saridakis E 2016 Modified Brans–Dicke cosmology with matter-scalar field interaction (arXiv:1602.02687)
[208] Kofman L A and Starobinskii A A 1985 *Sov. Astron. Lett.* **11** 271
[209] Koivisto T 2005 *Phys. Rev.* D **72** 043516
[210] Koivisto T and Mota D F 2005 *J. Cosmol. Astropart. Phys.* JCAP08(2005)021
[211] Koivisto T, Mota D F and Zumalacarregui M 2012 *Phys. Rev. Lett.* **109** 241102
[212] Kolb R and Turner M 1990 *The Physics of the Early Universe* (Redwood City, CA: Addison-Wesley)
[213] Komatsu E *et al* 2009 *Astrophys. J. Suppl.* **180** 330
[214] Komatsu E *et al* 2011 *Astrophys. J. Suppl.* **192** 18
[215] Koyama K, Maartens R and Song Y S 2009 *J. Cosmol. Astropart. Phys.* JCAP10(2009)017
[216] Krauss L M and Chaboyer B 2003 *Science* **299** 65
[217] Kristiansen J R, La Vacca G, Colombo L P L, Mainini R and Bonometto S A 2010 *New Astron.* **15** 609
[218] Kunz M, Corasaniti P-S, Parkinson D and Copeland E J 2004 *Phys. Rev.* D **70** 041301
[219] Landim R 2016 *Eur. Phys. J.* C **76** 31
[220] Laureijs R *et al* 2011 Euclid definition study report (arXiv:1110.3193)
[221] Layzer D 1963 *Astrophys. J.* **138** 174L
[222] Lesgourgues J, Valkenburg W and Gaztanaga E 2008 *Phys. Rev.* D **77** 063505
[223] Levi M *et al* 2013 The DESI experiment, a whitepaper for snowmass 2013 (arXiv:1308.0847)
[224] Lewis A, Challinor A and Lasenby A 2000 *Astrophys. J.* **538** 473
[225] Lewis A and Bridle S 2002 *Phys. Rev.* D **66** 103511
[226] Lewis A and Challinor A 2006 *Phys. Rep.* **429** 1
[227] Li M 2004 *Phys. Lett.* B **603** 1
[228] Li Y, Zhang J F and Zhang X 2014 *Phys. Rev.* D **90** 063005
[229] Li Y and Zhang X 2014 *Phys. Rev.* D **89** 083009
[230] Liddle A 2004 *Mon. Not. R. Astron. Soc.* **351** L49
[231] Liddle A 2007 *Mon. Not. R. Astron. Soc.* **377** L74
[232] Liddle A and Scherrer R J 1998 *Phys. Rev.* D **59** 023509
[233] Lima M and Hu W 2004 *Phys. Rev.* D **70** 043504
[234] Lima M and Hu W 2005 *Phys. Rev.* D **72** 043006
[235] Linder E V 2003 *Phys. Rev. Lett.* **90** 091301
[236] Linder E V and Cahn R N 2007 *Astrop. Phys.* **28** 481
[237] Loeb A 1998 *Astrophys. J. Lett.* **499** L111
[238] Macaulay E, Wehus I K and Eriksen H K 2013 *Phys. Rev. Lett.* **111** 161301
[239] Mainini R and Bonometto S 2007 *J. Cosmol. Astropart. Phys.* JCAP06(2007)020
[240] Mainini R and Mota D F 2012 *Astrophys. J.* **744** 3
[241] Majerotto E, Valiviita J and Maartens R 2009 *Mon. Not. R. Astron. Soc.* **402** 2344
[242] Manera M and Mota D 2006 *Mon. Not. R. Astron. Soc.* **371** 1373
[243] Marin F A, Beutler F, Blake C, Koda J, Kazin E and Schneider D P 2016 *Mon. Not. R. Astron. Soc.* **455** 4046
[244] Martinelli M, Honorez L, Melchiorri A and Mena O 2010 *Phys. Rev.* D **81** 103534
[245] Marulli F, Baldi M and Moscardini L 2012 *Mon. Not. R. Astron. Soc.* **420** 2377
[246] Matsubara T 2004 *Astrophys. J.* **615** 573
[247] Merloni A *et al* 2012 eROSITA science book: mapping the structure of the energetic universe (arXiv:1209.3114)
[248] Micheletti S, Abdalla E and Wang B 2009 *Phys. Rev.* D **79** 123506
[249] Micheletti S 2009 *J. Cosmol. Astropart. Phys.* **05** 009
[250] Mohammad F G, de la Torre S, Bianchi D, Guzzo L and Peacock J A 2016 *Mon. Not. R. Astron. Soc.* **458** 1948
[251] Morgan J S, Burgett W and Onaka P 2014 *Proc. SPIE* **9145** 18
[252] Mota D F and Bruck C 2004 *Astro. Astrophys.* **421** 71
[253] Mota D F 2008 *J. Cosmol. Astropart. Phys.* JCAP09(2008)006
[254] Multamaki T, Gaztanaga E and Manera M 2003 *Mon. Not. R. Astron. Soc.* **344** 761
[255] Murgia R, Gariazzo S and Forrergo N 2016 *J. Cosmol. Astropart. Phys.* **04** 014
[256] Nesseris S and Sapone D 2015 *Int. J. Mod. Phys.* D **24** 1550045
[257] Nolta M R *et al* 2004 *Astrophys. J.* **608** 10
[258] Nunes N J, Silva A C and Aghanim N 2006 *Astron. Astrophys.* **450** 899

[259] Nunes N J and Mota D F 2006 *Mon. Not. R. Astron. Soc.* **368** 751
[260] Oka A *et al* 2014 *Mon. Not. R. Astron. Soc.* **439** 2515
[261] Olivares G, Atrio-Barandela F and Pavón D 2005 *Phys. Rev.* D **71** 063523
[262] Olivares G, Atrio-Barandela F and Pavón D 2006 *Phys. Rev.* D **74** 043521
[263] Olivares G, Atrio-Barandela F and Pavón D 2008 *Phys. Rev.* D **77** 063513
[264] Olivares G, Atrio-Barandela F and Pavón D 2008 *Phys. Rev.* D **77** 103520
[265] Pace F *et al* 2014 *Mon. Not. R. Astron. Soc.* **447** 858
[266] Padmanabhan N *et al* 2012 *Mon. Not. R. Astron. Soc.* **427** 2132
[267] Padmanabhan T 2002 *Phys. Rev.* D **66** 021301
[268] Parker L E and Toms D J 2009 *Quantum Field Theory in Curved Spacetime: Quantized Fields and Gravity* (Cambridge: Cambridge University Press)
[269] Pavan A B, Ferreira E G M, Micheletti S, de Souza J C C and Abdalla E 2012 *Phys. Rev.* D **86** 103521
[270] Pavón D and Wang B 2009 *Gen. Relativ. Grav.* **41** 1
[271] Pavón D and Zimdahl W 2005 *Phys. Lett.* B **628** 206
[272] Peccei R D and Quinn H R 1977 *Phys. Rev. Lett.* **38** 1440
[273] Peebles P J E 1980 *Large Scale Structure of the Universe* (Princeton, NJ: Princeton University Press)
[274] Peebles P J E 1984 *Astrophys. J.* **284** 439
[275] Peebles P J E 1993 *Physical Cosmology* (Princeton, NJ: Princeton University Press)
[276] Peebles P J E and Ratra B *Rev. Mod. Phys.* **75** 59
[277] Pellicer C E *et al* 2012 *Mod. Phys. Lett.* A **27** 1250144
[278] Percival W J *et al* 2004 *Mon. Not. R. Astron. Soc.* **353** 1201
[279] Percival W J *et al* 2007 *Mon. Not. R. Astron. Soc.* **381** 1053
[280] Percival W J *et al* 2010 *Mon. Not. R. Astron. Soc.* **401** 2148
[281] Perlmutter S *et al* 1998 *Nature* **391** 51
[282] Perlmutter S *et al* 1999 *Astrophys. J.* **517** 565
[283] Pettorino V, Amendola L, Baccigalupi C and Quercellini C 2012 *Phys. Rev.* D **86** 103507
[284] Pettorino V and Baccigalupi C 2008 *Phys. Rev.* D **77** 103003
[285] Pires N, Zhu Z H and Alcaniz J S 2006 *Phys. Rev.* D **73** 123530
[286] Planck Collaboration I 2014 *Astron. Astrophys.* **571** 1
[287] Planck Collaboration XV 2014 *Astron. Astrophys.* **571** 15
[288] Planck Collaboration XVI 2014 *Astron. Astrophys.* **571** 16
[289] Planck Collaboration XVII 2014 *Astron. Astrophys.* **571** 17
[290] Planck Collaboration XIX 2014 *Astron. Astrophys.* **571** 19
[291] Planck Collaboration XX 2014 *Astron. Astrophys.* **571** 20
[292] Planck Collaboration I 2015 Overview of products and scientific results (arXiv:1502.01582)
[293] Planck Collaboration XIII 2015 Cosmological parameters (arXiv:1502.01589)
[294] Planck Collaboration XIV 2015 Dark energy and modified gravity (arXiv:1502.01590)
[295] Planck Collaboration XV 2015 Gravitational lensing (arXiv:1502.01591)
[296] Planck Collaboration XVIII 2015 Background geometry & topology (arXiv:1502.01593)
[297] Planck Collaboration XXIV 2015 Cosmology from Sunyaev–Zeldovich cluster counts (arXiv:1502.01597)
[298] Piazza F and Tsujikawa S 2004 *J. Cosmol. Astropart. Phys.* JCAP07(2004)004
[299] Polarski D and Gannouji R 2008 *Phys. Lett.* B **660** 439
[300] Postma M and Volponi M 2014 *Phys. Rev.* D **90** 103516
[301] Press W H and Schechter P 1974 *Astrophys. J.* **187** 425
[302] Pu B Y, Xu X D, Wang B and Abdalla E 2015 *Phys. Rev.* D **92** 123537
[303] Raccanelli A *et al* 2014 Measuring redshift-space distortions with future SKA surveys *Proc. Advancing Astrophysics with the Square Kilometre Array (AASKA14) (Giardini Naxos, Italy, 9–13 June, 2014)* (arXiv:1501.03821)
[304] Radicella N and Pavón D 2010 *J. Cosmol. Astropart. Phys.* JCAP10(2010)005
[305] Radicella N and Pavón D 2012 *Gen. Relativ. Grav.* **44** 685
[306] Ratra B and Peebles P J E 1988 *Phys. Rev.* D **37** 3406
[307] Raveri M, Baccigalupi C, Silvestri A and Zhou S-Y 2014 *Phys. Rev.* D **91** 061501
[308] Reichardt C L, de Putter R, Zahn O and Hou Z 2012 *Astrophys. J. Lett.* **749** L9
[309] Reid B A *et al* 2012 *Mon. Not. R. Astron. Soc.* **426** 2719
[310] Reif F 1965 *Fundamental of Statistical and Thermal Physics* (New York: Mc Graw Hill)
[311] Ribas Marlos O, Devecchi F P and Kremer G M 2008 *Europhys. Lett.* **81** 19001
[312] Ribas Marlos O, Devecchi F P and Kremer G M 2011 *Europhys. Lett.* **93** 19002
[313] Riess A G *et al* 1998 *Astron. J.* **116** 1009
[314] Riess A G *et al* 1999 *Astron. J.* **117** 707
[315] Riess A G *et al* 2007 *Astrophys. J.* **659** 98
[316] Riess A G *et al* 2011 *Astrophys. J.* **730** 119
[317] Ross A J *et al* 2015 *Mon. Not. R. Astron. Soc.* **449** 835
[318] Sachs R K and Wolfe A M 1967 *Astrophys. J.* **147** 73
[319] Saha B 2004 *Phys. Rev.* D **69** 124006
[320] Sahni V, Saini T D, Starobinsky A A and Ulam U 2003 *JETP Lett.* **77** 201
[321] Salvatelli V, Marchini A, Lopez-Honorez L and Mena O 2013 *Phys. Rev.* D **88** 023531
[322] Salvatelli V, Said N, Bruni M, Melchiorri A and Wands D 2014 *Phys. Rev. Lett.* **113** 181301
[323] Samushia L, Percival W J and Raccanelli A 2012 *Mon. Not. R. Astron. Soc.* **420** 2102
[324] Samushia H *et al* 2014 *Mon. Not. R. Astron. Soc.* **439** 3504
[325] Sánchez I E 2014 *Gen. Relativ. Garv.* **46** 1769
[326] Sandage A, Tamman G A and Saha A 2001 *Supernovae and Gamma-Ray Bursts: the Greatest Explosions Since the Big Bang* (Cambridge: Cambridge University Press) p 304
[327] Sandage A 1962 *Astrophys. J.* **136** 319
[328] Santos J, Alcaniz J S, Reboucas M J and Pires N 2007 *Phys. Rev.* D **76** 043519
[329] Sapone D, Kunz M and Amendola L 2010 *Phys. Rev.* D **82** 103535
[330] Santos M *et al* 2014 HI galaxy simulations for the SKA: number counts and bias *Proc. Advancing Astrophysics with the Square Kilometre Array (AASKA14) (Giardini Naxos, Italy, 9–13 June, 2014)* (arXiv:1501.03990)
[331] Schaefer B M 2008 *Mon. Not. R. Astron. Soc.* **388** 1403
[332] Scherrer R J 2004 *Phys. Rev. Lett.* **93** 011301
[333] Schwarz G E 1978 *Ann. Stat.* **6** 461
[334] Seljak U and Zaldarriaga M 1999 *Phys. Rev.* D **60** 043504
[335] Sen A 2002 *J. High Energy Phys.* JHEP04(2002)048
[336] Sen A 2002 *J. High Energy Phys.* JHEP07(2002)065
[337] Sen A 2002 *Mod. Phys. Lett.* A **17** 1797
[338] Sen A 2003 *Ann. Henri Poincare* **4** S31
[339] Sen A 2003 *Int. J. Mod. Phys.* A **18** 4869
[340] Sen A 2003 *Phys. Rev.* D **68** 106003
[341] Sen A and Scherrer R 2005 *Phys. Rev.* D **72** 063511
[342] Shahalam M, Pathak S D, Verma M M, Khlopov M Yu and Myrzakulov R 2015 *Eur. Phys. J.* C **75** 395
[343] Shen J Y, Wang B, Abdalla E and Keng S R 2005 *Phys. Lett.* B **609** 200
[344] Sievers J L *et al* 2013 *J. Cosmol. Astropart. Phys.* JCAP10(2013)060
[345] Simon J, Verde L and Jimenez J 2005 *Phys. Rev.* D **71** 123001
[346] Simpson F, Jackson B M and Peacock J A 2011 *Mon. Not. R. Astron. Soc.* **411** 1053
[347] Slosar A 2013 *J. Cosmol. Astropart. Phys.* JCAP04(2013)26
[348] Smith K M, Zahn O, Dore O and Nolta M R 2007 *Phys. Rev.* D **76** 043510
[349] Solevi P *et al* 2006 *Mon. Not. R. Astron. Soc.* **366** 1346

[350] Song Y-S and Percival W J 2009 *J. Cosmol. Astropart. Phys.* JCAP10(2009)004
[351] Spergel D N *et al* 2003 *Astrophys. J. Suppl.* **148** 175
[352] Spergel D N *et al* 2013 WFIRST-2.4: what every astronomer should know (arXiv:1305.5425)
[353] Stern D *et al* 2010 *J. Cosmol. Astropart. Phys.* JCAP02(2010)008
[354] Story K T 2013 *Astrophys. J.* **779** 86
[355] Sunyaev R A and Zeldovich Ya B 1972 *Comments Astrophys. Space Phys.* **4** 173
[356] Susskind L 1995 *J. Math. Phys.* **36** 6377
[357] Sutter P M and Ricker P M 2008 *Astrophys. J.* **687** 7
[358] Suzuki N *et al* 2012 *Astrophys. J.* **746** 85
[359] Swetz D S *et al* 2010 *Astrophys. J. Supp.* **194** 41
[360] Shaun A T, Abdalla F B and Lahav O 2010 *Phys. Rev. Lett.* **105** 031301
[361] Tegmark M *et al* 2004 *Phys. Rev.* D **69** 103501
[362] 't Hooft G 1993 Dimensional reduction in quantum gravity (arXiv: gr-qc/9310026)
[363] de la Torre S *et al* 2013 *Astron. Astrophys.* **557** 54
[364] Tsagas C G, Challinor A and Maartens R 2008 *Phys. Rep.* **465** 61
[365] Tsujikawa S 2007 *Phys. Rev.* D **76** 023514
[366] Tsujikawa S, Gannouji R, Moraes B and Polarski D 2009 *Phys. Rev.* D **80** 084044
[367] Tsujikawa S and Sami M 2004 *Phys. Lett.* B **603** 113
[368] La Vacca G and Colombo L P L 2008 *J. Cosmol. Astropart. Phys.* JCAP04(2008)007
[369] La Vacca G, Kristiansen J, Colombo L, Mainini R and Bonometto S 2009 *J. Cosmol. Astropart. Phys.* JCAP04(2009)007
[370] Valiviita J, Majerotto E and Maartens R 2008 *J. Cosmol. Astropart. Phys.* JCAP07(2008)020
[371] Valiviita J, Maartens R and Majerotto E 2010 *Mon. Not. R. Astron. Soc.* **402** 2355
[372] Valiviita J and Palmgren E 2015 *J. Cosmol. Astropart. Phys.* JCAP07(2015)015
[373] Verde L, Protopapas P and Jimenez R 2014 *Phys. Dark Universe* **5–6** 307
[374] Vergani L, Colombo L P L, La Vacca G and Bonometto S A 2009 *Astrophys. J.* **697** 1946
[375] Verma M M 2010 *Astrophys. Space Sci.* **330** 101
[376] Verma M M and Pathak S D 2014 *Int. J. Mod. Phys.* D **23** 1450075
[377] Viana P T P and Liddle A R 1996 *Mon. Not. R. Astron. Soc.* **281** 323
[378] Wang B, Gong Y G and Abdalla E 2005 *Phys. Lett.* B **624** 141
[379] Wang B, Lin C-Y and Abdalla E 2006 *Phys. Lett.* B **637** 357
[380] Wang B, Lin C-Y, Pavon D and Abdalla E 2008 *Phys. Lett.* B **662** 1
[381] Wang B, Zang J, Lin C Y, Abdalla E and Micheletti S 2007 *Nucl. Phys.* B **778** 69
[382] Wang Q and Fan Z 2009 *Phys. Rev.* D **79** 123012
[383] Wang Y and Mukherjee P 2007 *Phys. Rev.* D **76** 103533
[384] Way M J, Foster L V, Gazis P R and Srivastava A N 2009 *Astrophys. J.* **706** 623
[385] Wei H and Cai R G 2006 *Phys. Rev.* D **73** 083002
[386] Wei H and Zhang S N 2007 *Phys. Lett.* B **644** 7
[387] Weinberg S 1972 *Gravitation and Cosmology* (New York: Wiley)
[388] Weinberg S 1989 *Rev. Mod. Phys.* **61** 1
[389] Weinberg D H, Mortonson M J, Eisenstein D J, Hirata C, Riess A G and Rozo E 2013 *Phys. Rep.* **530** 87
[390] Weinberg D H *et al* 2013 Facilities for dark energy investigations (arXiv:1309.5380)
[391] Weller J and Lewis A M 2003 *Mon. Not. R. Astron. Soc.* **346** 987
[392] Wetterich C 1988 *Nucl. Phys.* B **302** 668
[393] Wetterich C 1995 *Astron. Astrophys.* **301** 321
[394] White M, Scott D and Silk J 1994 *Ann. Rev. Astron. Astrophys.* **32** 319
[395] Wintergerst N and Pettorino V 2010 *Phys. Rev.* D **82** 03516
[396] Wood-Vasey V M *et al* 2007 *Astrophys. J.* **666** 694
[397] Wu W L K 2014 *Astrophys. J.* **788** 138
[398] Xia J Q 2009 *Phys. Rev.* D **80** 103514
[399] Xia J Q 2013 *J. Cosmol. Astropart. Phys.* JCAP11(2013)022
[400] Xu X D, He J H and Wang B 2011 *Phys. Lett.* B **701** 513
[401] Xu X D, Wang B and Abdalla E 2012 *Phys. Rev.* D **85** 083513
[402] Xu X D, Wang B, Zhang P and Atrio-Barandela F 2013 *J. Cosmol. Astropart. Phys.* JCAP12(2013)001
[403] Xue S S 2015 *Nucl. Phys.* B **897** 326
[404] Yang T, Guo Z-K and Cai R-G 2015 *Phys. Rev.* D **91** 123533
[405] Yang W and Xu L 2014 *Phys. Rev.* D **89** 083517
[406] Yang W and Xu L 2014 *J. Cosmol. Astropart. Phys.* JCAP08(2014)034
[407] Yang W and Xu L 2014 *Phys. Rev.* D **90** 083532
[408] Yin S-Y, Wang B, Abdalla E and Lin C-Y 2007 *Phys. Rev.* D **76** 124026
[409] Zee A 2003 *Quantum Field Theory in a Nutshell* (Princeton, NJ: Princeton University Press)
[410] Zel'dovich Ya B 1972 *Mon. Not. R. Astron. Soc.* **160** 1
[411] Zhao G B 2015 Model-independent constraints on dark energy and modified gravity with the SKA *Proc. Advancing Astrophysics with the Square Kilometre Array (AASKA14) (Giardini Naxos, Italy, 9–13 June, 2014)* (arXiv:1501.03840)
[412] Zheng W, Li S Y, Li H, Xia J Q, Li M and Lu T 2014 *J. Cosmol. Astropart. Phys.* JCAP08(2014)30
[413] Zhou J, Wang B, Pavon D and Abdalla E 2009 *Mod. Phys. Lett.* A **24** 1689
[414] Zimdahl W, Pavon D and Chimento L P 2001 *Phys. Lett.* B **521** 133
[415] Zimdahl W 2005 *Int. J. Mod. Phys.* D **14** 2319
[416] Zimdahl W and Pavón D 2004 *Gen. Relativ. Grav.* **36** 1483
[417] Zimdahl W and Pavón D 2007 *Class. Quantum Grav.* **24** 5461
[418] Zlatev I, Wang L and Steinhardt P J 1999 *Phys. Rev. Lett.* **82** 896
[419] Zumalacarregui M Koivisto T S and Mota D F 2013 *Phys. Rev.* D **87** 083010
[420] Zuntz J, Bourliot T G, Ferreira P G and Starkman G D 2010 *Phys. Rev.* D **81** 104015